Generation and analysis of mouse lines with a defect in platelet secretion and application in mouse models of atherosclerosis and tumor metastasis

Dissertation

zur Erlangung des Doktorgrades

der Naturwissenschaften

vorgelegt beim Fachbereich 15

der Johann Wolfgang Goethe -Universität

in Frankfurt am Main

von

Dagmar Schumacher

aus Basel (Schweiz)

Max-Planck-Institut für Herz- und Lungenforschung,

Bad Nauheim (2012)

(D30)

vom Fachbereich 15 der

Johann Wolfgang Goethe - Universität als Dissertation angenommen.

Dekanin: Prof. Dr. Anna Starzinski-Powitz

Gutachter: Prof. Dr. Stefan Offermanns, Prof Dr. Amparo Acker-Palmer

Datum der Disputation:

Contents

Abbreviations

ATP	Adenosine triphosphate
ADP	Adenosine diphosphate
APC	Allophycocyanine
B16	B16F10 melanoma cells
BAC	Bacterial artificial chromosome
5-BDBD	5-(3-Bromophenyl)-1,3-dihydro-2H-benzofuro[3,2-e]-1,4-diazepin-2-one
bp	Basepair(s)
BSA	Bovine serum albumin
Calcein-AM	Calcein acetoxymethyl ester
CD40L	CD40 ligand (CD154)
cDNA	Complementary DNA
Cy5	Cyanine 5
DAPI	4',6-diamidino-2-phenylindole
DNA	Desoxyribonucleic acid
EDTA	Ethylendiamine tetraacetic acid
e.g.	Exempli gratia
Flp	FRT recombinase
FITC	Fluorescein isothiocyanate
FRT	Flp recognition target
g	Gram
g	Standard gravity (9.80665 m/s^2)
GAPDH	Glyceraldehyde 3-phosphate dehydrogenase
HCl	Hydrochloric acid
HEPES	4-(2-hydroxyethyl)-1-piperazineethanesulfonic acid
kDa	Kilodalton
LDLR	Low-density lipoprotein receptor
LLC1	Lewis lung carcinoma 1 cells
min	Minute(s)
mRNA	Messenger ribonucleic acid
MRS2500	(1R*,2S*)-4-[2-Iodo-6-(methylamino)-9H-purin-9-yl]-2-(phosphonooxy)bicyclo[3.1.0]hexane-1-methanol dihydrogen phosphate ester tetraammonium salt
Munc13	Mammalian uncoordinated-13
NaCl	Natriumchloride
NaOH	Natriumhydroxide
OCT	Optimum cutting temperature compound
PCR	Polymerase chain reaction

PDGF	Platelet-derived growth factor
PE	Phycoerythrin
PF4	Platelet factor 4 (CXCL4)
PRP	Platelet rich plasma
P2X	Purinergic ATP receptor, G Protein-coupled
P2Y	Purinergic ATP receptor, ion channel
qPCR	Quantitative polymerase chain reaction
RANTES	Regulated and normal T cell expressed and secreted (CCL5)
rpm	Rounds per minute
rRNA	Ribosomal ribonucleic acid
RT	Room temperature
s	Second(s)
S.D.	Standard deviation
SDS	Sodium dodecyl sulfate
S.E.M.	Standard error of the mean
siRNA	Small interfering ribonucleic acid
SNAP	Soluble NSF (N-ethylmaleimide-sensitive fusion protein)-attachment protein
SNARE	Soluble NSF attachment protein receptor
U46619	(Z)-7-[(1S,4R,5R,6S)-5-[(E,3S)-3-hydroxyoct-1-enyl]-3-oxabicyclo[2.2.1]heptan-6-yl]hept-5-enoic acid, thromboxane (TP) receptor agonist
VAMP	Vesicle-associated membrane protein
VE-cadherin	Vascular endothelial cadherin (CD144)
VEGF	Vascular endothelial growth factor
vWF	Von Willebrand factor

1   <u>Introduction</u>

Platelets are anucleate cellular fragments derived from megakaryocytes. Besides erythrocytes, they are the second largest group of blood cells, but they make up less than 0.5% of blood volume due to their small size (2-3 µm for human platelets; 1-2 µm for mouse platelets). Their primary function is attributed to hemostasis. In recent years their role in various pathological conditions is getting increasingly recognized and anti-platelet interventions may be a promising strategy in some diseases. The functionally relevant features, which enable platelets to contribute to such diverse outcomes, mainly comprise their ability to change their shape, to release different classes of granules and to interact with various other cell types.

Platelets contain three different kinds of granules: alpha and dense granules and lysosomes.

1.1   Secretory Machinery

1.1.1 Alpha granules

Alpha granules are the largest (200-500 nm) and most abundant type of vesicle in platelets (~50-80 per human platelet) (Sixma, Slot et al. 1989; Maynard, Heijnen et al. 2007). They can be identified via electron microscopy by 1) the peripheral membrane of the granule, 2) an electron dense nucleoid that contains chemokines and proteoglycan, 3) a less electron dense area adjacent to the nucleoid that contains fibrinogen, and 4) a peripheral electronluscent zone that contains von Willebrand factor (vWF), although not all four features need to be observed to qualify as an alpha granule (White and Krumwiede 2007). Immunostaining for established markers like vWF and fibrinogen may also be used to identify alpha granules. Reported cargo of alpha granules mainly comprises proteins and macromolecules and includes:

Protein class	Known alpha granule proteins
Adhesion proteins & surface receptors	P-selectin (CD62P), integrins (αIIbβ3, αVβ3), CD36, CD9, GLUT-3, fibrinogen, fibronectin, vitronectin, thrombospondin, vWF (von Willebrand factor)
Growth factors	VEGF, PDGF-B, TGF-β , EGF, IGF-1, bFGF, angiopoietin-1 and -2
Chemokines & cytokines	PF4, RANTES, SDF-1α, MCP-1, MCP-3, IL-1β, IL-8, MIP-1α, β-thromboglobulin, GRO-α, 12-HETE, NAP-2, ENA-78, CTAP-3,
Fibrinolytic agents	PAI-1, TAFI, 2-antiplasmin α2-Macroglobulin, plasminogen

Coagulation pathway	coagulation factors: V, XI, XIII; kininogen, multimerin
Immunologic molecules	B 1H globulin, factor D, C1 inhibitor, IgG

Table 1: **Well-established alpha granule molecules in literature.** Glut-3, glucose transporter type 3; PDGF-B, platelet-derived growth factor B; TGF-β, transforming growth factor beta; EGF, epidermal growth factor; IGF-1, insulin-like growth factor 1; bFGF, basic fibroblast growth factor; SDF-1α, stromal cell-derived factor 1 alpha; MCP, monocyte chemoattractant protein; IL, interleukin; MIP-1α, macrophage inflammatory protein 1 alpha; GRO-α, growth-regulated oncogene aplha; 12-HETE, 12-hydroxyeicosatetraenoic acid; NAP-2, neutrophil-activating protein 2; ENA-78, epithelial neutrophil-activating protein 78; CTAP-3, connective tissue-activating protein 3; PAI-1, plasminogen activator inhibitor 1; TAFI, thrombin-activatable fibrinolysis inhibitor (Rendu and Brohard-Bohn 2001; Maynard, Heijnen et al. 2007).

The major part of alpha granule content is acquired during budding in the megakaryocyte but proteins like fibrinogen are taken up via endocytosis in the circulation. There are several recent reports which suggest regulated differential sorting and exocytosis of alpha granule proteins, especially pro- and anti-angiogenic factors like VEGF and endostatin (Italiano, Richardson et al. 2008). Seghal et al. found non-overlapping localizations of fibrinogen and vWF in platelets (Sehgal and Storrie 2007). The molecular mechanisms involved still need to be elucidated. Substructural organization within the alpha granule often found includes dense nucleoid compartments, more translucent zones and tubular vWF structures in the periphery. P-Selectin was found to be associated with alpha and dense granule membranes in immunogold labeling (Stenberg, McEver et al. 1985; Israels, Gerrard et al. 1992; Youssefian, Masse et al. 1997). Alpha granule organization and components are highly variable and may differ between species.

Alpha granule release is slower than dense granule release (minutes instead of seconds) and may be differentially regulated by the kind of stimulus present (Italiano and Battinelli 2009). Alpha granules can fuse with each other upon platelet activation and are thought to be exocytosed mainly via the OCS (White 1999; White 1999; Gader, Ghumlas et al. 2008). Upon activation of platelets, a centralization of alpha granules is often observed, which precedes fusion with the OCS (White 1999; White and Krumwiede 2007). The major structural features of platelets, centralization of alpha granules upon stimulation and release of alpha granules are illustrated in figure 1 (White and Krumwiede 2007).
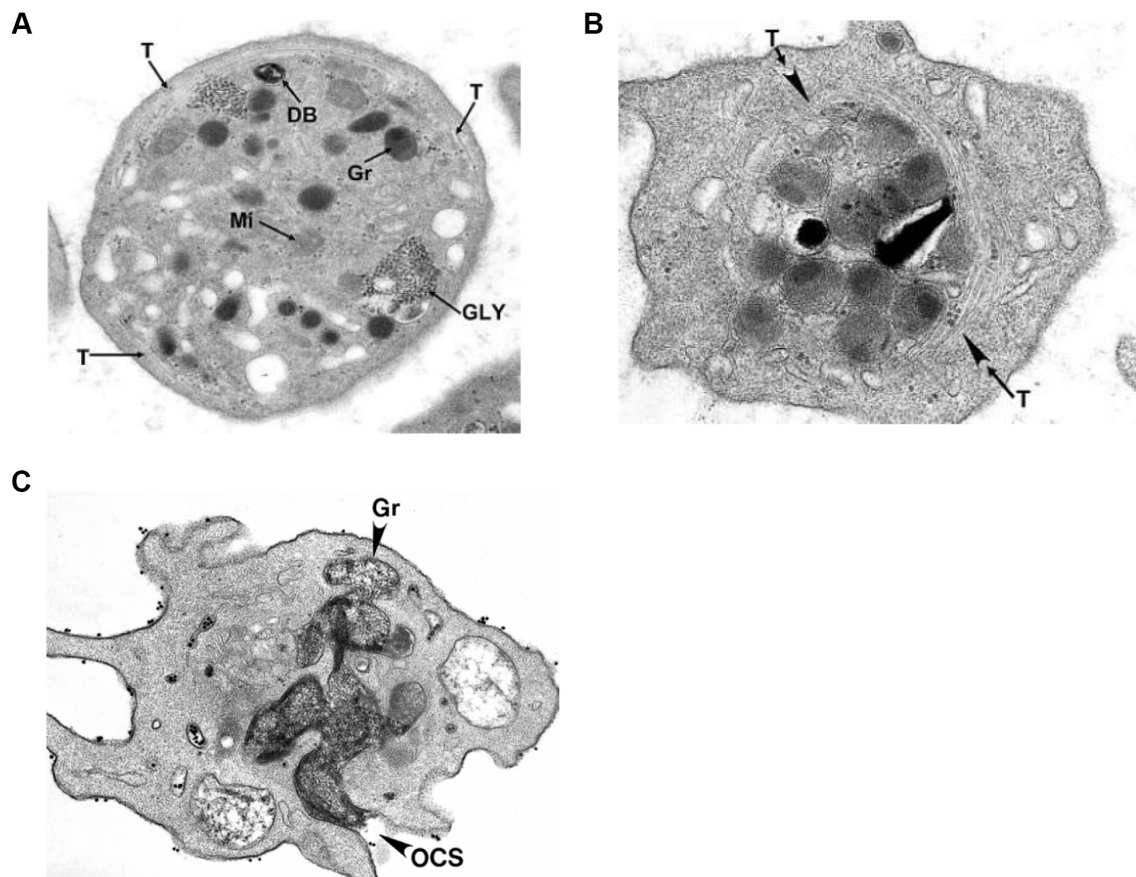
Figure 1: **Transmission electron microscopic images of fixed human platelets.** (A) Discoid platelet section in the equatorial plane revealing alpha granules (Gr), a few mitochondria (Mi), occasional dense bodies (DB) and glycogen (GLY) randomly dispersed in the cytoplasm. The discoid shape is maintained by a circumferential coil of microtubules (T) (Magnification x 27,000). (B) After exposure to thrombin, the platelet developed lamellapodia. Organelles have been transported to the center of the cell by the ring of microtubules (T) and microfilaments (Magnification x 50,000). (C) Platelet exposed to thrombin, fixed and stained with tannic acid. Together with osmic acid, tannic acid produces osmium black and stains fibrinogen in alpha granules (Gr), which have fused with each other and the channels of the open canalicular system (OCS) during secretion (Magnification x 37,000). (From: White and Krumwiede 2007).

1.1.2 Dense granules

Platelets contain approximately 6-10 electron-dense structures, which appear inherently opaque and have a characteristic bull eye-like shape in electron microscopic imaging. Some of these dense granules, also called dense bodies or δ-granules, show a whip-like tail (White and Krumwiede 2007; Gader, Ghumlas et al. 2008). Dense granules contain small molecules like ADP, ATP, GDP, GTP, Ca^{2+}, serotonin, histamine and polyphosphates (Ruiz, Lea et al. 2004; Maynard, Heijnen et al. 2007; White and Krumwiede 2007; Muller, Mutch et al. 2009). They are released within seconds upon stimulation (Ge, Woo et al.

2011) and their secretion is mainly mediated by F-actin, not microtubules (Ge, White et al. 2012). It was proposed that dense granules both fuse with the OCS and the outer membrane (Ge, White et al. 2009).

1.1.3 Lysosomes

Lysosomes are mainly considered as separated acidic degradative units rather than releasable granules. Several hematopoietic cells like macrophages (Tapper and Sundler 1990), cytotoxic T lymphocytes (Griffiths 1997) and platelets (Silverstein and Febbraio 1992) have so called secretory lysosomes. Lysosomes mainly store acid hydrolases able to degrade glycoproteins, glycolipids and glyco-aminoglycans like ADAM17 and ADAM10 which have been shown to cleave GPVI (Silverstein and Febbraio 1992). Cathepsins and hexosaminidase found in platelet lysosomes may play a role in clot remodeling or in further platelet activation (Ren, Ye et al. 2008). Although lysosomal release has been shown in vitro and hexosaminidase release at sites of local platelet activation has been observed in humans (Ciferri, Emiliani et al. 2000) physiological relevance remains controversial (Polasek 1989). Lysosomal release in vitro is only partial even at high agonist concentrations and needs high and maintained levels of strong platelet agonists (Ren, Wimmer et al. 2010).

1.2 Platelet activation

Platelet activation, shape change and release of granule contents are the mechanisms which govern platelet function in hemostasis, but also thrombotic events and other pathophysiological processes. A set of platelet surface receptors and platelet agonists are able to activate platelets. The context of platelet activation determines which molecules act on their respective platelet receptors and signaling cascades. Ultimately, the diverging pathways all lead to elevated intracellular calcium levels, followed by shape change (pseudopod formation), secretion of platelet granules and aggregation (crosslinking with nearby activated platelets). It is well established that rise in intracellular calcium results in exocytosis of platelet dense and alpha granules but the mechanisms are not yet fully elucidated (Ren, Ye, et al. 2008).

1.2.1 Main platelet receptors involved in platelet activity

Under hemostatic conditions, platelets do not adhere to the vessel wall as endothelial cells lining the vessel lumen synthesize platelet inhibitors and protect the underlying extracellular matrix from being exposed. Endothelial cells produce prostaglandin I_2 (PGI$_2$) from arachidonic acid (Moncada, Gryglewski et al. 1976; Weksler, Marcus et al. 1977), which binds to the platelet IP receptor and stimulates adenylyl cyclase, leading to cAMP formation and inhibition of platelet activation (Stegner and Nieswandt 2011). In addition, endothelial cells synthesize NO which inhibits a rise in intracellular Calcium levels mainly through cyclic GMP (cGMP) and the cGMP-dependent protein kinase type I (PKG I) (Dangel, Mergia et al.

2010). Once endothelial cells get activated, they expose P-Selectin and multimeric structures of von Willebrand factor (vWF) on their surface which enables platelets, leukocytes and platelet-leukocyte aggregates to "roll" on endothelium, slow down and form tight interactions with the vessel wall through various surface receptors. On platelets, the initial interaction is mainly mediated by glycoprotein receptor GPIbα, which binds to vWF (Munnix, Cosemans, et al. 2009). Under high shear stress, as observed in small vessels, the GPIbα-binding domain of vWF (A1) unfolds and this unfolding is thermodynamically coupled to binding to GPIbα (Auton, Zhu et al. 2010). GPIb is associated with GPV and GPIX (GPIb-V-IX complex). If the endothelial barrier is disrupted and the extracellular matrix gets exposed, platelets encounter molecules such as collagen, vWF, fibrinogen, fibronectin, vitronectin and laminin, which immediately bind to their respective platelet receptors. Collagen from the ECM activates and binds platelets mainly through GPVI and its co-receptor FcγII with a supporting role for integrin α2β1 in the formation of stable thrombi (Munnix, Cosemans, et al. 2009). Binding of GPVI and GPIbα by their respective ligands activates platelets and leads to an intracellular rise in calcium levels which in turn causes release of secondary mediators and recruitment of other platelets. Release of dense granule ADP and ATP as well as formation of thromboxane A_2 and thrombin are the main mediators amplifying activation via autocrine and paracrine feedback loops. Upon platelet activation, thromboxane A_2 is generated through liberation of arachidonic acid from the plasma membrane, metabolization to prostaglandin H_2 and transformation to thromboxane A_2 by thromboxane synthase (McNicol and Israels 2003). Thromboxane A_2 is released and binds to TP receptor subtypes α or β on platelets to potentiate activation. Thrombin generation by the coagulation cascade is facilitated on the surface of activated platelets through exposure of phosphatidylserine which enhances coagulation factor binding and activation (Sims and Wiedmer 2001). Human platelets express mainly PAR1 and PAR4 Thrombin receptors on their surface whereas mouse platelets exhibit PAR3 and PAR4. In humans, PAR1 seems to be the central receptor for thrombin signaling while PAR4 mediates a slower, more prolonged activation (Covic, Gresser et al. 2000). In mice, PAR3 is the primary mediator of thrombin action and PAR4 may serve as "co-activator" (Bender, Hofmann et al. 2010).

Agonist stimulation of platelets and the resulting PLC activation is followed by formation of IP_3 and DAG, which leads to a rise in intracellular calcium levels and in the end, triggers the switch of a "low-affinity state" of integrin αIIbβ3 to a "high-affinity state". This influences the efficiency of integrin αIIbβ3 to bind to its ligand fibrinogen, which enhances platelet aggregation and further "outside-in" signaling of integrin αIIbβ3 to stabilize aggregates. Therefore, activation of integrin αIIbβ3 is termed the "final common pathway" of platelet activation (Nieswandt, Varga-Szabo et al. 2009; Stegner and Nieswandt 2011). Stable thrombi are formed by crosslinking activated platelets with each other through adhesive plasma proteins like fibrinogen and vWF. The C-type lectin receptor CLEC-2 recently discovered as platelet surface receptor (Suzuki-Inoue, Fuller et al. 2006)

binds to the tumor-associated ligand podoplanin, HIV-1 and the snake venom rhodocytin in addition to its role in hemostasis and thrombosis. Blocking CLEC-2 on platelets with a specific antibody inhibits their ability to form stable aggregates under flow in vitro and leads to an enhanced bleeding time and a marked defect in thrombus formation in vivo (May, Hagedorn et al. 2009). The known platelet activating pathways are summarized in figure 2. Prostaglandin E2, epinephrine and serotonin can potentiate platelet activation mechanisms described above but are not sufficient to trigger major platelet responses on their own (Stegner and Nieswandt 2011).
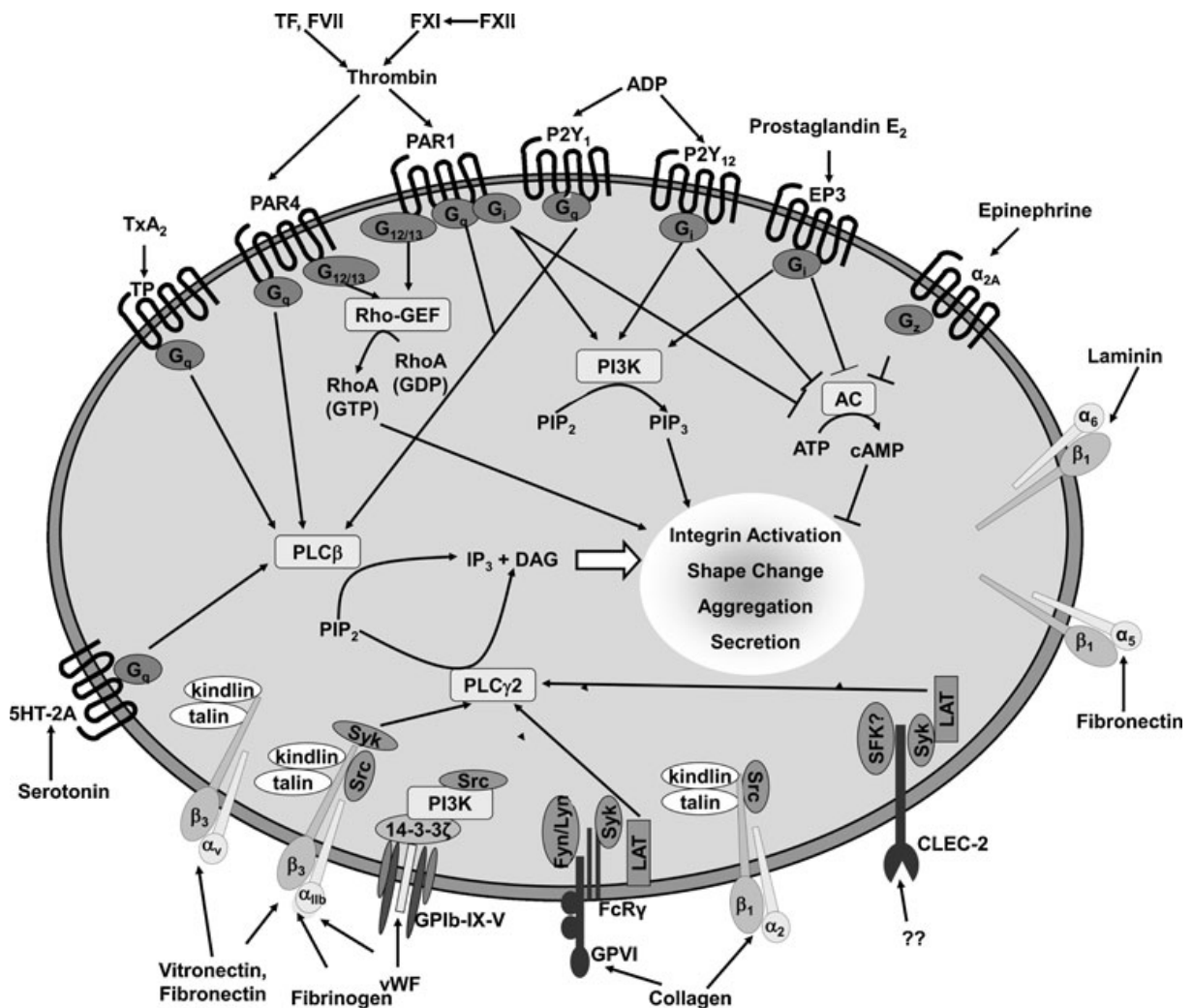
Figure 2: **"Platelet receptors and important signaling molecules leading to platelet activation.** Soluble agonists stimulate G protein-coupled receptors, triggering pathways involving the corresponding G proteins. Cross-linking of GPVI or CLEC-2 results in activation of phospholipase (PL) Cγ2. TF tissue factor, TxA2 thromboxane A2, TP TxA2 receptor, PAR protease-activated receptor, RhoGEF Rho-specific guanine nucleotide exchange factor, PI3K phosphoinositide-3-kinase, AC adenylyl cyclase, PIP2 phosphatidylinositol-4,5-bisphosphate, PIP3 phosphatidylinositol-3,4,5-trisphosphate, IP3 inositol-1,4,5-trisphosphate, DAG diacylglycerol." (Excerpt from: Stegner and Nieswandt 2011).

Figure 3 displays the most important signaling cascades and interactions of platelets upon exposure of extracellular matrix (Stegner and Nieswandt 2011).
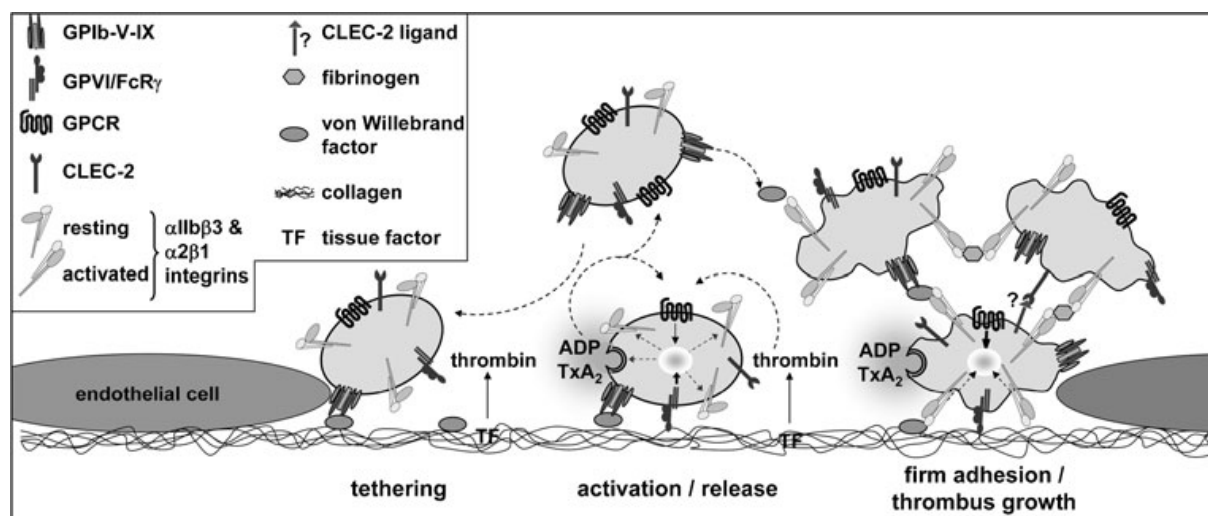
Figure 3:   **"Model for platelet adhesion to the subendothelial matrix at sites of vascular injury and subsequent thrombus formation.** The initial contact (tethering) to the ECM is mediated predominantly by GPIb–vWF interactions. In a second step, GPVI–collagen interactions initiate cellular activation followed by the shift of integrins to a high-affinity state and the release of second-wave agonists, most importantly ADP, ATP, and thromboxane A_2 (TxA_2). In parallel, exposed tissue factor locally triggers the formation of thrombin, which in addition to GPVI, mediates cellular activation. Finally, firm adhesion of platelets to collagen through activated α2β1 (directly) and αIIbβ3 (indirectly via vWF or other ligands) results in sustained GPVI signaling, enhanced release of soluble agonists and procoagulant activity. Released ADP, ATP, and TxA_2 amplify integrin activation on adherent platelets and mediate thrombus growth by activating additional platelets. The forming thrombus is stabilized by signaling through CLEC-2, whose ligand/counter-receptor remains to be identified, and other receptors." (Excerpt from: Stegner and Nieswandt 2011).

Apart from the main platelet receptors discussed above there are a couple of others, which have minor or supportive roles or are relevant in other contexts. Describing their function is beyond the scope of this introduction, for review see e.g. Munnix, Cosemans, et al. 2009; Coller 2011; Stegner and Nieswandt 2011. Table 2 gives an overview of the human platelet receptors known so far (Coller 2011; Stegner and Nieswandt 2011).

Receptor class	Receptors present on human platelets
Integrins	αIIbβ3, αVβ3, α2β1, α5β1, α6β1
Leucine-rich repeat receptors	GPIbα, GPIbβ, GPV, GPIX
Immunoglobulin repeat receptors	PECAM-1, GPVI, FcγRIIA, CLEC-2
Selectins	P-selectin
Tetraspanins	CD9, CD151, TSSC6, CD63, Tspan9

G protein-coupled seven transmembrane receptors	PAR-1, PAR-4, $P2Y_1$, $P2Y_{12}$, thromboxane–prostanoid receptors TPα and TPβ, prostaglandin receptors IP_1 and EP_3, $α_{2A}$-adrenergic receptor, arginine vasopressin receptor V_{1A}, serotonin receptor $5-HT_{2A}$, adenosine receptors A_{2A} and A_{2B}

Table 2: **Known receptors on human platelets** (Coller 2011; Stegner and Nieswandt 2011).

1.3 Platelet exocytosis

1.3.1 SNARE proteins

Regulated exocytosis is a very conserved process. It has been intensely studied especially in the context of neuronal signal transduction. The key proteins and signaling events discovered in neurotransmitter release were found in all secreting hematopoietic cells studied so far (Logan, Odemuyiwa et al. 2003). At the center of the exocytotic process, members of three classes of SNARE proteins bound either to the vesicle membrane (VAMPs) or the outer cell membrane (SNAP-23/-25 and syntaxins) align close to the plasma membrane, overcome the rejection of the two lipid bilayers and mediate fusion between the two. VAMPs and syntaxins contain one coiled-coil domain and SNAP-23/-25 two, all of them are close to the membrane anchor domains of the three protein classes. The coiled-coil domains are called "SNARE motifs" and they can form a very stable four-helix bundle, which brings the opposing membranes in close proximity. In the resting state, another regulatory domain consisting of three parallel α-helices (Habc domain) folds onto the SNARE motif of syntaxin. The Sec-1/Munc18-1 (SM) protein Munc18-1 is believed to bind to this inactive syntaxin conformation and keep it unavailable for contact with the other two SNAREs. Usually, elevated calcium levels trigger release of Munc18-1, opening of syntaxin and SNARE complex formation. Small GTPases from the Rab3 family are also involved in alignment of the three SNAREs. After fusion and release of vesicle content, NSF attachment proteins (SNAPs, no relation to SNAP-23/-25) and *N*-ethylmaleimide senstitive factor (NSF) bind to the SNARE core complex and disassemble it through the ATPase activity of NSF. The components of the exocytotic machinery are recycled and Munc18-1 binds again to inactive syntaxin (Chen and Scheller 2001; Jahn, Lang et al. 2003; Sollner 2003; Hong 2005; Rizo and Rosenmund 2008). Figure 4 illustrates the exocytotic process in the single steps described above (Chen and Scheller 2001).
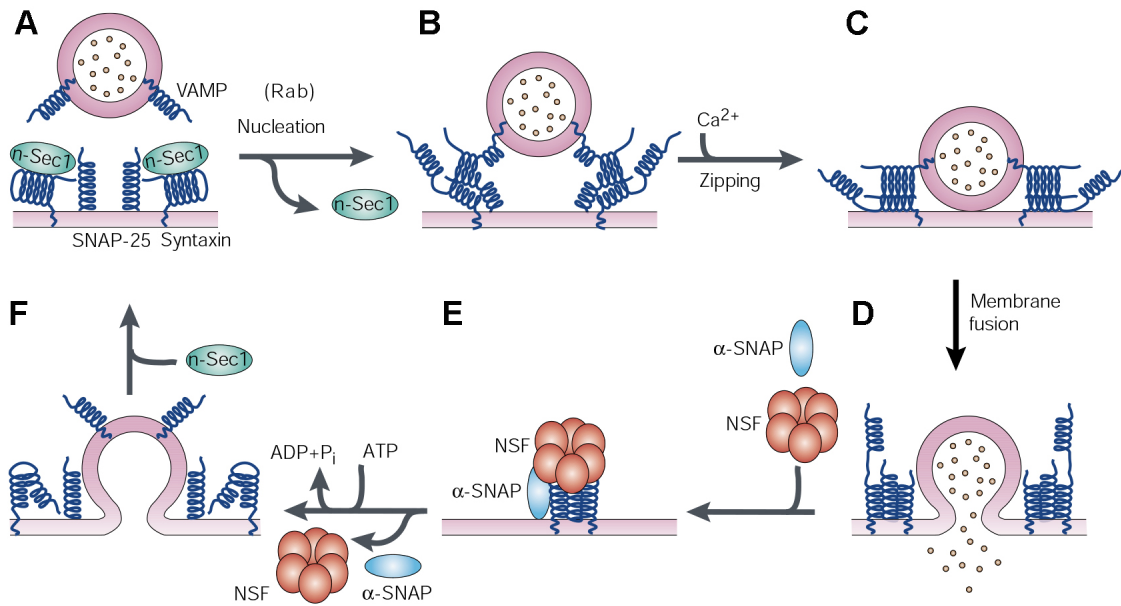
Figure 4: **SNARE-mediated exocytosis and recycling.** (A) VAMP is bound to the vesicle membrane and has one coiled-coil "SNARE motif" reaching out into the cytosol. SNAP-25 (or SNAP-23) and syntaxin are bound to the outer cell membrane an have one and two cytosolic coiled-coil domains, respectively. Munc18-1 (n-Sec1) keeps the two syntaxin coiled-coil domains in an "inactive" state folded onto each other. (B) The signals triggering exocytosis (mostly elevation of intracellular calcium levels) lead to release of Munc18-1 (n-Sec1) and that together with the small GTPase Rab leads to alignment of the SNARE motifs of the three SNARE proteins ("nucleation") and (C) calcium-supported "zippering" from the N-terminal ends of the SNARE motifs to the C-terminal ends. (D) The two membranes fuse with each other and the vesicle content is released. (E) NSF and SNAP are recruited to the SNARE complex and (F) through the ATPase activity of NSF, the SNARE complex is disassembled and recycled. (From: Chen and Scheller 2001).

According to literature, human and mouse platelets contain the following isoforms of the three SNARE protein families: SNAP-23, syntaxin-2, -4, and -7, and VAMP-2, -3, VAMP-7/TI-VAMP, and VAMP-8 with the later being the most abundant (Ren, Ye et al. 2008). SNAP-23 is involved in all exocytotic events in platelets. Syntaxin-2 and -4 are the main syntaxin isoforms contributing to platelet secretion (Flaumenhaft, Rozenvayn et al. 2007), with syntaxin-2 being important for dense granule release (Chen, Bernstein et al. 2000) but functionally overlapping with syntaxin-4 in alpha granule and lysosomal release (Chen, Lemons et al. 2000; Ren, Ye et al. 2008). VAMP-3 and VAMP-8 have been shown to play a role in platelet secretion (Flaumenhaft, Croce et al. 1999; Feng, Crane et al. 2002; Polgar, Chung et al. 2002) but VAMP-3 knockout mice have normal granule release (Schraw, Rutledge et al. 2003), indicating that VAMP-8 can compensate for a loss of VAMP-3.

It is well established that the light chains of botulinum toxins and tetanus toxin can be efficiently applied to interfere with granule secretion in various cell lines in vitro (Schiavo,

Matteoli et al. 2000), a finding, which was also confirmed for isolated, permeabilized platelets (Ren, Barber et al. 2007). Upon entering the hosts' body, *Clostridium* toxins are taken up by nerve endings and lead to shut-down of neuromusculur signal transmission by cleaving specific members of the SNARE protein families and impeding transmitter release. The light chain encodes the zinc metalloproteinase capable of cleaving respective SNARE proteins, thus making them unavailable or even act in a dominant-negative manner for SNARE complex formation. Table 3 shows the *Clostridium* toxins and their target SNARE proteins.

Toxin	Target SNARE protein(s)
TeNT	VAMP-1, -2, -3
BoNT-A	SNAP-25 (not SNAP-23)
BoNT-B	VAMP-1, -2
BoNT-C	Syntaxin-1, -2, -3, SNAP-25 (not SNAP-23)
BoNT-D	VAMP-1, -2
BoNT-E	SNAP-23, -25
BoNT-F	VAMP-1, -2
BoNT-G	VAMP-1, -2

Table 3:   *Clostridium* **toxins and their respective SNARE protein targets.** TeNT, tetanus toxin; BoNT-A to -G, botulinum toxin A to G. (Humeau, Doussau et al. 2000; Schiavo, G., M. Matteoli, et al. 2000; Dolly and Aoki 2006).

1.3.2   Munc13 proteins

Several proteins have been identified, which can influence regulated exocytosis via acting directly or indirectly on SNARE proteins. One of these proteins is the Munc13 protein family, which is exclusively present in the "active zone", the area close to the plasma membrane where readily releasable vesicles are transported and fusion takes place. Munc13 is required in the "docking" and "priming" step of SNARE-mediated exocytosis, meaning the process of bringing the two membranes in close proximity, disassembling syntaxin and Munc18-1 and alignment of the three SNARE proteins. The mechanisms by which Munc13 achieves its effect are still not clear, it is suggested that activated Munc13 might lower the energy barrier for fusion or play a role in release of Munc18-1 from syntaxin (Hong 2005; Basu, Betz et al. 2007). Anyway, deletion of Munc13 usually has severe consequences, e.g. deletion in neurons (Rosenmund, Sigler et al. 2002), chromaffin cells (Ashery, Varoqueaux et al. 2000), cytotoxic T cells (Feldmann, Callebaut et al. 2003) and neutrophils (Brzezinska, Johnson et al. 2008) results in strong reduction of regulated exocytosis of the respective granule cargo. It has been demonstrated that Munc13-4, the ubiquitous isoform present in platelets (Ren, Ye et al. 2008) controls dense granule release in platelets together with Rab27a and b (Shirakawa, Higashi et al. 2004). The Munc13 proteins comprise four family members, Munc13-1 to Munc13-4. While Munc13-1 to Munc13-3 are brain-specific, there are two ubiquitous isoforms, ubMunc13-2, a Munc13-2

variant, and Munc13-4 which is the more prevalent and functionally important isoform in most secretory cell types studied so far (Feldmann, Callebaut et al. 2003; Brzezinska, Johnson et al. 2008; Ren, Ye et al. 2008). The diagram below shows the structure of Munc13 proteins (figure 5). Munc homology domains (MHD) serve as bindind sites to SNAP-23 and -25 (Abdullah, Bundy et al. 2003; Basu, Betz et al. 2007), C1 domain can bind diacylglycerol (DAG) and C2 domains are calcium sensing domains.
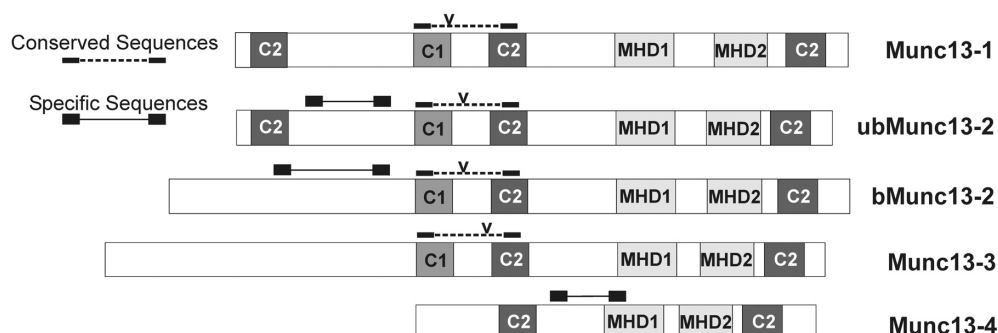
Figure 5: **Schematic representations of the Munc13 isoforms and most of their functional domains.** MHD: Munc homology domain; C1: Diacylglycerol (DAG) binding domain; C2: Calcium sensing domain; ubMunc13-2: ubiquitous Munc13-2 variant; bMunc13-2: brain-specific Munc13-2 variant. (From: Abdullah, Bundy et al. 2003).

The Bruce Beutler laboratory established a mouse line with a functional null-mutant of Munc13-4 (Munc13-4^{Jinx}). The *Jinx* mutation was first identified in a screen of the mouse cytomegalovirus (MCMV) resistome which comprised 3500 G(3) germline mutant mice (Crozat, Georgel et al. 2006). The NK cell phenotype related to the MCMV resistance was described by Crozat et al. in 2007 (Crozat, Hoebe et al. 2007). They mapped the *Jinx* mutation to an intron in the C-terminus of Munc13-4 causing a frame shift and thus a premature stop codon (figure 6 A). They observed no expression of wild-type Munc13-4 mRNA in *Jinx* mice (figure 6 B).

Figure 6: **Location of *Jinx* mutation** in the genomic sequence of the Jinx mutation in the Munc13-4 gene (*Unc13d^{Jinx}*) (A), which causes a premature stop codon in the C-terminal Munc homology domain (MHD). **Effect of the *Jinx* mutation at the mRNA level** (B). KpnI cuts the WT cDNA twice with a 3,467-bp amplification fragment leading to 1,922-, 1,221-, and 324-bp bands. In the *Jinx* mutant, the 53-

bp insertion contains an additional KpnI site, giving 1,922-, 596-, 678-, and 324-bp bands. In the mutant cDNA pool, no WT transcript was detectable. C2, Ca2+-binding domain; MHD, MUNC homology domain; DUF, DUF1041 domain. (From: Crozat, Hoebe et al).

1.4 Platelets and atherosclerosis

1.4.1 Platelet Factor 4

Macrophages play an important role in atherogenesis. They differentiate from blood monocytes, migrate to the subendothelial space and further develop into lipid-enriched foam cells. A critical factor in monocyte differentiation is M-CSF and ApoE-deficient knock-out mice show a reduction in atherosclerotic plaque formation. However, in recent years, evidence is accumulating that Platelet Factor 4 (PF4; CXCL4) secreted by activated platelets and deposited at sites of vascular damage can lead to a specific pro-atherogenic macrophage differentiation profile which is characterized by a loss of the hemoglobin-haptoglobin (Hb-Hp) scavenger receptor CD163 and the consequential inability to express the atheroprotective enzyme heme oxygenase-1 in response to Hb-Hp complexes. Thus, hemoglobin clearance after plaque rupture is impaired and knockout of the PF4 gene in ApoE-deficient mice leads to a reduction in atherogenesis (Gleissner, Shaked et al. 2010). A recent review even suggests to call the characteristic macrophage differentiation upon stimulation with PF4 "M4" because it is clearly distinct from the established macrophage phenotypes (Gleissner 2012) (figure 7).
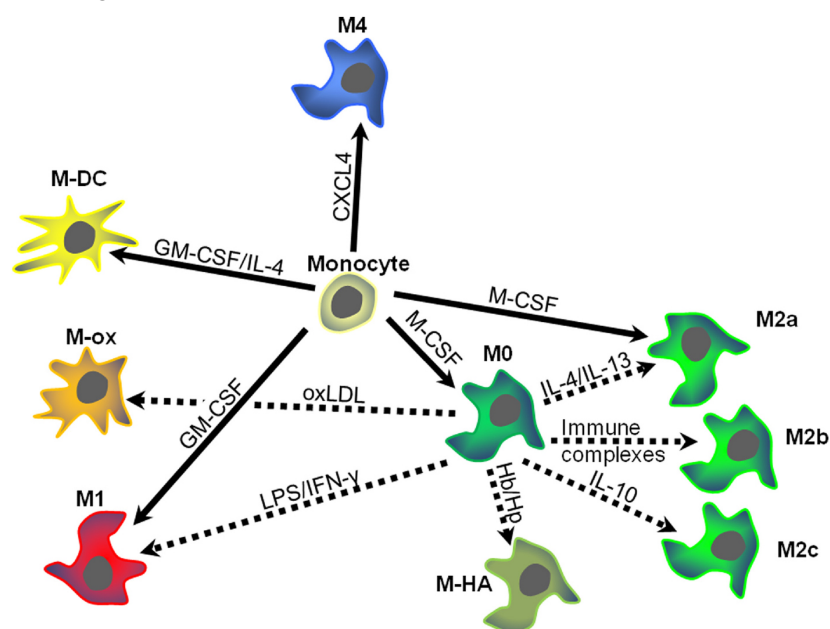
Figure 7: Schematic overview of heterogenic macrophage populations in atherosclerotic plaques. Different growth factors, chemokines or lipoproteins may induce differential development in monocytes entering the plaque micromilieu. "Dotted arrows indicate monocyte-macrophage differentiation, while solid arrows signify macrophage polarization. Arrows are labeled with the key drivers of differentiation or polarization. Colors and distances indicate similarities

and differences between the different macrophage types. M-DC, dendritic cells; M-ox, foam cells induced by oxidized low density lipoprotein (oxLDL); M-HA, hemorrhage-associated macrophages; CXCL4, platelet factor 4; GM-GSC, granulocyte-macrophage colony-stimulating factor; Hb/Hp, hemoglobin-haptoglobin complexes; IFN-γ, interferon-gamma; IL, interleukin; LPS, lipopolysaccharide." (Excerpt from: Gleissner 2012).

PF4, together with another alpha granule protein, RANTES (CCL5), was also shown to enhance T cell effector differentiation (Gerdes, Zhu et al. 2011).

1.4.2 Other pro-inflammatory mediators released from platelets

Platelet CD40 ligand (CD40L) is another molecule released from activated platelets, which has been implicated in atherogenesis. CD40L-deficient platelets show impaired aggregation and thrombus stability. In ApoE-deficient, atherosclerosis-prone mice, injection of CD40L-deficient platelets but not wild-type platelets decreased plaque formation (Lievens, Zernecke et al. 2010). Several molecules released from platelet dense granules have been implicated in inflammation and atherogenesis. Dense-granule-derived polyphosphates have been shown to upregulate bradykinin production, which in turn stimulates the generation of the pro-inflammatory cytokines IL1β and TNFα (Muller, Mutch et al. 2009). The protein 14-3-3ζ was identified in dense granules from human platelets with a proteomics approach and shown to be present in atherosclerotic plaques from patients' samples with aneurysms (Hernandez-Ruiz, Valverde et al. 2007). Serotonin has mitogenic effects on endothelial cells (Pakala, Willerson et al. 1994) and smooth muscle cells (Hodivala-Dilke, McHugh et al. 1999) in vitro and could contribute to the proliferation of these cell types characteristic for atherosclerotic plaque formation in vivo.

1.5 Platelets and Cancer

1.5.1 Historical overview

Armand Trousseau was the first to describe a relation between cancer and platelets as early as 1865 (Armand Trousseau, Phlegmasia alba dolens, in: Clinique Medicale de l'Hotel-Dieu de Paris, Vol 3, 2nd Edition, Ballière, Paris, 1865, pp 654-712). He noted that patients with thromboembolism had an increased risk to host an occult tumor and vice versa, patients with a diagnosed tumor were more likely to develop thrombotic events. Since then, evidence has gathered showing a prominent role of platelets also in the leading cause of cancer-related deaths today, the formation of distant metastases. Gasic et al. reported in 1968 that pharmacologic reduction of platelets in the circulation leads to a reduction of experimental pulmonary metastasis and that this decrease can be restored by infusion of platelets (Gasic, Gasic et al. 1968). Development of depleting antibodies for platelets allowed verifying the observations made by Gasic in an experimental setting where platelets were virtually absent (Pearlstein, Ambrogio et al. 1984). Crissman and

colleagues demonstrated for the first time that platelets are associated with tumor cells shortly after vascular arrest (Crissman, Hatfield et al. 1988), a finding, which was later also reported by other groups (Im, Fu et al. 2004). In the 1990s, it was first shown that platelets bind to tumor cells and protect them against lysis from natural killer (NK) cells (Nieswandt, Hafner et al. 1999). The strong reduction in metastasis in platelet-depleted mice could be repeated with genetic depletion of platelets (Camerer, Qazi et al. 2004). As early as 1973, it was shown that the ability of tumor cells to activate platelets correlates with their metastatic potential (Gasic, Gasic et al. 1973; Pearlstein, Salk et al. 1980) and in 2012, confirmation for a major role of platelet activation in the clinical context was provided by a large post-hoc analysis of cardiovascular outcome trials (Rothwell, Wilson et al. 2012). Rothwell and colleagues found a 15% reduction in cancer-related deaths with intake of daily low-dose aspirin, which inhibits platelet activation, starting 5 years after initiation of therapy.

1.5.2   Platelet effects on primary tumors

Platelets store a multitude of pro-angiogenic factors in alpha granules such as VEGF, PDGF, bFGF (FGF2), EGF, IGF and angiopoietin, and several anti-angiogenic factors such as angiostatin, thrombospondin-1, endostatin, TGFβ and S1P (Jain, Harris et al. 2010; Gay and Felding-Habermann 2011). All of these molecules have been shown to influence tumor angiogenesis (Gay and Felding-Habermann 2011; Claesson-Welsh 2012). Several reports have found differential release of pro- and anti-angiogenic stimuli from platelets in response to certain stimuli (Ma, Perini et al. 2005; Italiano, Richardson et al. 2008; Bambace, Levis et al. 2010; Peterson, Zurakowski et al. 2010; Chatterjee, Huang et al. 2011; Nylander, Osman et al. 2012), which implies that release of these mediators can be tightly controlled as is required in tumor microenvironment (Spano and Zollo 2012). Platelet depletion reportedly leads to hemorrhage in primary tumors (Ho-Tin-Noe, Goerge et al. 2008) and the authors conclude that constant release from platelet granules prevents excessive leakage from newly formed tumor vessels since infusion of resting platelets restored vessel integrity whereas infusion of degranulated platelets did not.

1.5.3   Platelet effects on tumor metastasis

Tumor metastasis is the leading cause of cancer death and is a complex and still incompletely understood process. Tumor cells of the primary tumor need to acquire an invasive phenotype, enter the circulation and withstand shear forces and immune cell attacks before they extravasate in the target organ and grow in the organ parenchyma (Sahai 2007; Joyce and Pollard 2009; Nguyen, Bos et al. 2009; Chaffer and Weinberg 2011).
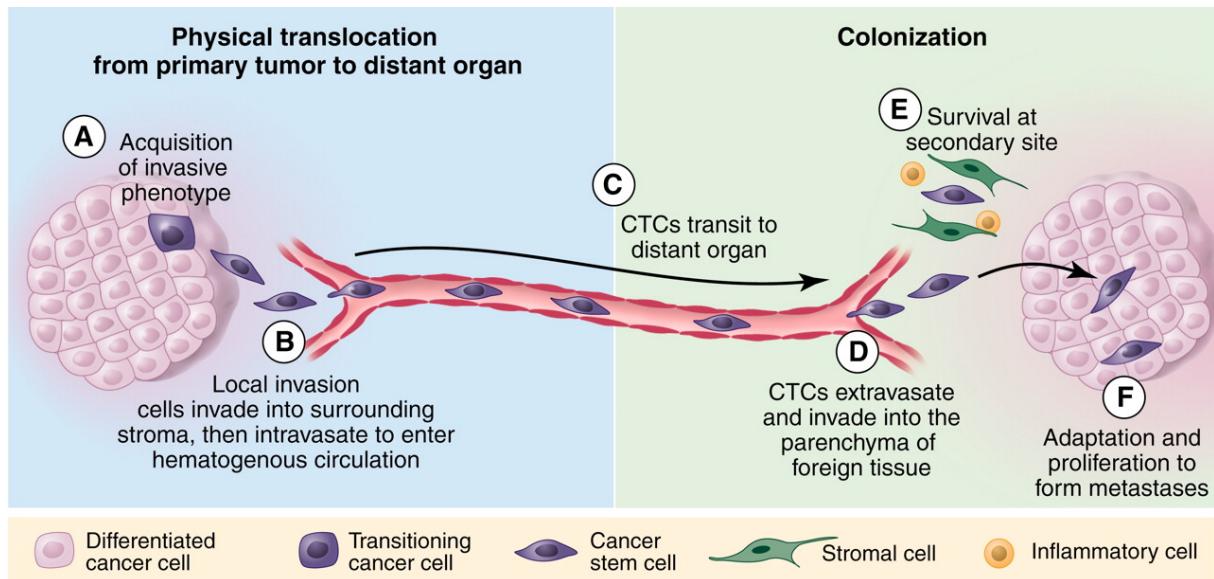
Figure 8: **Overview of the main events involved in formation of metastases from a primary tumor.** Tumor cells need to acquire an invasive phenotype (A), invade the circulation (B), travel to the target organ (C), extravasate (D), survive (E) and proliferate (F) in the organ parenchyma. (From: Chaffer and Weinberg 2011).

As mentioned above, the contribution of platelets to tumor metastasis is well established (Gasic, Gasic et al. 1968; Pearlstein, Ambrogio et al. 1984; Camerer, Qazi et al. 2004). The effects of almost complete absence of platelets due to anti-platelet antibodies or genetic depletion on the number of experimental metastasis are dramatic: a reduction of more than 94% compared to controls was reported (Pearlstein, Ambrogio et al. 1984; Camerer, Qazi et al. 2004; Coupland, Chong et al. 2012). To achieve such a pronounced reduction in metastasis, it is sufficient to deplete platelets at the time of tumor cell injection (Coupland, Chong et al. 2012), indicating that platelets play an important role during vascular arrest and extravasation of tumor cells. Several mechanisms have been proposed how platelets mediate these effects. Platelets were shown to bind to tumor cells and protect them from NK cell lysis in vitro (Nieswandt, Hafner et al. 1999) and in vivo (Palumbo, Talmage et al. 2005; Placke, Kopp et al. 2011). Circulating tumor cells of patients display co-expression of platelet markers (Placke, Orgel et al. 2012). NK cells are the primary immune cells efficiently clearing tumor cells from the circulation (Gorelik, Wiltrout et al. 1982; Hanna 1985). It has been suggested that platelets form a cloak around circulating tumor cells, thereby shielding them against recognition from NK cells (Nieswandt, Hafner et al. 1999) and that releasate from platelets modulates NK cell function, partially by downregulating the NK cell activating receptor NKG2D on NK cells (Placke, Kopp et al. 2010; Placke, Kopp et al. 2011). However, a recent study found no correlation between platelet-mediated and NK cell-mediated effects on tumor cell metastasis (Coupland, Chong et al. 2012).

Several platelet surface receptors have been implicated in tumor metastasis. P-selectin-deficient mice exhibit at strong reduction in experimental metastasis (Kim, Borsig et

al. 1998) and some of the anti-metastatic effects of heparins or related compounds have been ascribed to their inhibitory action on P-selectin (Kim, Borsig et al. 1998; Varki and Varki 2002; Li, Luo et al. 2010; Gong, Mi et al. 2012). However, it is difficult to discriminate between contributions of endothelial versus platelet P-selectin and the importance of P-selectin in metastasis depends on the target organ (Coupland, Chong et al. 2012; Matsui, Amano et al. 2012).

A role for the important platelet surface receptor integrin αIIbβ3 in tumor cell induced platelet aggregation (TCIPA) was first described in 1987 (Bastida, Almirall et al. 1987; Grossi, Fitzgerald et al. 1987; Nierodzik, Klepfish et al. 1995). Integrin αIIbβ3 was shown to bind to integrin αvβ3 on tumor cells expressing this receptor and this interaction lead to increased adhesion of melanoma cells to endothelial cells in vitro (Lonsdorf, Kramer et al. 2012). Blockade of integrin αIIbβ3 with specific antibodies reduced the formation of metastasis in several tumor cell lines (Karpatkin, Pearlstein et al. 1988; Erpenbeck and Schon 2010).

Contradictory results have been obtained for an involvement of GPIbα in platelet-tumor cell interactions, depending on tumor cell line studied and experimental settings (Erpenbeck and Schon 2010). Mice constitutively lacking GPIbα showed a reduction in metastasis (Bergmeier, Rackebrandt et al. 2000), whereas injection of blocking antibodies against GPIbα evoked a dramatic increase in experimental metastasis (Jain, Zuka et al. 2007). Lack of GPIbα leads to defects in platelet and megakaryocyte biogenesis similar to Bernard Soulier syndrome and resulting effects thus exceed the impact of anti-GPIbα antibodies, which could in part explain these differing observations (Erpenbeck and Schon 2010).

Blockade of the major platelet collagen receptor, GPVI, does not influence experimental metastasis (Erpenbeck and Schon 2010).

Figure 9 shows effects of platelet depletion (A), anti-GPIbα antibody (B), anti-integrin αIIbβ3 antibody (C), anti-GPVI antibody (D) and global deletion of P-selectin on B16 melanoma metastasis in the lung (Erpenbeck and Schon 2010).
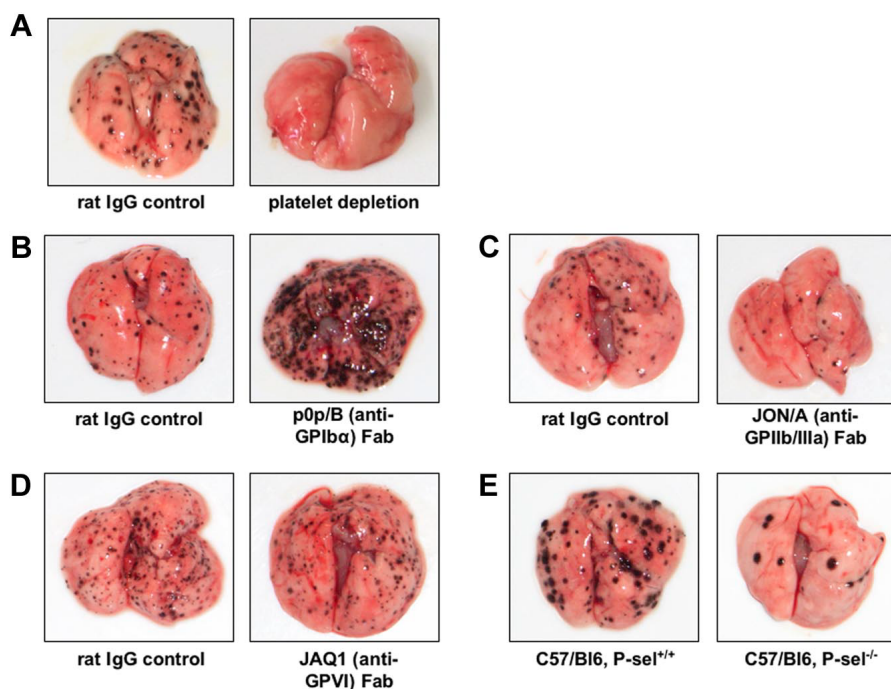
Figure 9: "**Examples for modulation of pulmonary melanoma metastasis through targeted interference with platelet receptors.** In all experiments (performed by L.E. in the laboratory of M.P.S.), C57/BL6 mice were intravenously injected with 2.5 x 10^5 B16F10 melanoma cells, and pulmonary metastasis was evaluated after 10 to 14 days. (A) Antibody-mediated depletion of platelets prevents metastasis formation. (B) Inhibition of platelet GPIbα by function-blocking, monovalent Fab fragments results in a marked increase of pulmonary melanoma metastases. (C) Inhibition of αIIbβ3 by specific Fab fragments decreases the number of metastatic melanoma nodules in the lung. (D) Antibody-mediated blockade of GPVI does not significantly influence pulmonary melanoma metastasis. (E) P-selectin deficiency causes marked reduction of pulmonary melanoma metastasis." (Excerpt from: Erpenbeck and Schon 2010).

The recently discovered platelet receptor CLEC-2 (Suzuki-Inoue, Fuller et al. 2006) has been implicated in interactions with tumor cells expressing podoplanin (Aggrus) on their surface (Suzuki-Inoue 2011) as was found for e.g. B16 melanoma cells (Lowe, Navarro-Nunez et al. 2012). Podoplanin is known to cause platelet aggregation (Lowe, Navarro-Nunez et al. 2012) and there is data suggesting that presence of podoplanin on tumor cells is connected with metastasis and poor clinical outcome (Mishima, Kato et al. 2006; Yuan, Temam et al. 2006).

Thrombin is one of the most important and potent agonists in normal platelet function. Tissue factor exposure on cells together with coagulation factors leads to thrombin generation in the circulation. It has been shown that a number of tumor cells expose tissue factor on their surface and metastatic potential and tumor angiogenesis correlate with tissue factor expression for colorectal and melanoma cell lines (Voigtlander, Rand et al. 2002). In addition, some tumor cells themselves express thrombin receptors on their surface and this also correlates with their metastatic potential (Zigler, M., T. Kamiya et al. 2011). Thrombin-

stimulated tumor cells can bind more efficiently to platelets and endothelial cells and form more pulmonary metastases in a mouse model (Erpenbeck and Schon 2010).

Figure 10 summarizes possible interactions of circulating tumor cells with platelets and other cell types (Gay and Felding-Habermann 2011).
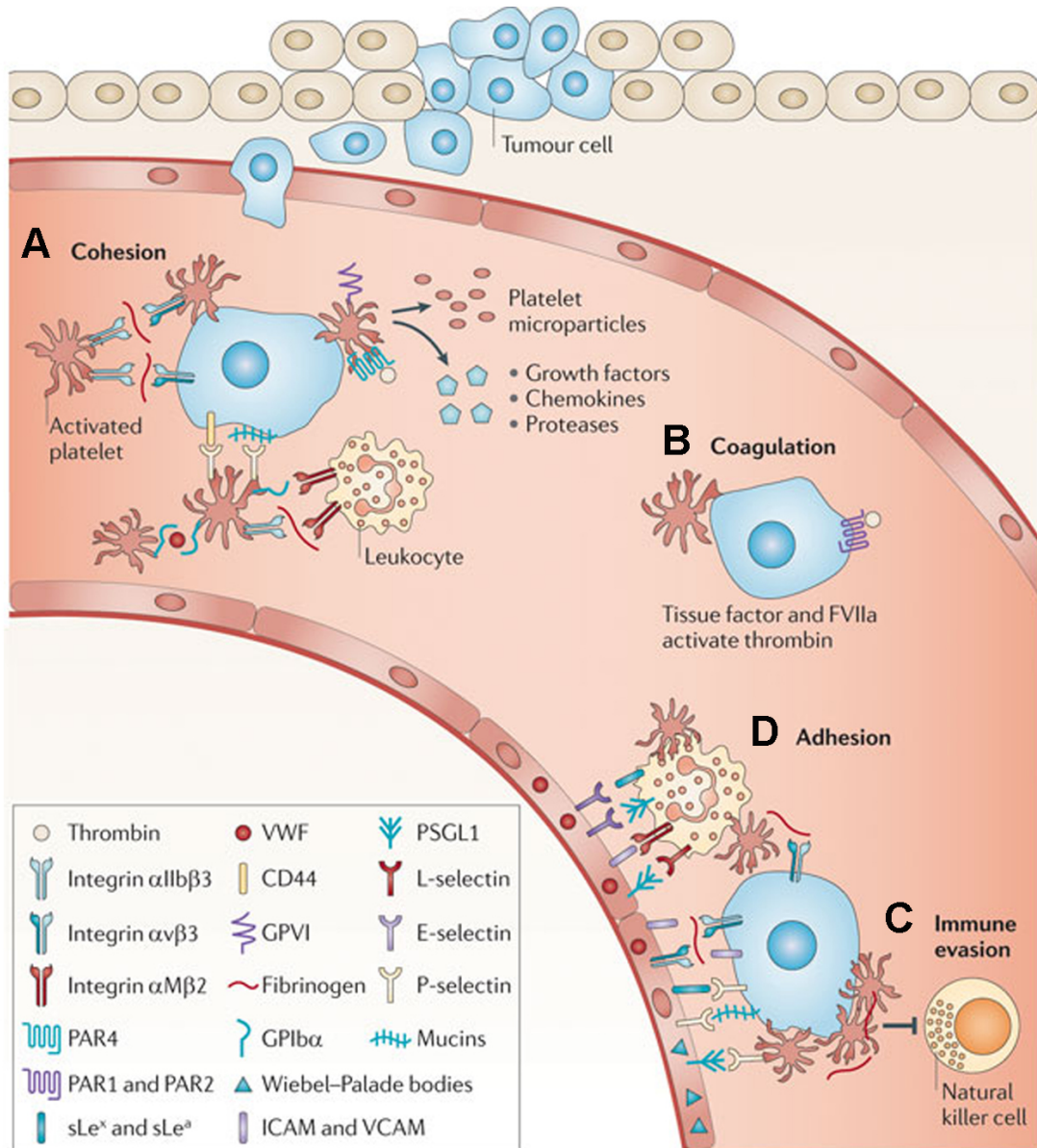
Figure 10: Tumor cell and platelet interactions in the circulation. (A) Upon entering the circulation, tumor cells activate platelets, stimulate platelet secretion and bind platelets to their surface. Interactions with other platelets and potentially leukocytes are enabled through cross-linking with fibrinogen and vWF. (B) Tissue factor exposure on tumor cells together with factor (F) VIIa leads to thrombin generation, which further activates platelets and can also stimulate PAR receptor-expressing tumor cells. (C) Platelet-covered tumor cells are protected against lysis by NK cells during transit. (D) In the microcirculation, platelets bound to tumor cells may brigde interactions with endothelial cells and facilitate vascular arrest. (From: Gay and Felding-Habermann 2011).

2   <u>Aims of this study</u>

Platelets contain a large number of secretable mediators able to influence various pathophysiological processes. Mostly indirect evidence is accumulating that platelets play a role in detrimental diseases like atherosclerosis and cancer. We sought to

- **(I)**   generate and
- **(II)**   describe genetically modified mouse lines with defective platelet secretion but otherwise unaltered morphology and function and
- **(III)**   to study the effects of specific defects in platelet granule secretion in murine models of atherosclerosis and tumor progression.

3 <u>Materials</u>

3.1 Laboratory equipment

Agarose gel electrophoresis equipment	Bio Rad, GE
Analytical balance	Satorius, GE
Apact 4 S Plus aggregometer	Diasys Greiner, GE
Bio Photometer Eppendorf	Eppendorf, GE
Biofuge pico Heraceus	Heraceus, GE
Coombs and chambers for electrophoresis	Workshop University Heidelberg, GE
Cryotome	Leica, GE
DynaMag cell separation magnet	Invitrogen, USA
Eppendorf centrifuge 5417	Eppendorf, GE
Eppendorf centrifuge 5810R	Eppendorf, GE
FACSCalibur flow cytometer	BD Biosciences, GE
FACSCanto flow cytometer	BD Biosciences, GE
Flexstation	Molecular Devices, USA
Flow chamber system	Workshop University Heidelberg, GE
Fluorometer/ Luminometer	Thermo Fisher Scientific, USA
Gel Doc 2000 system	BioRad, GE
Gene Quant pro Photometer	Amersham Bioscience/Biochrom, UK
GenePulser	Bio Rad, GE
Gradient Cycler PTC 200 DNA Engine	Bio Rad, GE
Innova 4300 incubator shaker	New Brunswick Scientific, USA
Leica DFC 280 camera	Leica, GE
Leica DMLS2 microscope	Leica, GE
Leica SP5 confocal microscope	Leica, GE
Lightcycler 480 qPCR cycler	Roche, GE
Magnetic Mini-Stirrer	HANNA, GE
Magnetic mixer	Variomag, GE
Microtome	Leica, GE
Microwave heater	Panasonic, GE
NanoDrop ND1000 Spectrophotometer	Biozym, GE
Neubauer counting chamber	Karl Hecht, GE
Olympus IX81 microscope	Olympus, JP
Owen WTB-Binder incubator plates	Binder, GE

pH 211 Microprocessor pH meter	HANNA, GE
Photospectrometer	Thermo Fisher Scientific, USA
Refrigerators, 4 °C, -20 °C, -80°C	Liebherr Premium, GE
Thermomixer compact Eppendorf	Eppendorf, GE
Two-syringe infusion pump KDS200	KD Scientific, USA
Vortex	A. Hartenstein, GE
Water bath	Eppendorf, GE
Western blot equipment	Bio Rad, GE
Zeiss Axio Observer.Z1	Zeiss, GE

Table 4:   Laboratory equipment used in this study.

3.2   Software

CellQuestPro	BD Bioscience, GE
Blast	NIH, USA
End Note X1	Thomson Reuters
FACSDiva	BD Bioscience, GE
GraphPadPrism 5	GraphPad Software, USA
Image J	NIH, USA
Microsoft Office 2007	Microsoft, USA
ND-1000 V3.1.0	Nanodrop, USA
Adobe Design Suite CS6	Adobe Systems Incorporated, USA
Quantity One	BioRad, GE
Vector NTI 10 advance	Invitrogen, GE

Table 5:   Software used in this study.

3.3   Laboratory supplies

Accucount flurescent particles	Spherotech, USA
Acryl-cuvettes	Sarstedt Nümbrecht, GE
Agar-plates	Brand, GE
Amaxa nucelofector cell electroporator	Lonza, CH
Apact 4 S Plus cuvettes	Diasys Greiner, GE
Bacteria culturing tube, 5 ml	Brand, GE
Beakers	Brand, GE
Capillares 10 µl	Kabe, GE
Cell culture dishes	Greiner Bio One, GE
Cell culture pipettes	BD Bioscience, GE
Cell culture plates	Greiner Bio One, GE
Cell sieve 70 µm	BD Falcon, GE

Cryosection slides	Thermo Fisher Scientific, USA
Dynabeads cell separation beads	Invitrogen, USA
Nunc Maxisorp ELISA plates	Nunc, Thermo Scientific, USA
Eppendorf tubes 0.5 ml, 1.5 ml and 2 ml	Eppendorf, GE
FACS tubes	BD Bioscience, GE
Falcon tubes 15, 50 ml	BD Bioscience, GE
Filter paper	Neolab, GE
Gel casting platform	Bio Rad, GE
Gel combs	Bio Rad, GE
Genepulser cell electroporator	Bio Rad, GE
Gilson pipettes	Gilson, USA
Glass bottles, Kolben	Brand, GE
Glass cylinders	Brand, GE
Microscop coverslip	Hartenstein, GE
Microscope slides	Hartenstein, GE
Needle 27G, 24G	BD Bioscience, GE
Pasteur pipette	Greiner BioOne, GE
PCR wells	Roche, GE
Pipette tips (10 µl, 200 µl, 1000 µl)	Brand, GE
Plastic pipette 5 ml	Greiner BioOne, GE
Scalpel	Dahle, Rödental, GE
Surgical tools	Megro/Ratiomed, GE
Syringe 1 ml	BD Bioscience, GE
Syringe filter, 0.22 µm	Roth, GE
Transwell plate 8 µm pore size	Corning, USA

Table 6:   Laboratory supplies used in this study.

3.4   Chemicals

Agar	AppliChem, GE
Agarose	Invitrogen, GE
Ampicillin sodium salt	AppliChem, GE
ADP	Sigma, GE
Apyrase grade VII	Sigma, GE
ATP	Sigma, GE
ATPγS (adenosine 5'-O-(3-thio)triphosphate)	Jena Bioscience, GE
5-BDBD (5-(3-Bromophenyl)-1,3-dihydro-2H-benzofuro[3,2-e]-1,4-diazepin-2-one)	Tocris, USA
Bromo phenol blue	Sigma, GE
BSA (bovine serum albumin)	Sigma, GE

BSA essentially fatty acid free	Sigma, GE
Calcein AM (Calcein acetoxymethyl ester)	Sigma, GE
Calcium chloride dehydrate ($CaCl_2$ x $3H_2O$)	AppliChem, GE
Carbon dioxide (CO_2)	ZBT, GE
Chloramphenicol	Sigma, GE
Chloroform	Sigma, GE
CRP (collagen-related peptide)	Gift from Bernhard Nieswandt
DAPI (4',6-diamidino-2-phenylindole)	Sigma, GE
dATP	Promega, GE
dCTP	Promega, GE
dGTP	Promega, GE
Di-sodium hydrogenphosphat-2-hydrate	Riedel-de Haën, GE
DNA loading dye 6x	Fermentas, GE
dTTP	Promega, GE
EDTA (ethylendiamine tetraacetic acid)	Roth, GE
Ethanol absolute	ZBT, GE
Ethidium bromide	Merck, GE
Ferric chloride ($FeCl_3$)	Sigma, GE
Fiblillar type I collagen	Nycomed, GE
FITC-dextran 70 kDa	Sigma, GE
FITC-dextran 70 kDa, lysine-fixable	Invitrogen, USA
Fluo-4 AM (2-{[2-(2-{5-[bis(carboxymethyl)amino]-2-methylphenoxy}ethoxy)-4-(2,7-difluoro-6-hydroxy-3-oxo-3H-xanthen-9-yl)phenyl](carboxymethyl)amino}acetic acid acetoxymethyl ester)	Molecular Probes, USA
Flurbiprofen ((±)-2-fluoro-α-methyl-[1,1'-biphenyl]-4-acetic acid)	Cayman Chemical, USA
Glucose D(+)	Merck, GE
Glutaraldehyde solution 25%	Merck, GE
Glycerol 99%	Merck, GE
Glycine	AppliChem, GE
Heparin-sodium	B.Braun Melsungen, GE
HEPES (4-(2-hydroxyethyl)-piperazin-1-ethansulfonicacid)	AppliChem, GE
High Range Latter	Fermentas, GE Hydrogen
Hydrogen chloride (HCl)	AppliChem, GE
Hydrogen peroxide	Sigma, GE
Isoflurane	Abbot Laboratories, USA

Isopropanol 99% (2-propanol)	Roth, GE
Ketamine ((RS)-2-(2-Chlorophenyl)-2-(methylamino)cyclohexanone)	Kepro, NL
L-arabinose	Sigma, GE
Ligation buffer	New England BioLabs, GE
Magnesium chloride hexahydrate	Merck, GE
Mineral oil	Sigma, GE
MRS2500 (1R*,2S*)-4-[2-Iodo-6-(methylamino)-9H-purin-9-yl]-2-(phosphonooxy)bicyclo[3.1.0]hexane-1-methanol dihydrogen phosphate ester tetraammonium salt)	Tocris, USA
Nonidet P-40 (Ethylphenyl-polyethylene glycol)	AppliChem, GE
Oil Red O (1-([4-(Xylylazo)xylyl]azo)-2-naphthol, 1-[2,5-dimethyl-4-(2,5-dimethylphenylazo)phenylazo]-2-naphthol)	Sigma, GE
OPD (1,2-phenylenediamine dihydrochloride) tablet	Dako, DK
Para-formaldehyde	Sigma, GE
Phenol	Roth, GE
Phenol/ chloroform	Roth, GE
Potassium chloride	AppliChem, GE
Rhodocytin	Gift from Bernhard Nieswandt
SDS (sodium dodecyl sulfate)	AppliChem, GE
Sepharose CL4b	Sigma, GE
Smart Ladder marker 200-10 000bp	Eurogentec, GE
Sodium chloride	AppliChem, GE
Sodium hydroxide	Roth, GE
Sodium hydrogencarbonate-monohydrate	Sigma, GE
Sodium-di-hydrogenphosphate-monohydrate	Neolab, GE
Spermidin 100 mM	Sigma, GE
Sucrose	Sigma, GE
Tamoxifen	Sigma, GE
Tetracycline	Sigma, GE
Thrombin from bovine plasma	Sigma, GE
Tris (Trishydroxymethylaminomethan)	AppliChem, GE
Trisodium-salt-dihydrate	Sigma, GE
Trypton	AppliChem, GE
Trypton	Roth, GE
U46619	Cayman Chemical, USA
UTP	Sigma, GE

Xylazine (N-(2,6-dimethylphenyl)-5,6-dihydro-4H-1,3-thiazin-2-amine)	Kepro, NL
Yeast extract	AppliChem, GE

Table 7:   Chemicals used in this study.

3.5   Antibodies

Antigen	Company
Asialo GM1, mouse	Wako, JP
β-actin, mouse	Acris Antibodies, GE
CD3ε, mouse	BD Pharmingen, GE
CD9, mouse	Emfret, GE
CD41, mouse	BD Pharmingen, GE
CLEC-2, mouse	Gift from Bernhard Nieswandt, GE
GPIbα, mouse	Emfret, GE
GPV, mouse	Emfret, GE
GPVI, mouse	Emfret, GE
GPIX, mouse	Emfret, GE
Integrin αIIb, mouse	Emfret, GE
Integrin αIIbβ3, mouse	Emfret, GE
Integrin αIIbβ3 active conformation, mouse	Emfret, GE
Integrin β1, mouse	Emfret, GE
Ly6G, mouse	BD Pharmingen, GE
Ly6G, mouse	Biolegend, USA
Munc13-4, mouse	Santa Cruz, USA
Myc peptide	Novus, USA
NK1.1, mouse	BD Pharmingen, GE
PF4, mouse	R&D Systems, USA
P-selectin, mouse	BD Pharmingen, GE
SNAP-23, mouse	Synaptic Systems, GE
SNAP-25, mouse	Synaptic Systems, GE
Syntaxin-1A, mouse	Synaptic Systems, GE
Syntaxin-1B, mouse	Synaptic Systems, GE
Syntaxin-2, mouse	Synaptic Systems, GE
Syntaxin-3, mouse	Synaptic Systems, GE
Syntaxin-4, mouse	Synaptic Systems, GE
Syntaxin-5, mouse	Synaptic Systems, GE
Syntaxin-5, mouse	Synaptic Systems, GE
Syntaxin-6, mouse	Synaptic Systems, GE
Syntaxin-7, mouse	Synaptic Systems, GE

VAMP-1, mouse	Synaptic Systems, GE
VAMP-2, mouse	Synaptic Systems, GE
VAMP-3, mouse	Synaptic Systems, GE
VAMP-4, mouse	Synaptic Systems, GE
VAMP-5, mouse	Synaptic Systems, GE
VAMP-6, mouse	Synaptic Systems, GE
VAMP-7 (TI-VAMP), mouse	Novus, USA
VE-cadherin (CD144), mouse	BD Pharmingen, GE
vWF, human	Dako, DK
vWF-HRP, human	Dako, DK

Table 8: **Antibodies used in this study.**

3.6 Enzymes

Antarctic phosphatase	New England Biolabs, USA
CIP (Calf intestinal alkaline phosphatase)	New England Biolabs, USA
Dispase	Sigma, GE
Proteinase K	AppliChem, GE
Restriction enzymes	New England Biolabs, USA
RNaseA	New England Biolabs, USA
Taq polymerase	Promega, USA
T4 DNA ligase	New England Biolabs, USA
VentR DNA polymerase	New England Biolabs, USA
vWF-HRP, human	Dako, DK

Table 9: **Enzymes used in this study.**

3.7 Buffers and solutions

Self-made buffers and solutions were prepared in fresh double-distilled and deionised water. Buffers and solutions used during cloning were autoclaved. Concentrations are indicated as final concentrations.

PBS (phosphate buffered saline)	8.0 g/l NaCl, 0.2 g/l KCl, 1.44 g/l Na2HPO4, 0.24 g/l KH2PO4, pH 7,4
10x digestion buffer1/2/3	New England Biolabs, USA
10x Taq-buffer	200 mM Tris-HCL (pH 8.4), 500 mM KCl
Mini/Maxi-preparation-buffers: B1-B3	
B1:	50 mM Tris, 10 mM EDTA, 100 ug/mL RnaseA, pH 8.0 with HCl
B2:	0.2 M NaOH, 1% SDS
B3:	3 M potassium-acetat, pH 5.5 with 100% acetic acid
Eosin solution	Sigma, GE

Haematoxylin solution	Sigma, GE
Injection buffer	10 mM Tris-HCL pH 7.5, 0.1 mM EDTA, 100 mM-NaCl
Kaiser's glycerol gelatine	Merck Millipore, GE
Loading buffer (6x)	0.25 % bromo phenol blue, 0.25% xylene cyanol, 30 % glycerol
OCT (Optimum cutting temperature compound)	Thermo Fisher Scientific, USA
Red blood cell lysis buffer	Sigma, GE
Sterile saline (0.9 % NaCl) solution	B.Braun Melsungen, GE
TAE-buffer	40 mM Tris acetate, 1 mM EDTA, pH 8.0
Tail-buffer	0.1 M EDTA, 0.5 % SDS, 50 mM Tris pH 8, 0.5 mg / ml Proteinase K
TE-buffer	10 mM Tris-HCL, 1 mM EDTA, pH 7.5
Thermo Polymerase buffer	New England Biolabs, USA

Table 10:   Buffers and solutions used in this study.

3.8   Cell culture media & solutions

All self-made culture media were autoclaved before using.

BSA (bovine serum albumin), sterile	Invitrogen, USA
DMEM medium	Invitrogen, USA
DMEM/F12 medium	Invitrogen, USA
EGM2 medium	Lonza, CH
EC growth supplement with heparin	Promocell, USA
FBS (fetal bovine serum)	Invitrogen, USA
Glutamine, sterile	Invitrogen, USA
HBSS (Hank's balanced salt solution)	Invitrogen, USA
LB-medium	5 g/l yeast extract, 10 g/l trypton, 7 g/l NaCl, dissolved in ddH$_2$O
LB-medium for plates	5 g/l yeast extract, 10 g/l trypton, 7 g/l NaCl, 10 g agar per liter LB-medium, dissolved in ddH$_2$O
Non-essential amino acids, sterile	Invitrogen, USA
PBS, sterile	Invitrogen, USA
Penicillin/ streptomycin, sterile	Invitrogen, USA
RPMI medium	Invitrogen, USA
SOB-Mg medium	20 g/l trypton, 5 g/l yeast extract, 10 mM NaCl, 10 mM KCl, dissolved in ddH2O
Trypsin EDTA	Invitrogen, USA

Table 11:   Cell culture media and solutions used in this study.

3.9 Kits

Amaxa cell line nuclofector kit V	Lonza, CH
Celltrace CFSE (Carboxyfluorescein diacetate succinimidyl ester) labeling kit	Invitrogen, USA
Counter-Selection-BAC modification kit	Gene Bridges, GE
Enliten ATP kit	Promega, USA
High pure PCR product purification kit	Roche, GE
Lightcycler 480 probes master	Roche, GE
Mini RNA isolation kit	Qiagen, GE
PF4 ELISA kit	Raybiotech, USA
RNase-free DNase set	Qiagen, GE
Transcriptor high fidelity cDNA synthesis kit	Roche, GE
Universal probe library set, human	Roche, GE
Universal probe library set, mouse	Roche, GE

Table 12:   Kits used in this study.

3.10 Vectors & BAC

706-Flp	Gene Bridges, GE
pBigT	Addgene, USA
pBS(II)KS(+) (pBluescript II KS(+))	Agilent Technologies, USA
phCre2_ERT2	Gift from Günter Schütz
RP24-98A BACs	BAC/PAC Resources, Oakland, USA

Table 13:   Vectors and BAC used in this study.

3.11 Bacterial strain

DH10B: Genotype: *F- mcrA. (mrr-hsdRMS-mcrBC) φ80lacZ.M15 .lacX74recA1 endA1 araD139. (ara, leu)7697 galU galK ë- rpsL nupG*
Invitrogen, USA

3.12 Cell lines

B16F10	ATCC, USA
CF-PAC1	ATCC, USA
HUVEC	Lonza, CH
LLC1	ATCC, USA
MS1 (Mile Sven 1)	Gift from Boris Strilić
SH-SY5Y	ATCC, USA

Table 14:   Cell lines used in this study.

3.13 Mouse strains

C57Bl/6J (referred to as "wild-type mice")	Jackson Laboratory, USA
LDLR KO (B6.129S7-Ldlrtm1Her/J)	Jackson Laboratory, USA
P2Y$_2$ KO (B6.129P2-P2ry2tm1Bhk/J)	Jackson Laboratory, USA
Munc13-4 mutant (Unc13d^{Jinx})	Scripps Research Institute, USA

Table 15:   Mouse strains used in this study.

4 <u>Methods</u>

4.1 Cloning

4.1.1 Cloning of PF4-BAC-toxin constructs

Materials: BAC vector RP24-98A4 containing PF4 gene was from BAC/PAC Resources, Oakland, CA; primers were from Invitrogen; cloning enzymes were from New England Biolabs; pBluescript II KS(+) phagemid vector was from Agilent Technologies; pBigT plasmid carrying the BGH-pA was from Addgene; phCre2_ERT2 plasmid containing the FRT-flanked ampicillin resistance gene was a kind gift from Günter Schütz, DKFZ, Heidelberg; Counter-Selection BAC Modification Kit for E/T cloning was from Gene Bridges; 706-Flp plasmid containing the flippase recombinase gene was from Gene Bridges

The cloning process was similar for the three toxin light chains used in this study (tetanus toxin (TeNT), botulinum toxin C and E (BoNT-C, BoNT-E)). The sequence used for the PF4-TeNT construct corresponds to the original *Clostridium tetani* sequence of the toxin light chain containing the zinc metalloproteinase capable of cleaving certain SNARE proteins but not binding to cell surface receptors and internalization. For both BoNT-E and BoNT-C light chain sequences, Entelechon designed and produced sequences optimized for expression in *Mus musculus*. To engineer the 5' homology arms for E/T cloning, approximately 100-150 basepairs (bp) upstream and downstream sequence of the PF4 gene on BAC vector RP24-98A4 was amplified by PCR and a restriction site was introduced via the 5' primer while the 3' primer carried 8 bases overlapping with the first bases of the respective toxin light chains. Then, 300-800 bp of the 5' end of the toxin light chains were amplified by PCR until a unique restriction site in the toxin and construct was reached at the 3' end. The 5' primer carried eight nucleotides overlapping with the 3' end of the 5' homology arm. Via overlap PCR with the modified 5' homology arms and the modified 5' partial sequence of the respective toxin light chain PCR products as templates and the 5' primer of the 5' homology arm and the 3' primer of the partial toxin sequence as primers, the 5' homology arm and the partial toxin sequence were joined and cloned into the pBluescript II KS(+) (pBSIIKS(+)) phagemid vector which was used as a cloning backbone. The remaining parts of the toxin light chains were cloned into the PBSIIKS+ vector via the unique restriction sites. The BGH-polyA (BGH-pA) tail was excised from the pBigT plasmid and introduced immediately 3' of the toxin. The Ampicillin-resistance cassette was excised from the phCre2_ERT2 plasmid including the FRT-sites flanking the gene and placed behind the 3' end of the BGH-pA. In analogy to the 5' homology arm, the 3' homology arm was produced by amplifying approximately 150 bp of the genomic sequence immediately 3' of the PF4 stop codon with the RP24-98A4 BAC as template. Via the primers, restriction sites were introduced into the PCR products on both ends and these restriction sites were used to clone the 3' homology arms behind the 3' end of the ampicillin-resistance cassette. To replace the PF4 gene in the RP24-98A4 BAC construct

with the final construct assembled in the pBSIIKS(+) cloning vector, E/T cloning was employed. This method is based on recombination of DNA strands carrying homologous sequences mediated by the λ phage-derived proteins Redα and Redβ. Redα is a 5' to 3' exonuclease, which produces 3' single strand DNA overhangs. Redβ binds to 3' overhangs and promotes annealing to homologous DNA. The Counter-Selection BAC Modification E/T cloning kit from Gene Bridges was used for homologous recombination of the toxin constructs into the RP24-98A4 BAC vector and selection of recombined clones was achieved by testing for ampicillin resistance. In a final step, the ampicillin resistance cassette was removed employing the 34 bp FRT sites flanking the cassette, which are recognized by the *Saccharomyces cerevisiae*-derived enzyme flippase encoded in the 706-Flp plasmid used here. The sequence between the FRT sites is excised by the flippase leaving just an eight bp core of each FRT site in the construct. The final BAC construct containing the toxin light chain and the BGH-pA instead of the PF4 gene was verified by PCR with primers binding upstream of the 5' homology arm and in the toxin light chain sequence and a second pair binding inside the BGH-pA and downstream of the 3' homology arm to test for correct location. In addition, the construct was sequenced starting upstream and downstream of the inserted sequence. Restriction digests of the modified RP24-98A4 BAC DNA with three different restriction enzymes was performed yielding specific cleavage patterns of the complete genomic sequence carried by RP24-98A4 BAC. This assures integrity of the complete sequence and would detect multiple insertions of the toxin constructs in unwanted places. The purified BAC construct was linearized and injected into mouse oocytes. Injection into mouse pronuclei was performed at the Interfakultäre Biomedizinische Forschungseinrichtung (IBF) of the University of Heidelberg.

4.1.2 Cloning of PF4-BAC-SNAP-23 constructs

Materials: BAC vector RP24-98A4 containing PF4 gene was from BAC/PAC Resources, Oakland, CA; primers were from Invitrogen; cloning enzymes were from New England Biolabs; pBluescript II KS(+) phagemid vector was from Agilent Technologies; pBigT plasmid carrying the BGH-pA was from Addgene; phCre2_ERT2 plasmid containing the FRT-flanked ampicillin resistance gene was a kind gift from Günter Schütz, DKFZ, Heidelberg; Counter-Selection BAC Modification Kit for E/T cloning was from Gene Bridges; 706-Flp plasmid containing the flippase recombinase gene was from Gene Bridges

Two genetically modified dominant-negative transgenic constructs of the SNAP-23 gene were designed for this study. The first mutant lacked the last eight amino acids (24 bp) of the original SNAP-23 *Mus musculus* sequence and was termed SNAP-23 Δ8. This truncated variant was generated by mRNA isolation from mouse platelets, subsequent cDNA production and amplification of the desired sequence via PCR with primers introducing a short (eight bp) overlapping sequence with the 5' homology arm and a restriction site on the 3' end. The second construct contained three mutations and was termed SNAP-23 Ala as three polar amino acids were replaced by the unipolar alanine. The

first was asparagine to alanine (N to A) at position 53 in the protein sequence (Accession ID BAA20345), the second glutamic acid to alanine at position 150 (E to A) and the third glutamine (Q to A) to alanine at position 157. For higher expression, the first intron of murine IgCμ heavy chain and the third intron of IgCε heavy chain were inserted after position 99 and position 422 in the cDNA sequence (Accession ID AF007169), where intron 3-4 and intron 6-7 are located in the genomic SNAP-23 sequence (accession ID MGI109356). The further cloning procedure was analogous to the PF4-toxin cloning process described above except that a triple myc tag was inserted immediately upstream of the SNAP-23 start codon in both SNAP-23 mutants to enable detection of expression of the transgene. In the final BAC constructs, the PF4 gene in BAC RP24-98A4 was thus replaced by a triple myc tag, the SNAP-23 Δ8 mutant or the SNAP-23 Ala mutant, respectively, and a BGH-pA tail. The purified BAC constructs were linearized and injected into mouse oocytes. Injection into mouse pronuclei was performed at the Interfakultäre Biomedizinische Forschungseinrichtung (IBF) of the University of Heidelberg.

4.2 Platelet-specific methods

4.2.1 Platelet preparation

Materials: All chemicals were from Sigma

Blood was collected from 2-4 mice or healthy volunteers and was anti-coagulated with citrate. Platelet-rich plasma (PRP) was prepared by centrifugation at 150 × g for 7 min. The PRP was centrifuged at 350 × g for 7 min, and the platelet pellet was gently resuspended in HEPES/Tyrode's buffer (TB; 10 mM HEPES/NaOH, pH 7.4, 5.56 mM glucose, 0.3% w/v BSA (essentially fatty acid free), 137 mM NaCl, 12 mM $NaHCO_3$, 2.7 mM KCl, 0.36 mM NaH_2PO_4, 1 mM $MgCl_2$). Platelet concentrations were determined by hemacytometer.

4.2.2 Western blotting

Materials: Antibodies against mouse Syntaxin-1A, Syntaxin-1B, Syntaxin-2, Syntaxin-3, Syntaxin-4, Syntaxin-5, Syntaxin-6, Syntaxin-7, Syntaxin-8, SNAP-23, SNAP-25, VAMP-1, VAMP-2, VAMP-3, VAMP-4, VAMP-5, VAMP-8 were from Synaptic Systems; VAMP-7 (TI-VAMP) was from Novus; anti-Munc13-4 antibody was from Santa Cruz, anti-myc antibody was from Novus; anti-PF4 antibody was from R&D Systems; anti-β-actin antibody was from Acris Antibodies

Washed mouse platelets were centrifuged at 350 x g for 7 min, and the pellet was re-suspended in Laemmli buffer. The samples were lysed at 90°C for 5 min and the lysate of 5×10^6 to 1×10^7 (as a second essay when no signal was detected with the lysate of 5×10^6 platelets at the appropriate size) platelets per lane was separated on a SDS polyacrylamide gel. Munc13-4 levels were detected using a mouse anti-Munc13-4 antibody. An anti-β-actin antibody was used as loading control.

4.2.3 Flow cytometry

Materials: ADP and thrombin were from Sigma; U46619 was from Cayman Chemicals; collagen-related peptide (CRP), rhodocytin and the antibody against CLEC-2 were generous gifts from Dr. Bernhard Nieswandt; antibodies against mouse GPIbα, GPV, GPVI, GPIX, integrin β1, integrin αIIb, integrin αIIbβ3, active integrin αIIbβ3 (JON/A) and CD9 were from Emfret; antibodies against mouse CD41 and P-selectin were from BD Pharmingen

For flow cytometry, washed platelets were adjusted to 1×10^6 platelets/ml with Tyrode's buffer, and 25 µl were stimulated with the indicated agonists (if applicable) for 10 min at 37°C. Samples were then stained with the indicated labeled antibodies for 20 min at room temperature and directly analyzed by flow cytometry (FACSCanto; BD Pharmingen). Platelets were gated by forward/sideward scatter (FSC/SSC) characteristics and identified by anti-CD41 staining.

4.2.4 Aggregometry

Materials: fibrillar type I collagen was from Nycomed; U46619 was from Cayman Chemicals; $CaCl_2$ was from Sigma; cuvettes for Apact 4S Plus aggregometer were from Diasys Greiner

Washed platelet suspensions of the indicated mouse genotypes were adjusted to a concentration of 3×10^8 platelets/ml. Platelet suspensions, stock solution of $CaCl_2$ (40 mM) and aggregometer (Apact 4S Plus; Diasys Greiner) were pre-warmed to 37°C. Agonists were diluted in Tyrode's buffer in 20-fold higher concentrations than the final concentration. 185 µl of platelet suspension was added to a cuvette containing a magnetic stirrer, 5 µl of $CaCl_2$ stock solution was added (1 mM final concentration) and baseline of aggregometer was set. Measurement and stirring was started. 10 µl of agonist was added and the time point noted. Measurement was recorded for 900 s. Values below zero display platelet shape change after addition of agonist, values above zero mark platelet aggregation in percent relative to the baseline set at the beginning. Before starting a new assay, platelets were tested for pre-activation by running a sample without agonist. The corresponding platelet suspension was used in further experiments if the aggregation curve stayed stable in the range of approximately -2% to +2% around baseline for at least 300 s.

4.2.5 Platelet count

Materials: EDTA was from Sigma; Accucount fluorescent particles were from Spherotech; anti-CD41 antibody was from BD Pharmingen

100 µl of blood per mouse was taken in EDTA (5 mM final concentration), and a defined concentration of fluorescent particles was added. Platelets were stained with a FITC-labeled antibody against CD41 for 30 min at RT. Using flow cytometry, platelets were counted as CD41 positive events relative to the number of fluorescent particles.

4.2.6   PF4 release

Materials: Mouse PF4 ELISA kit was from Raybiotech, thrombin was from Sigma

10 µl aliquots of supernatant from platelets (1 x 10^8/ml) treated with agonist or tumor cells (1 x 10^6/ml) were assayed in triplicates in a standard mouse PF4 ELISA Kit according to manufacturer's instructions. Absorption at 450 nm was measured in a spectrophotometer (Thermo Scientific). Level of PF4 in the samples was calculated by comparison with a PF4 standard dilution series.

4.2.7   vWF release

Materials: ELISA plate was from Nunc; anti-vWF antibodies and OPD tablets were from Dako; H_2O_2 and chemicals for buffer preparation were from Sigma

50 µl aliquots of supernatant from platelets (1 x 10^8/ml) treated with agonist or tumor cells (1 x 10^6/ml) were assayed in triplicates in an ELISA plate coated with a human vWF capturing antibody. The samples were analyzed with a secondary HRP-labeled vWF antibody and substrate solution containing OPD tablets and H_2O_2 according to Dako's general ELISA procedure. Absorption at 490 nm was measured in a spectrophotometer (Thermo Scientific). Levels of vWF in the samples were calculated compared to a vWF standard dilution series.

4.2.8   ATP release

Materials: Enliten ATP kit was from Promega; thrombin was from Sigma; U46619 was from Cayman Chemical; fibrillar type I collagen was from Nycomed

ATP secretion by platelets was determined using a luciferin/luciferase ATP kit. For this purpose, 10 µl aliquots of supernatant from platelets (1 x 10^8/ml) treated with agonist or 1 x 10^6 tumor cells/ml were mixed with 100 µl of ATP reagent, and light emission was measured using a luminometer (Thermo Scientific). Raw data were collected as relative light units integrated over 0.1 s and calibrated using an ATP standard.

4.2.9   Flow chamber

Materials: Heparin-natrium was from B.Braun Melsungen; fibrillar type I collagen was from Nycomed; BSA was from Sigma

Heparinized blood (final concentration 5 U/ml) of wild-type and Munc13-4-deficient mice was mixed 1:1 with Tyrode's buffer and was applied to a flow chamber set-up containing collagen-coated coverslips. Before the experiment, coverslips were blocked in 5% BSA (essentially fatty acid free) for 2 hours at RT, fixed to the flow chamber and rinsed with Tyrode's buffer supplemented with heparin (5 U/ml). The transparent flow chamber had a slit depth of 50 µm and was connected to a syringe filled with the diluted blood samples. Perfusion was carried out at room temperature using a pulse-free pump with a wall shear

rate of 1000 s^{-1}. Perfusion was stopped after 5 min and chambers were rinsed with Tyrode's buffer for 2 min. Coverslips were analyzed by taking 5 randomly chosen brightfield images per coverslip on a stereomicroscope (Zeiss Axio Observer Z.1) and measuring the plaque-covered area with ImageJ (NIH).

4.2.10 Adhesion to Collagen

Materials: Heparin-natrium was from B.Braun Melsungen; fibrillar type I collagen was from Nycomed; BSA was from Sigma

The adhesion assay with collagen was performed similar to the flow chamber experiments with some modifications. Briefly, washed platelets (1 x 10^8/ml) of wild-type and Munc13-4-deficient mice were applied to the flow chamber set-up instead of whole blood samples, transported into the flow chamber containing the collagen-coated coverslip with a low shear rate (100 s^{-1}) and let to adhere to the collagen fibers for 10 min. After that, coverslips were rinsed with Tyrode's buffer for 2 min and analyzed as described above.

4.2.11 Interaction of tumor cells with CFSE-labeled platelets

Materials: Carboxyfluorescein diacetate succinimidyl ester (CFSE) CellTrace was from Invitrogen

Isolated mouse platelets (1 x 10^8/ml) were stained with CFSE for 30 min and washed in Tyrode's buffer. B16 tumor cells resuspended in TB (1 x 10^6/ml) were mixed 1:1 with platelets and incubated for 30 min on a shaker at 37°C and 200 rpm. Platelet-tumor cell suspensions were analyzed in triplicates by flow cytometry (FACSCanto; BD Pharmingen). Mean fluorescence intensities of tumor cells were identified by for-ward/sideward scatter (FSC/SSC) in the FITC channel.

4.3   Cell culture methods

4.3.1   Cell culture

Materials: Medium and additives were from Invitrogen; B16F10, LLC1, SH-SY5Y, CF-PAC1 cell lines were from ATCC, HUVEC were from Lonza

All cells were incubated at 37°C and 5% CO$_2$. Human umbilical vein endothelial cells (HUVECs) were grown in EGM2 medium and passages below passage six were used for all experiments. All other cell lines were cultured in the presence of 10% FBS and penicillin/streptomycin each at 100 units/ml in RPMI (B16F10 melanoma cells), DMEM and 2 mM glutamine (Lewis lung carcinoma 1 (LLC1) and Mile Sven 1 (MS1) endothelial cells), DMEM, 2 mM glutamine and 100 µM non-essential amino acids (SH-SY5Y neuroblastoma and CF-PAC1 adenocarcinoma cells).

4.3.2 Transswell transmigration assay

Materials: Transswell plates were from Corning; transfection kit was from Amaxa; siRNA was from Quiagen; 5-BDBD and MRS2500 were from Tocris; calcein-AM and apyrase grade VII were from Sigma; flurbiprofen was from Cayman Chemical; adenosine 5'-O-(3-thio)triphosphate (ATPγS) was from Jena Bioscience

MS1 cells (8×10^3 at seeding in 50 µl) or HUVEC (6×10^3 at seeding in 50 µl) were cultured for 2 days on 96-transwell plates with polyester membranes of 8-µm pore size with medium changes every day. For knockdown experiments, 4×10^5 MS1 cells were transfected using Nucleofector Kit V with different sets of siRNA against the P2Y$_2$ receptor and 1.2×10^4 cells in 50 µl were seeded to the upper compartment. Where indicated, MS1 cells were pre-incubated with 5-BDBD (1 µM) or MRS2500 (100 nM) for 30 min. Before the experiment, exemplary wells of each condition were visually checked by calcein-AM staining of the endothelial monolayer and only plates with 100% confluency were used. For transmigration, the medium from the upper compartment was removed and 50 µl of a 1:1 mixture of platelets (2×10^8/ml) with calcein-AM-labeled tumor cells (8×10^5/ml) in TB was added to the upper com-partment alone or with flurbiprofen (100 nM) or apyrase (20 U/ml). ATPγS (10 µM) was added in the absence of platelets. For supernatant experiments, human platelets (5×10^7/ml) or mouse platelets (2×10^8/ml) were incubated for 30 min at 37°C alone or with tumor cells (1.6×10^6/ml) and centrifuged at 350 x *g* for 10 min. The supernatant was mixed 1:1 with Tyrode's buffer (for MS1 cells) or cell culture medium (for HUVECs) containing calcein-AM-labeled tumor cells (8×10^5/ml) and 50 µl were added to the upper compartment. In all experiments, 250 µl TB or culture medium were added to the lower compartment, and tumor cells were allowed to transmigrate over night. On the next day, the non-transmigrated tumor cells from the upper compartment were removed and only the transmigrated tumor cells on the lower side of the filter or the bottom of the transwell were imaged (Zeiss Axio Observer.Z1 and Olympus IX81) and quantified with ImageJ (NIH). Each experiment was performed at least 3 times with a minimum of 5 wells per experiment.

4.3.3 Endothelial barrier function

Materials: Transswell plates were from Corning; FITC-dextran 70 kDa (FITC-DX) and apyrase grade VII were from Sigma

The permeability assay was performed as described for the transwell assay with some modifications. Briefly, MS1 cells were cultured on transwell filters and the supernatant of platelets alone or platelets stimulated with tumor cells was mixed 1:1 with Tyrode's buffer containing 2 mg/ml 70 kDa FITC-DX of which 50 µl were added to the upper compartment in the absence or presence of apyrase (20 U/ml). 250 µl Tyrode's buffer were added to the lower compartment. After 90 min, the amount of passed FITC-DX to the lower compartment was measured (FlexStation3, Molecular Devices). For visualization of changes in the

endothelial barrier, MS1 cells were stimulated for 1 h with supernatants from tumor cells alone or from tumor cells after stimulation with platelets in the absence or presence of apyrase (20 U/ml). Cells were further processed for staining and imaging.

4.3.4 Immunostaining and Imaging

Materials: Para-formaldehyde, sucrose and DAPI were from Sigma; OCT was from Thermo Fisher Scientific; anti-VE-Cadherin antibody was from BD Pharmingen; Alexa Fluor (AF) 594-conjugated secondary antibody and AF488-conjugated phalloidin were from Molecular Probes; Cy5-conjugated secondary antibody was from Dianova

Cells or tissues were fixed with 4% para-formaldehyde. Tissues were further cryopreserved in 30% sucrose, embedded in OCT, and cryosectioned at 16 µm. Cells or sections were stained with rat anti-VE-Cadherin and Alexa Fluor (AF) 594- or Cy5-conjugated secondary antibodies. DAPI was used to stain cell nuclei, and AF488-conjugated phalloidin to stain F-actin. Images were acquired using a Leica SP5 confocal microscope and analyzed using ImageJ (NIH).

4.3.5 mRNA expression analysis by qPCR

Materials: Dispase was from Sigma; PBS, BSA, FBS magnetic beads and magnet, DMEM/F12 medium, penicillin/streptomycin were from Invitrogen; anti-CD144 antibody was from BD Pharmingen; EC growth supplement with heparin was from PromoCell; Mini RNA isolation kit was from Qiagen; Transcriptor High Fidelity cDNA Synthesis kit, Master mix and probes for qPCR using Universal Probe Library System were from Roche

For isolation of mouse primary pulmonary endothelial cells, lungs were minced and digested in 50 U/ml dispase for 1 h at 37°C with shaking (350 rpm). After filtration, the cells were washed in PBS containing 0.5% BSA. Cells were incubated with anti-CD144 antibody-coated magnetic beads for 1 h at room temperature, washed, and isolated with a magnet (Invitrogen). Cells were grown in DMEM/F12 supplemented with 10% FBS, penicillin/ streptomycin, and EC growth supplement with heparin on fibronectin-coated wells. Cells were harvested, and RNA was isolated with a standard RNA isolation kit according to manufacturer's instructions. RNA was transcribed using a kit and quantitative PCR was performed employing the Universal Probe Library System on a Lightcycler 480 instrument (Roche). Primers were designed with the online tool provided by Roche. For each gene, at least the two top result primers were tested and the pair with the higher efficiency and reproducibility was used for quantification. Relative expression levels for mouse and human genes were obtained by normalizing with 18S rRNA and H3F3A or 18S rRNA and GAPDH values, respectively. Sequences for forward (Fw) and Reverse (Rev) primers of mouse and human receptors are depicted from 5' to 3' end. Primers for mouse P2Y receptors are displayed in table 16.

Gene name	Primer orientation	Sequence	Probe number
P2Y1	Fw	CTGTGTGGACCCCATTCTTT	19
	Rev	TCGGGACAGTCTCCTTCTGA	19
P2Y2	Fw	TGGTACTGGCCGTCTTCG	4
	Rev	AG-TAGAGGGTGCGCGTGA	4
P2Y4	Fw	CGGCGACTGTATCGACCT	17
	Rev	GAGAGAACGGAGCCGAGAA	17
P2Y6	Fw	GCAGTCTTTGCTGCCACA	42
	Rev	GTGGGCTCAGGTCGTAGC	42
P2Y12	Fw	TGCTGTACACCGTCCTGTTC	107
	Rev	AAATCCTCATTGCCAAGCTG	107
P2Y13	Fw	ATGTGTGAGATGGGGAAAGG	18
	Rev	CTGACTACTGTGGTGGTCTTCG	18
P2Y14	Fw	TCTTAGAAGACACCCAGTCTTTCC	69
	Rev	AAATAGATACGAGTGTTGCTTGGA	69

Table 16: **Primer sequences for mouse P2Y receptors** from 5' to 3' end used for qPCR and designed with the Assay Design Center online tool provided by Roche (http://www.roche-applied-science.com/sis/rtpcr/upl/index.jsp?id=UP030000, November 1st, 2012)

Primer sequences for mouse P2X primers are shown in table 17.

Gene name	Primer orientation	Sequence	Probe number
P2X1	Fw	TGTAAGCCCCTGTCCCATC	19
	Rev	TCCTGCAGAGGACATGTGG	19
P2X2	Fw	GCTCCAGCTCTGCTCTGACT	77
	Rev	TTTGTCCCATATGCTGGTCA	77
P2X3	Fw	TTTCATCAACCTCCCCTCTG	100
	Rev	GACAGTACCCCATCACCCATA	100
P2X4	Fw	AGAGGAATATCCTCCCCAACAT	10
	Rev	GCGCATTATAAATGCACGAC	10
P2X5	Fw	CACAGTCATCAACATTGGTTCC	45
	Rev	AGGTAGATAAGTACCAGGTCACAGAAG	45
P2X6	Fw	AGCTGCGGCTAAAGTTGC	18
	Rev	GGCTGCAGAAGCCATGTT	18
P2X7	Fw	CAGTCACTGGAGGAACTGGAA	17
	Rev	CCAAAGGAAACACACCGATT	17

Table 17: **Primer sequences for mouse P2X receptors** from 5' to 3' end used for qPCR and designed with the Assay Design Center online tool provided by Roche (http://www.roche-applied-science.com/sis/rtpcr/upl/index.jsp?id=UP030000, November 1st, 2012).

Primers for mouse housekeeping genes are shown in table 18.

Gene name	Primer orientation	Sequence	Probe number
18S rRNA	Fw	GCAATTATTCCCCATGAACG	48
	Rev	GGGACTTAATCAACGCAAGC	48
H3F3A	Fw	AGGCAAGTGAGGCCTACCA	56
	Rev	TAAGCACGTTCTCCGCGTAT	56

Table 18: **Primer sequences for mouse housekeeping genes** from 5' to 3' end used for qPCR and designed with the Assay Design Center online tool provided by Roche (http://www.roche-applied-science.com/sis/rtpcr/upl/index.jsp?id=UP030000, November 1st, 2012).

Primers for human P2Y receptors are displayed in table 19.

Gene name	Primer orientation	Sequence	Probe number
P2Y1	Fw	ATGTTCTGTGTCCCCTTGGT	26
	Rev	AAATCAAAGCTCTCACAATTAATCC	26
P2Y2	Fw	TAACCTGCCAC-GACACCTC	41
	Rev	CTGAGCTGTAGGCCACGAA	41
P2Y4	Fw	CATCACCCGCACCATTTACT	64
	Rev	TTCAGTACTCGGCAGTCAGC	64
P2Y6	Fw	CTGCCCACAGCCATCTTC	42
	Rev	GCTGAGGTCATAGCAGACAGTG	42
P2Y11	Fw	GTTGGTGGCCAGTGGTGT	17
	Rev	CCGCATGATGTGGTAGGG	17
P2Y12	Fw	CATGATTCTGACTTTTCCATTCA	48
	Rev	TGACACACAAAAGTTCTCAGTGG	48
P2Y13	Fw	TTTCTTGACCGGCATCC	21
	Rev	AGCTGGGGATGTGAACAAAC	21
P2Y14	Fw	CTTGCGGTATATGAAAGAATTCAC	82
	Rev	AAGAAATAAATAATAGGGTCCAAGCA	82

Table 19: **Primer sequences for human P2Y receptors** from 5' to 3' end used for qPCR and designed with the Assay Design Center online tool provided by Roche

(http://www.roche-applied-science.com/sis/rtpcr/upl/index.jsp?id=UP030000, November 1st, 2012).

Primer sequences for human P2X primers are shown in table 20.

Gene name	Primer orientation	Sequence	Probe number
P2X1	Fw	TCCCCAGGAAGTCTCCTACC	13
	Rev	CCCTGAGCTTCTGGCAAAC	13
P2X2	Fw	CAAGGTGATCGTGGTGAGG	15
	Rev	CGATGAATACGTACCACACGAA	15
P2X3	Fw	CTTGCACGAGAAGGCTTACC	76
	Rev	CTTGGTTACCACCGAGGACT	76
P2X4	Fw	TGGGACCCAGACCGACTA	66
	Rev	GGCGTGTCGTACTCGAACA	66
P2X5	Fw	GTCAGAAGGGGAACGGATCT	17
	Rev	AATTCACGTGCTCCTGTGG	17
P2X6	Fw	TCCCTGCTGGTTGAGAAGAG	23
	Rev	GCCTCATCCTTGCTTTCG	23
P2X7	Fw	ATGTCAAGGGCCAAGAAGTC	64
	Rev	AGGAATCGGGGGTGTGTC	64

Table 20: **Primer sequences for mouse P2X receptors** from 5' to 3' end used for qPCR and designed with the Assay Design Center online tool provided by Roche (http://www.roche-applied-science.com/sis/rtpcr/upl/index.jsp?id=UP030000, November 1st, 2012).

Primers for human housekeeping genes are shown in table 21.

Gene name	Primer orientation	Sequence	Probe number
18S rRNA	Fw	GCAATTATTCCCCATGAACG	48
	Rev	GGGACTTAATCAACGCAAGC	48
GAPDH	Fw	GCATCCTGGGCTACACTGA	82
	Rev	CCAGCGTCAAAGGTGGAG	82

Table 21: **Primer sequences for human housekeeping genes** from 5' to 3' end used for qPCR and designed with the Assay Design Center online tool provided by Roche (http://www.roche-applied-science.com/sis/rtpcr/upl/index.jsp?id=UP030000, November 1st, 2012).

4.3.6 Calcium mobilization assay

Materials: Fluo-4 AM was from Molecular Probes; Hanks balanced salt solution (HBSS) was from Invitrogen, UTP was from Sigma

Changes in intracellular Ca^{2+} concentration were measured with the calcium sensitive dye Fluo-4. Briefly, upon knockdown, MS1 cells were incubated with 4 µM Fluo-4 at 37°C for 30 min in Hanks balanced salt solution (HBSS) containing 1 mM $CaCl_2$ and then washed 2 times with HBSS. Samples were analyzed for 20 sec to establish a base line and then stimulated with 10 µM UTP. Changes in fluorescence emission were measured using a plate reader (FlexStation3, Molecular Devices).

4.4 In vivo experiments

4.4.1 Genetic mouse models

Control C57BL/6J animals, LDL receptor-deficient mice (B6.129S7-Ldlrtm1Her/J) and P2Y2-deficient mice (B6.129P2-P2ry2tm1Bhk/J) were obtained from The Jackson Laboratory (Bar Harbor, ME). The Munc13-4 mutant mouse line (Unc13d^{Jinx}) was kindly provided by Bruce Beutler (Department of Genetics, The Scripps Research Institute, La Jolla, USA). All experimental animal procedures were approved by the Regierungspräsidien Darmstadt and Karlsruhe.

4.4.2 Tail bleeding time

Materials: Isoflurane was from Abbott Laboratories; NaCl was from Sigma

Age-matched wild-type and Munc13-4 mice were kept under isoflurane anesthesia throughout the experiment. 15 ml falcon tubes were filled with sterile 0.9% NaCl solution and pre-warmed to 37°C. a sterile scalpel was used to cut 2 mm off the end of the tail and the tail was immediately immersed into the saline-filled falcon tube. Blood flow and time after tail cut were monitored and bleeding was counted as terminated if blood flow stopped longer than 30 s. To avoid critical loss of blood, the experiment was terminated after 20 min if blood flow had not stopped until that time.

4.4.3 FeCl$_3$ thrombosis model

Materials: Xylazine and ketamine were from Kepro; 0.9% sterile NaCl solution was from B.Braun Melsungen, FeCl$_3$ was from Sigma

21 days old wild-type and Munc13-4 mice were anesthetized with xylazine (6 mg/kg bodyweight) and ketamine (100 mg/kg bodyweight). The heatable stage of an inverse microscope (Zeiss Axio Observer.Z1) and 0.9% sterile saline solution were pre-heated to 37°C. Through a lateral abdominal incision, the small intestine was carefully pulled out with saline-soaked cotton buds. A jejunal artery was arranged on the microscopic stage in a way that blood flow could be monitored. A filter paper with a width of 1 mm was soaked in 10%

FeCl$_3$ solution and applied on a fat-free part of the artery for 30 s. After removal of the filter paper, the time to complete occlusion of the vessel was measured. A vessel was considered completely occluded if no fluid movement was observed for 1 min. The experiment was terminated by killing the animal after 60 min if the artery was not occluded until that time. Only one artery was used per animal.

4.4.4 Atherosclerosis model

Materials: High fat (21%), high cholesterol (1.5%) diet was from Sniff Spezialdiäten GmbH; para-formaldehyde, sucrose, EDTA, isopropanol and Oil Red O were from Sigma; xylazine and ketamine were from Kepro; Kaiser's glycerol gelatine was from Merck Millipore

12 weeks old male LDL receptor knockout mice were lethally irradiated with 9.5 Gray and transplanted with 5 x 10^6 bone marrow cells each derived from the femur and ossa cruris of age-matched male wild-type and Munc13-4-deficient mice. Control mice receiving only irradiation and no bone marrow transplantation died within 10 days after irradiation. Mice were let to recover on normal chow for four weeks. After this time, mice were fed a high fat (21%), high cholesterol (1.5%) diet for 16 weeks with weekly monitoring of bodyweight. Mice were anesthetized with xylazine (6 mg/kg bodyweight) and ketamine (100 mg/kg bodyweight) and perfused with PBS and 4% para-formaldehyde. The aorta was excised from ascending aorta to bifurcation and immersed overnight in a solution containing 4% para-formaldehyde, 5% sucrose and 20 mM EDTA in PBS. The next day, fat and adventitia were carefully removed from the vessel and the aortas were opened with one longitudinal cut through the whole aortic segment. Aortas were rinsed with 60% isopropanol for 2 min and stained for 15 min in a 0.3 % Oil Red O (w/v) solution in 60% isopropanol. Afterwards, aortas were rinsed with 60% isopropanol for 10 min. Isopropanol was removed and replaced by PBS and aortas were mounted with Kaiser's glycerol gelatin. Oil Red O-stained lipid-containing plaque areas were measured as percent relative to total aortic area with ImageJ (NIH).

4.4.5 Tumor models

Materials: B16F10 and LLC1 cell lines were from ATCC; PBS was from Invitrogen; isoflurane was from Abbott Laboratories, para-formaldehyde, haematoxylin and eosin solutions were from Sigma

B16F10 melanoma cells or LLC1 cells were harvested and resuspended in PBS. Mice (at 8-10 weeks of age) were anesthetized with isoflurane and 1 x 10^6 B16 or LLC1 cells in 100 µl PBS were were injected subcutaneously to their flanks. Mice with B16 primary tumor were sacrificed 19 days and mice with LLC1 tumor 21 days after injection of tumor cells, and primary tumors as well as lung metastases were analyzed. Alternatively, 125 µl of a tumor cell (5 x 10^4 cells) suspension was injected to the lateral tail vein of mice, and lung metastases were analyzed 12 days later. Animals were perfused with PBS and para-

formaldehyde. Primary tumors were removed and weighed. For analysis of pulmonary metastases, the lungs were removed and fixed in para-formaldehyde. Lungs were then cut in 5 μm sections and one section every 200 μm throughout the whole lung was screened histologically, the number of metastases was counted and assigned to the respective size category: small (diameter: <0.1 mm), medium (diameter: 0.1-1.0 mm) or large (diameter: >1.0 mm).

4.4.6   Analysis of endothelial barrier function in vivo

Materials: B16F10 cell line was from ATCC; sterile saline was from B.Braun Melsungen; isoflurane was from Abbott Laboratories; fixable FITC-dextran 70 kDa and PBS were from Invitrogen; para-formaldehyde, haematoxylin and eosin solution and sucrose were from Sigma

Mice were anesthetized using isoflurane and 100 μl of fixable FITC-dextran with a molecular weight of 70 kDa) in 0.9% saline was injected retroorbitally at a concentration of 15 mg/kg. One min later, 1×10^5 B16 tumor cells in 125 μl PBS were injected via the lateral tail vein. After 3 hours, animals were sacrificed, and lungs were carefully excised. Lungs were fixed in para-formaldehyde, cryo-preserved in 30% sucrose and further processed for immunostaining and imaging.

4.4.7   NK cell depletion

Materials: anti-asialo GM1 depleting antibody was from Wako; sterile saline was from B.Braun Melsungen; B16F10 cell line was from ATCC; EDTA and red blood cell lysis buffer were from Sigma; antibodies against mouse NK1.1 and CD3ε were from BD Pharmingen

NK cells were depleted with an anti-asialo GM1 depleting antibody. 25 μl of antibody solution diluted 1:4 in 0.9% saline per animal was injected i.v.. One day after initial injection of antibody, 5×10^4 B16 tumor cells in PBS were injected in the tail vein of mice. Injection of antibody was repeated every 3.5 days throughout the experiment. Animals were sacrificed on day 12 after tumor cell injection, and the number of lung metastases was determined as described above. NK cell levels were determined via flow cytometry before the first injection of antibody (=basal) and on day 7 and 12 after injection of tumor cells. For this purpose, 50 μl of blood per mouse was taken in EDTA (5 mM final concentration), red blood cells were lysed and NK cells were stained with an APC-labeled antibody against NK1.1 and a FITC-labeled antibody against CD3ε for 30 min at RT. NK cells were identified as NK1.1 and CD3ε positive events and expressed as percent of granulocyte population (identified in a fixed gate in forward/sideward scatter).

4.4.8   Neutrophil depletion

Materials: anti-Ly6G depleting antibody was from Biolegend; sterile saline was from B.Braun Melsungen; B16F10 cell line was from ATCC; EDTA and red blood cell lysis buffer were from Sigma; FITC-labeled anti-Ly6G antibody was from BD Pharmingen

Neutrophils were depleted with an anti-Ly6G depleting antibody. 25 µg of antibody solution diluted 1:4 in 0.9% saline per animal was injected i.v.. Three hours after initial injection of antibody, 5×10^4 B16 tumor cells in PBS were injected in the tail vein of mice. Injection of antibody was repeated every 3 days throughout the experiment. Animals were sacrificed on day 8 after tumor cell injection, and the number of lung metastases was determined as described above. Neutrophil levels were determined via flow cytometry before the first injection of antibody (basal) and on day 5 and 8 after injection of tumor cells. For this purpose, 50 µl of blood per mouse was taken in EDTA (5 mM final concentration), red blood cells were lysed and Neutrophils were stained with a FITC-labeled antibody against Ly6G for 30 min at RT. Neutrophils were expressed as percent of granulocyte population (identified in a fixed gate in forward/sideward scatter).

4.5   Statistical analysis

If not stated otherwise, one representative of at least 3 independently performed experiments is shown. All raw data was analyzed with Student's t-test. Depicted are mean values ± S.D. or ± S.E.M. as indicated in the figure legends. Statistical significance was defined as *, $P<0.05$; **, $P<0.01$; ***, $P<0.001$; n.s., not significant.

5   Results

5.1   Generation of mouse lines with a specific platelet secretion defect

5.1.1   Establishing a mouse line with specific platelet granule secretion defect via heterologous toxin expression

In order to study the role of platelet secretion in various pathological contexts, we sought to establish and describe a mouse line with defined platelet secretion abnormalities but with intact general platelet morphology and function. In a first approach, we generated mouse lines with heterologous expression of *Clostridium* toxins, specifically Botulinum toxin C (BoNT-C) and E (BoNT-E) and Tetanus toxin (TeNT) under the promoter of platelet factor 4 (PF4). The toxins were chosen with respect to their ability to render those proteins of the SNARE superfamily non-functional, which are expressed in platelets and known to contribute to granule release. BoNT-C cleaves syntaxin-1, -2 and -3 and SNAP-25, but not SNAP-23. BoNT-E cleaves SNAP-23 and SNAP-25. TeNT cleaves VAMP-1, -2 and -3 (Humeau, Doussau et al. 2000; Schiavo, G., M. Matteoli, et al. 2000; Dolly and Aoki 2006). PF4 expression is restricted to platelets and the promoter is activated in late stages of thrombopoiesis, shortly before fragmentation from megakaryocytes. It is also one of the most abundant proteins in platelets, which lead us to assume that expression of the toxins under control of the PF4 promoter can reach sufficient levels to affect granule exocytosis.

BoNT-C

Botulinum toxin C (BoNT-C) cleaves members of the syntaxin protein family and recognizes an Arginine-Alanine (RA)-motif towards the C-terminal end of the protein (Humeau, Doussau et al. 2000). It is still not well described which other amino acids around this motif or influencing secondary and tertiary structure of the protein are required for cleavage by Botulinum toxin C. Based on the known RA-motif and similarity of amino acids surrounding this motif, we predicted members of the mouse syntaxin family which can be potentially cleaved by Botulinum toxin C as limited experimental data is available (Table 22). We also determined the protein levels of the syntaxin protein for which a specific antibody was available.

Protein name	Sequence Accesion ID	Cleavage by BoNT-C expected	Expressed in mouse platelets
Syntaxin-1A	NP_058081	Yes	No
Syntaxin-1B	NP_077725	Yes	No
Syntaxin-2	NP_031967	Yes	Yes
Syntaxin-3	NM_152220	Yes	No
Syntaxin-4	NM_009294	No	Yes

Syntaxin-5	NM_019829	No	Yes
Syntaxin-6	NM_021433	No	Yes
Syntaxin-7	NM_016797	?	No
Syntaxin-8	NM_018768	No	Yes
Syntaxin-11	XM_920202	Yes	Not determined
Syntaxin-12	NM_133887	No	Yes
Syntaxin-16	NM_172675	Yes	Yes
Syntaxin-17	NM_026343	Yes	Not determined
Syntaxin-18	NM_026959	No	Not determined
Syntaxin-19	NM_026588	No	Not determined

Table 22: **Expected cleavage of syntaxin proteins by BoNT-C** derived from sequence similarity to known cut protein and protein expression in mouse platelets as determined by Western blot. Some SNARE proteins are very conserved and no specific antibody is commercially available so the expression by Western blot could not be determined.

According to literature (Flaumenhaft, Rozenvayn et al. 2007), syntaxin-2 and -4 are the main isoforms involved in platelet secretion. Syntaxin-2 is cleaved by BoNT-C, but syntaxin-4 is not. For generation of transgenic mice, a BAC-construct based on BAC RP24-98A4, which covers approximately 100'000 base pairs upstream and downstream of the mouse PF4 gene, was generated. The PF4 gene was replaced by RedE/T-mediated homologous recombination with a construct previously assembled in the pBluescript II KS(+) (pBSIIKS(+)) cloning vector. This construct contained the sequence of the clostridial BoNT-C light chain optimized for murine codon usage (Entelechon), followed by a BGH-pA tail and a stop codon. A schematic overview of the final BAC construct is given in figure 11.
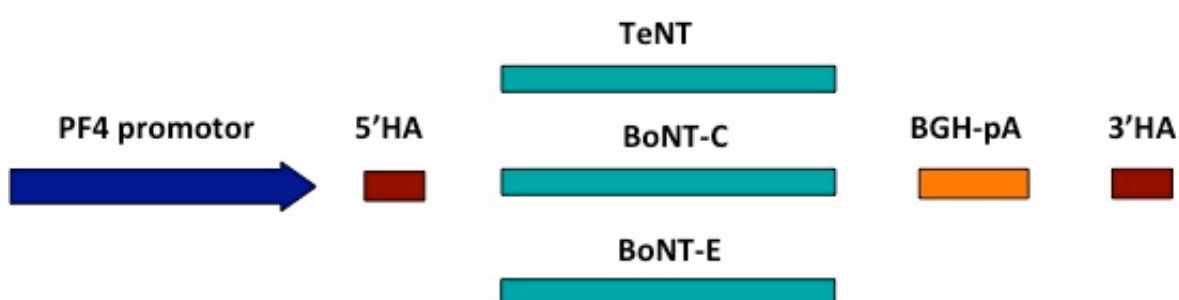
Figure 11: Schematic overview over the BAC constructs. The BAC vector consists of approximately 100'000 upstream (PF4 promotor) and downstream (not shown) regulatory sequence of the PF4 gene. Approximately 150 base pairs adjacent to the PF4 start and stop codon were included in the cloning vector to mediate homologous recombination to the BAC vector (5'HA, 3'HA). The toxin light chain sequence replaced the PF4 gene and was followed by a polyA tail and a stop codon (not shown).

The final BAC construct was sequenced in a region extending approximately 100-200 base pairs upstream and downstream of the inserted toxin and the integrity of the whole BAC sequence was screened by digestion with four different restriction enzymes to avoid multiple insertions of the toxin. The cleavage band pattern shown in figure 12 corresponds to the expected bands from in silico predictions.
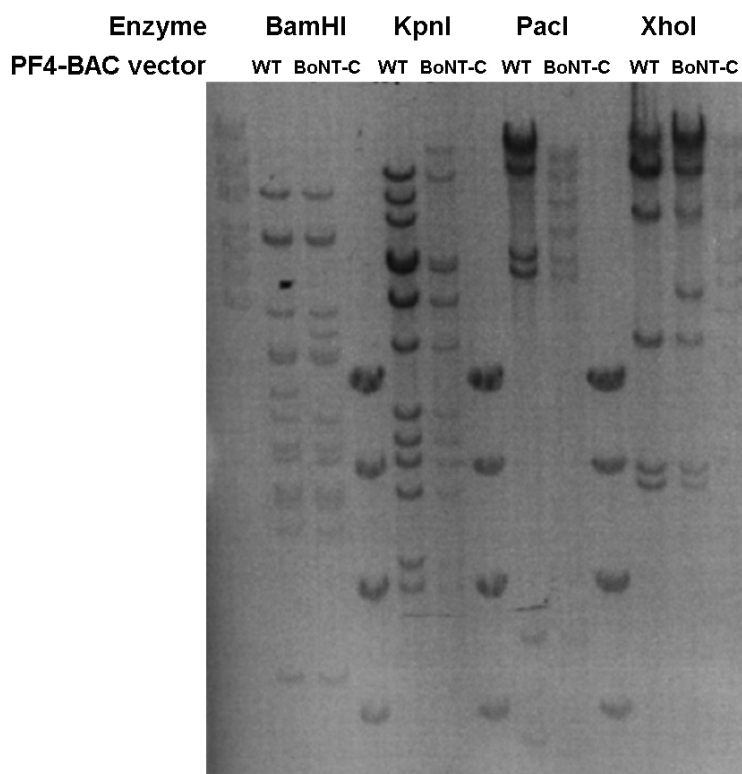

Enzyme	BamHI		KpnI		PacI		XhoI	
PF4-BAC vector	WT	BoNT-C	WT	BoNT-C	WT	BoNT-C	WT	BoNT-C

Figure 12: Restriction digest of the final PF4-BAC construct in which the PF4 gene was replaced with the BoNT-C construct. PF4-BAC wild-type (WT) and PF4-BoNT-C-BAC (BoNT-C) DNA was cut with BamHI, KpnI, PacI and XhoI. The wild-type and genetically modified band patterns matched the in silico predictions. Bands larger than approximately 25,000 kDa could not be resolved.

In addition, sequencing was performed with primers binding upstream of the 5' homology and in the construct as well as from inside the construct further downstream than the 3' homology arm. This construct was purified and perinuclear injection into mouse oocytes produced 61 pups of which 5 mice showed integration of the transgene in tail DNA PCR. To test for cleavage of syntaxin-2 in platelets, we used a specific antibody against the N-terminal region of syntaxin-2, which was able to recognize the full-length protein and the cleaved version (Synaptic Systems). The Western blot below (figure 13) shows lysed platelets isolated from each of the five transgene-positive founder mice blotted for syntaxin-2. The cleaved product of syntaxin-2 is expected to weigh approximately 4 kDa less than the full-length protein.
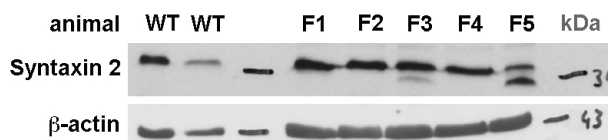
Figure 13: **Western blot for cleavage of syntaxin-2** of platelets isolated from the five PCR-positive founder mice (F1-F5) obtained from the PF4-BoNT-C line and two littermate control mice (WT). The anti-syntaxin-2 antibody used (Synaptic Systems) was able to detect the cleaved product. β-actin served as loading control.

Only two of the five founders showed the BoNT-C cleavage product. The amount of cleaved product relative to full-length syntaxin-2 was approximately 15% for founder 3 and 60% for founder 5. Founder 5 was mated for further experiments and the cleavage rate of syntaxin-2 could be confirmed for its offspring (data not shown).

BoNT-E

BoNT-E cleaves members of the SNAP protein family. It is known which amino acids surrounding the cleavage site are needed for recognition by the toxin light chain (Chen and Barbieri 2006; Chen and Barbieri 2007). For SNAP-23, which has been shown to be involved in platelet exocytosis (Flaumenhaft, Croce et al. 1999; Lemons, Chen et al. 2000), and SNAP-25, there is experimental evidence of cleavage of murine SNAP-23 by BoNT-E (Vaidyanathan, Yoshino et al. 1999). SNAP-29 and SNAP-91, which are not expressed in mouse platelets are also members of the SNAP family but their physiological function is less well defined and is probably more related to intracellular transport and fusion mechanisms. Nevertheless, based on the known recognition motif for BoNT-E, their protein sequences show considerable variation in the respective region and cleavage by BoNT-E is unlikely. The BAC construct used for generation of transgenic mice was similar to the construct used for BoNT-C. The same BAC carrying the PF4 gene (RP24-98A4) was used and a version of the BoNT-E light chain optimized for expression in mice (Entelechon) followed by a BGH-pA tail and a stop codon replacing the PF4 gene was inserted. To verify the final BAC sequence, the same tests as mentioned for the PF4-BoNT-C construct were applied (sequencing, PCR and restriction digest) and results confirmed identity with the in silico sequence (data not shown). Following injection into mouse oocytes, 57 pups were born, of which four showed integration of the transgene. A specific antibody against SNAP-23 (Synaptic Systems) was used to determine cleavage of this protein in the platelets of founder animals by BoNT-E (figure 14).
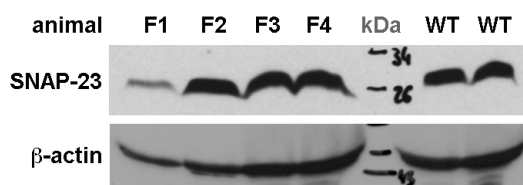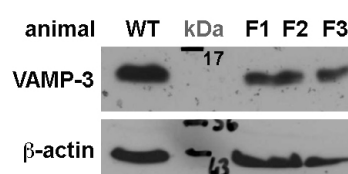
Figure 14: **Western blot for cleavage of SNAP-23** of platelets isolated from the four PCR-positive founder mice (F1-F4) obtained from the PF4-BoNT-E line and two littermate control mice (WT). Membranes were probed with anti-SNAP-23 antibody (Synaptic Systems), β-actin served as loading control.

The anti-SNAP-23 antibody was not able to detect the cleaved product because a C-terminal peptide was used for immunization, as this is the only part of the protein distinct from SNAP-25. Thus, SNAP-23 cleavage by BoNT-E could only be estimated by comparing the amounts of SNAP-23 in relation to β-actin. Founder 1 is the only animal which has a low signal for SNAP-23 in platelets, but total amount of platelets was also less as measured with the anti-β-actin antibody. From this result, it was inconclusive if any of the founders for this mouse line had significant cleavage of SNAP-23. To avoid stress for the founder animal, founder 1 was mated and only the next generation of mice was tested again for reduction in SNAP-23 levels.
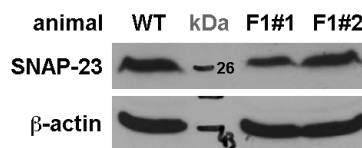
Figure 15: **Western blot of platelets isolated from two mice of the F1 generation** from founder 1 in the PF4-BoNT-E line (F1#1, F1#2) and a littermate control (WT). Membranes were probed with anti-SNAP-23 antibody and β-actin served as loading control.

Offspring #1 shows a marked reduction of approximately 40% in SNAP-23 while its sibling #2 shows only a minor reduction if any (figure 15).

TeNT

Tetanus toxin recognizes a specific motif in VAMP proteins described in literature for VAMP-1 (Schiavo, Matteoli et al. 2000). Based on sequence similarity, we predicted that VAMP-2 and -3 are also cleaved by TeNT whereas VAMP-4, -5 and -8 are unlikely to be cleaved (Table 23). This would mean, that one VAMP isoform known to contribute to platelet secretion is cleaved (VAMP-3), while the other one is not (VAMP-8) (Ren, Ye et al. 2008). Specific antibodies were used to determine expression in mouse platelets.

Protein name	Sequence Accesion ID	Cleavage by TeNT expected	Expressed in mouse platelets
VAMP-1	NP_033522	Yes	No
VAMP-2	NP_033523	Yes	Yes
VAMP-3	NP_033524	Yes	Yes
VAMP-4	NP_058076	No	No
VAMP-5	NP_058568	No	No
VAMP-7 (TI-VAMP)	NP_035645	No	?
VAMP-8	AAC23665	No	Yes

Table 23: **Expected cleavage of syntaxin proteins by TeNT** derived from sequence similarity to known cut protein and protein expression in mouse platelets as determined by Western blot. For VAMP-7 it could not be determined whether the signal detected roughly at the expected size was specific.

The anti-VAMP-7 antibody did not detect a band of the expected size although expression in platelets was claimed (Ren, Barber et al. 2007). However, VAMP-7 was not shown to be involved in platelet secretion and is also known for its role in endosomal trafficking (Chaineau, Danglot et al. 2009). The PF4-TeNT construct was assembled as described for the other toxins except that the original Clostridial toxin light chain sequence was used instead of a modified version. The antibody against VAMP-3 used to screen the five transgene-positive mice of the PF4-TeNT oocyte injection was raised against a peptide comprising the N-terminal part of the protein with 10 amino acids overlapping into the C-terminal end that is cleaved by TeNT. It is thus unclear if this antibody is able to detect the cleaved version of VAMP-3 or not. Western blot of platelet lysates from the three founder mice is shown below (figure 16).

Figure 16: **Western blot for cleavage of VAMP-3** of platelets isolated from the three PCR-positive founder mice (F1-F3) obtained from the PF4-TeNT line and two littermate control mice (WT). Membranes were probed with anti-VAMP-3 antibody (Synaptic Systems), β-actin served as loading control.

From these results, it is inconclusive whether VAMP-3 levels were decreased in the transgenic mice. All three founders were mated for further analysis. Western blots of the F1 generation indicated a small if any reduction in the amount of VAMP-3 in platelets (data not shown).

Functional analysis of the PF4-toxin mouse lines

The cleavage rates of the toxins for the respective SNARE proteins in the transgenic founder animals was not as high as expected with 60% of syntaxin-2 cleaved for PF4-BoNT-C, around 40% of SNAP-23 cleaved for PF4-BoNT-E and uncertain cleavage of VAMP-3 by PF4-TeNT constructs. In the mouse line with the best cleavage rate, PF4-BoNT-C, syntaxin-4 might be able to compensate for a reduction in syntaxin-2. SNAP-23 is the only SNAP protein described previously in platelet release (Flaumenhaft, Croce et al. 1999; Lemons, Chen et al. 2000) and thus the PF4-BoNT-E transgenic mice were more likely to show functional consequences of the reduction in SNAP-23 in alpha and dense granule release than the other two mouse lines. We used P-selectin exposure on the surface of thrombin-activated and secreting platelets determined by a labeled antibody in flow cytometry to measure release of secretory granules. No difference in P-selectin exposure was observed in offspring from the founder mice of the toxin transgenic lines and littermate controls. Figure 17 shows representative results from transgenic mice of the PF4-BoNT-E line.
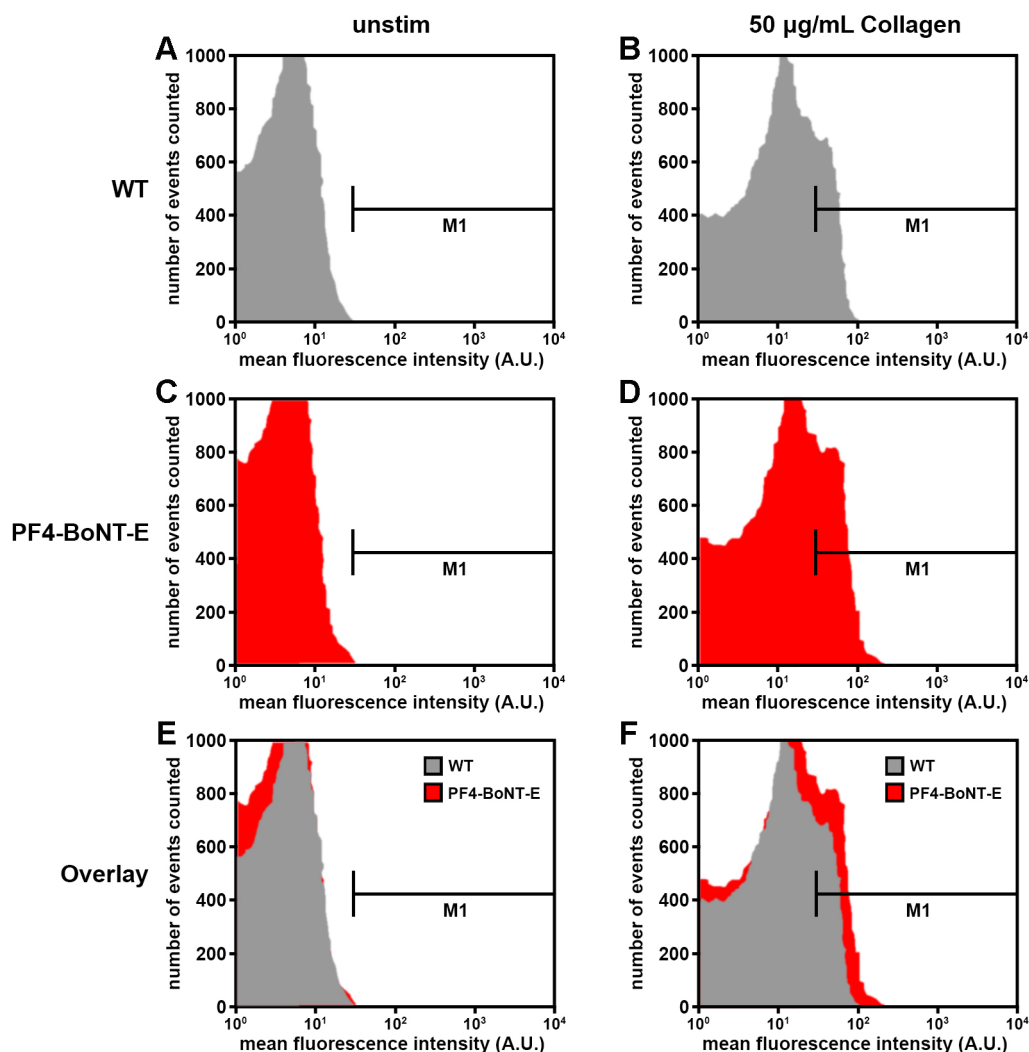
Figure 17: P-Selectin exposure on platelet surfaces in transgenic toxin mice was determined with a FITC-labeled anti-P-selectin antibody (emfret) in flow cytometry. Platelets from wild-type (WT) and PF4-BoNT-E transgenic (PF4-BoNT-E) mice were isolated, left untreated (unstim.) or stimulated with collagen (Nycomed) for 15 min and identified with a PE-labeled anti-CD41 antibody (BD) (number of events counted). A gate was set (M1) to visualize increase in P-selectin exposure upon stimulation.

The steepness and end point of light transmission curves in aggregometry is influenced by both alpha and dense granule secretion, especially in response to low doses of collagen because only a limited number of platelets is activated via direct contact to the large and heavy collagen fibrils. Thus, for fast and efficient platelet aggregation, secondary mediators are important. No difference in light transmission exceeding accidental variation between toxin transgenes and controls was observed upon stimulation with various agonist concentrations, represented by data from mice of the PF4-BoNT-E line stimulated with 0.3 µg/ml collagen (Figure 18).
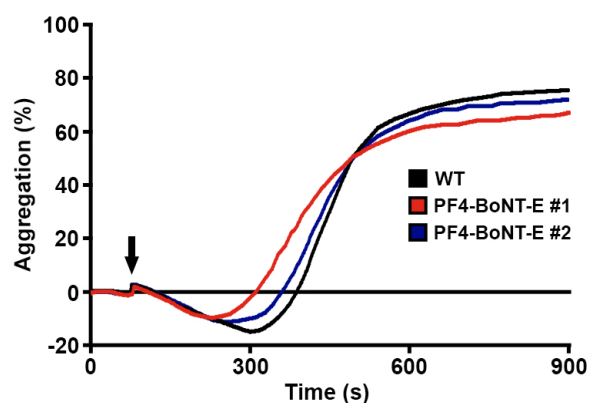
Figure 18: Light transmission curves of platelet suspensions (3×10^8/ml) **before and after addition (arrow) of 0.3 µg/ml collagen**. The x-axis shows the time from start of measurement to 900 s, the y-axis shows percentage of aggregation. The arrow indicates application of agonist and the curves show light transmission curves of platelets isolated from several wild-type (WT), and two PF4-BoNT-E transgene positive animals (PF4-BoNT-E #1, #2).

Re-injection of the PF4-BoNT-C and PF4-BoNT-E constructs in mouse oocytes produced 10 and 6 transgenic animals but only weaker cleavage (10-40 %) of syntaxin-2 and no obvious cleavage for SNAP-23, respectively (data not shown). Breeding homozygous mice and crossing the mouse lines to combine the transgenes also did not lead to a phenotype in in vitro platelet release assays (data not shown), so the project was discontinued.

5.1.2 Establishing a mouse line with specific platelet granule secretion defect via expression of dominant-negative SNAP-23 mutants

SNAP-23 is the central single protein in the formation of the exocytotic SNARE core complex which is expressed in platelets and necessary for platelet exocytosis (Flaumenhaft, Croce et al. 1999; Chen, Bernstein et al. 2000; Chen, Lemons et al. 2000; Lemons, Chen et al. 2000). Hence, loss of SNAP-23 cannot be compensated for by other proteins and should strongly affect platelet granule release. Our next approach to interfere with platelet release thus focused on creating dominant-negative SNAP-23 variants which would again be expressed in mice under the control of the promoter of the platelet-specific, highly abundant protein PF4.

SNAP-23 delta 8 mutant

The C-terminal end of SNAP-23 mediates binding to VAMP and thus engagement in exocytotic core complex formation. If the last exon of SNAP-23 is deleted, exocytosis is severely disturbed in mast cells (Vaidyanathan, Puri et al. 2001) and regulated exocytosis in rat pancreatic acinar cells is inhibited by C-terminal truncation of SNAP-23 (Huang, Sheu et al. 2001). In platelets, studies with permeabilized platelets (Chen, Bernstein et al. 2000; Chen, Lemons et al. 2000; Lemons, Chen et al. 2000) and culture-derived platelets (Gillitzer, Peluso et al. 2008) have shown that presence of a C-terminally truncated SNAP-23 can strongly reduce platelet alpha and dense granule secretion. Based on these findings, we designed a construct, which lacked the last 8 amino acids of SNAP-23 (SNAP-23 Δ8). SNAP-23 RNA was isolated from mouse platelets, transcribed into cDNA and amplified with primers covering SNAP-23 from start codon to 24 base pairs before the stop codon. The rest of the BAC-construct was designed as described for the toxin vectors except for a triple myc tag which was inserted immediately upstream of the SNAP-23 ATG (figure 19) to monitor construct expression in vivo.

Figure 19: Schematic overview over the BAC constructs. The BAC vector consists of approximately 100'000 upstream (PF4 promoter) and downstream (not shown) regulatory sequence of the PF4 gene. Approximately 150 base pairs adjacent to the PF4 start and stop codon were included in the cloning vector to mediate homologous recombination to the BAC vector (5'HA, 3'HA). A triple myc tag and the SNAP-23 Δ8 mutant replaced the PF4 gene and were followed by a polyA tail and a stop codon (not shown).

Nine transgenic animals were obtained after blastocyst injection. The calculated mass for the SNAP-23 peptide sequence (accession ID BAA2c345) is 23.2 kDa, but the anti-SNAP-23 antibody detected a signal at approximately 26 kDa. The transgenic PF4-SNAP-23 Δ8 mutant has a mass of 22.58 kDa, so it is unlikely that the two proteins can be distinguished in a normal Western blot. No extra band below 26 kDa was detected in the Western blot probed for SNAP-23 (Figure 20). No specific band was detected in a second blot incubated with an anti-myc antibody (data not shown), which suggests that the myc-tagged transgenic SNAP-23 Δ8 was not expressed in these animals.
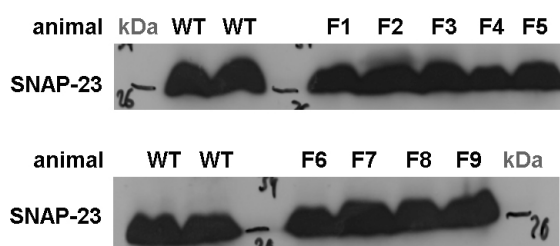
Figure 20: **Western blot of platelets isolated from the nine PCR-positive founder mice** (F1-F9) obtained from the **PF4-SNAP-23 Δ8 line** and four littermate control mice (WT). Anti-SNAP-23 antibody was applied to check for expression of mutant SNAP-23.

Nevertheless, the founder animals were mated and the offspring was analyzed in the functional assays described for the toxin transgenes but platelet function was not perturbed (data not shown).

SNAP-23 Ala mutant

We designed a second SNAP-23 mutant based on the observation by Sorensen et al. (Sorensen, Matti et al. 2002) that three amino acids in SNAP-25 are particularly important for SNAP-mediated exocytosis. When these three sites are mutated to the unpolar amino acid alanine, the binding of divalent cations is perturbed and exocytosis in chromaffin cells is strongly reduced. SNAP-23 and -25 are very conserved and the corresponding regions and mutated amino acids identical or almost identical in both proteins (Figure 21).

SNAP-25 12
EEMQRRADQLADESLESTRRMLQLVEESKDAGIRTLVMLDEQGEQLERIEEGMDQINKDM
SNAP-23 7
-EEVQLRAHQVTDESLESTRRI-LGLAI-ESQDAGIKTI-TMLDEQGEQLNRIEEGMDQINKDM

SNAP-25 72
KEAEKNLTDLGKFCGLCVCPCNKLK----SSDAYKKAWG----------NQDGVVASQPARVVDER-
SNAP-23 67
REAEKTLTELNKCCGLCICPCNRTKNFESGKNYKATWGDGGDNSPSNVVSKQPSRITNGQ

SNAP-25 125
--EQM----AISGGFIRRVTNDARENEMDENLEQVSGIIGNLRHMALDMGNEIDTQNRQIDRI
SNAP-23 127
PQQTTGAASGGYIKRITNDAREDEMEENLTQVGSILGNLKNMALDMGNEIDAQNQQIQKI

SNAP-25 182
MEKADSNKTRIDEANQRATKMLGS
SNAP-23 187
TEKADTNKNRIDIANTRAKKLIDS

Figure 21: Murine sequences of SNAP-25 (Accession ID: NP_035558) **and SNAP-23** (Accession ID: BAA20345) **aligned** (BLAST, NCBI). Mutated amino acids in the SNAP-23 Ala mutant are highlighted in red. Original amino acids were replaced by the unpolar amino acid alanine.

We thus hypothesized that mutation of these three amino acids would affect SNAP-23 function similarly to SNAP-25. A high expression level was essential for this dominant negative approach to work so we sought to optimize the construct in this respect. Lacy-Hulbert et al. report 30-fold enhanced expression of their construct when they introduced short intron sequences derived from the first intron of murine IgCμ heavy chain and the third intron of IgCε heavy chain at two original splice sites in GFP and bacteriophage P1-derived cre recombinase cDNA sequences (Lacy-Hulbert, Thomas et al. 2001). We also inserted the first intron of murine IgCμ heavy chain and the third intron of IgCε heavy chain, both of which are rather short, at two sites in SNAP-23 cDNA sequence which contained introns prior to processing. A schematic overview of the construct is displayed in figure 22.
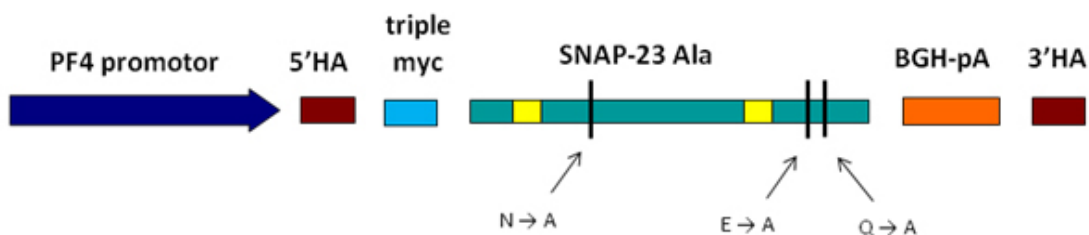
Figure 22: Schematic representation of the PF4-SNAP-23 Ala construct. The BAC vector for PF4-SNAP-23 Ala consists of approximately 100'000 upstream (PF4 promoter) and downstream (not shown) regulatory sequence of the PF4 gene. Approximately 150 base pairs adjacent to the PF4 start and stop codon were included in the cloning vector to mediate homologous recombination to the BAC vector (5'HA, 3'HA). A triple myc tag and the SNAP-23 Ala mutant replaced the PF4 gene and were followed by a polyA tail and a stop codon (not shown). Yellow parts in SNAP-23 represent the first intron of IgCμ heavy chain (5') and the third intron of IgCε (3'). Arrows indicate site and identity of mutated amino acids.

The SNAP-23 Ala sequence containing the three mutations and the two introns were synthetized (Entelechon) and cloned into the final construct. Thirteen PCR-positive founder animals were obtained after blastocyst injection of PF4-SNAP-23 Ala. In the platelets of three of the positive founders, a band at around 32 kDa was detected in Western blot when probed with anti-myc antibody after long exposure (>20 min), suggesting expression of the construct in platelets (figure). However, in a second Western blot stained for SNAP-23, only

the band of endogenous SNAP-23 running at approximately 26 kDa was observed even after long exposure of the film (figure 23).
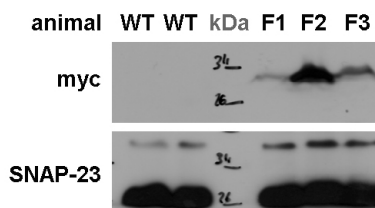

Figure 23: **Western blot of platelets isolated from the PF4-SNAP23 Ala PCR-positive founder mice.** Shown are the three mice that displayed a signal in anti-myc staining (upper panel; F1-F3). In the lower panel, platelet lysates of the same mice were probed with anti-SNAP-23 antibody. Two littermate control mice (WT) were processed in parallel.

These findings indicate that the PF4-SNAP-23 Ala construct was indeed expressed in platelets but expression levels compared to endogenous SNAP-23 levels were very low. Accordingly, no difference in P-selectin exposure and aggregometry between mutants and wild-type controls were observed (data not shown). Using transgenic SNAP-23 mutants to interfere with platelet secretion was thus abandoned.

5.2 Analysis of the *Jinx* mouse line, a genetically modified null-mutant of the Munc13-4 gene

5.2.1 Basal analysis

The Munc13 protein family is involved in the priming and docking step of SNARE-mediated exocytosis. It has been demonstrated that Munc13-4, the isoform present in platelets (Ren, Ye et al. 2008), controls dense granule release in platelets together with Rab27a and b (Shirakawa, Higashi et al. 2004). The Bruce Beutler laboratory generated a mouse line with a functional null-mutant of Munc13-4 (Munc13-4^{Jinx}). Given the major role of Munc13 in regulated exocytosis, we hypothesized that Munc13-4 deficiency should cause a major platelet secretion defect. We first determined Munc13-4 protein levels in *Jinx* platelets and found no detectable production of Munc13-4 protein (figure 24 A). Therefore, the *Jinx* mouse line will be termed "Munc13-4 KO" or Munc13-4-deficient" for clarity from here on. Western blot analysis of platelet lysates from isolated wild-type and Munc13-4 KO platelets probed with an antibody against the alpha granule protein PF4 showed no difference in PF4 protein levels between both genotypes (figure 24 B). Platelet numbers determined with flow cytometry in whole blood were not changed in Munc13-4 KO mice compared to wild-type animals (figure 24 C). Transmission electron microscopy revealed intact platelet morphology and normal granule numbers in Munc13-4 KO platelets (figure 24 D; Ren, Wimmer et al. 2010).
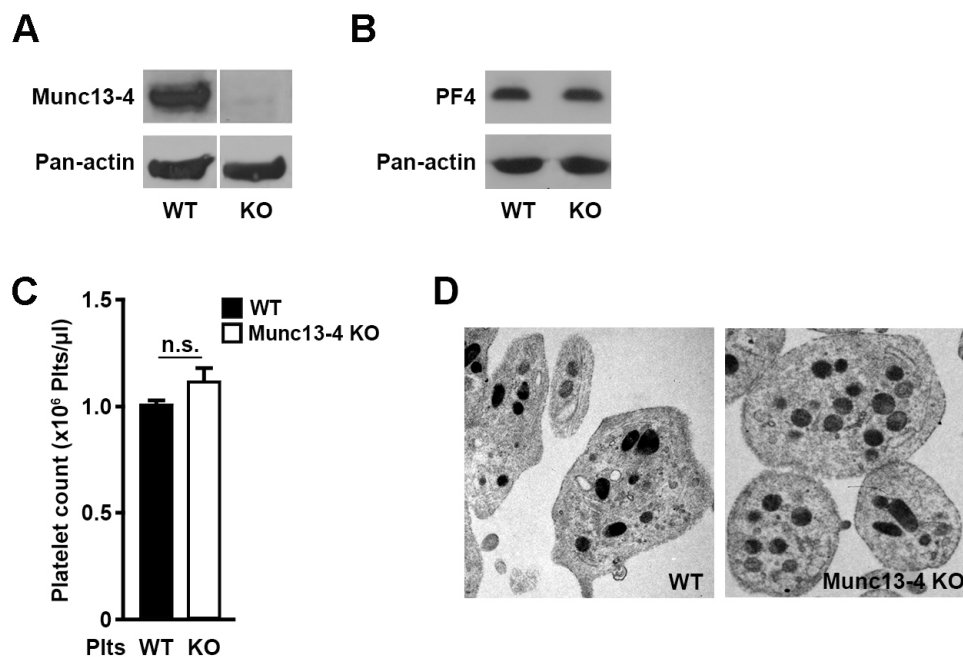
Figure 24: **Basic analysis of the phenotype of Munc-13-4-deficient platelets.** (A) Platelet extracts from wild-type (WT) and Munc-13-4-deficient mice (KO) were analyzed by Western blotting using an anti-Munc13-4 antibody (n = 3). Pan-actin staining served as loading control. (B) Platelet extracts from wild-type (WT) and Munc-13-4-deficient mice (KO) were analyzed by Western blotting using an anti-PF4 antibody (n = 3). Pan-actin staining served as loading control. (C) Platelet numbers of wild-type (WT) and Munc-13-4-deficient mice (KO) were determined by flow cytometry as described in methods (n = 3). (D) Wild-type (WT) and Munc13-4 KO (Munc13-4 KO) platelet morphology was visualized with transmission electron microscopy (magnification x 10,000). Shown are mean values ± S.D.; n.s., not significant.

We next investigated whether basal surface expression of important platelet receptors is altered in Munc13-4 KO platelets. Therefore, we stained isolated Munc13-4 and wild-type platelets with antibodies against GPIb, GPV, GPVI, GPIX, integrin α2, integrin β1, integrin αIIbβ3, CD9 and CLEC-2 and measured their relative fluorescence intensities in flow cytometry (figure 25). There was no difference between wild-type and Munc13-4 KO platelets in the expression level of the surface receptors tested except for a small but significant reduction in CD9 and CLEC-2 levels in Munc13-4 KO platelets.
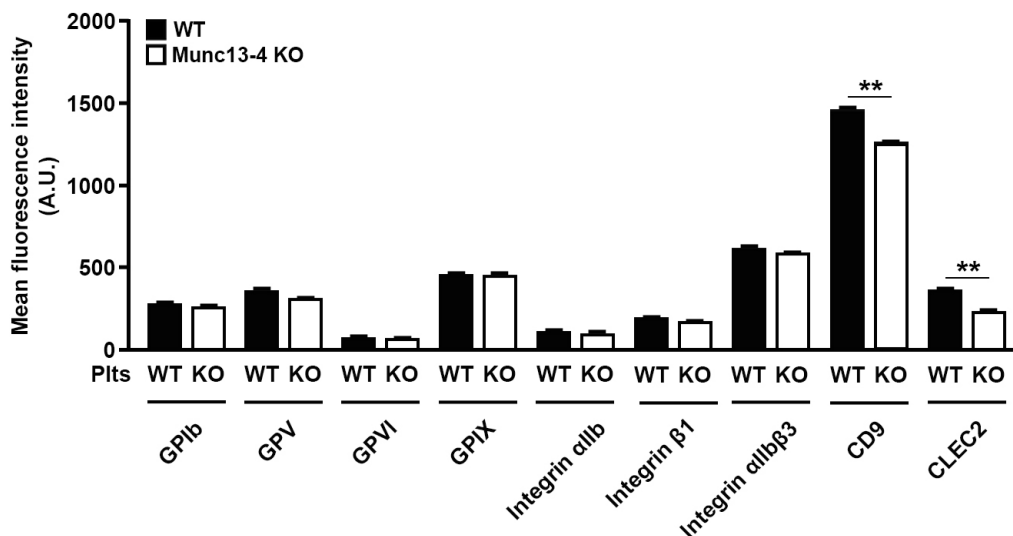
Figure 25: Basal surface receptor expression on Munc13-4 KO platelets. Washed platelets from wild-type (WT) and Munc-13-4-deficient mice (KO) were stained with labeled antibodies against the indicated and staining was quantified by flow cytometry (n = 3). Shown are mean values ± S.D.; **, $P < 0.01$.

Integrin αIIbβ3 activation leads to a calcium-dependent conformational change that can be monitored with a specific antibody (JON/A, Emfret) recognizing an epitope that is only exposed in the activated conformation. Wild-type and Munc13-4 KO platelets were stimulated with increasing concentrations of thrombin (figure 26 A) or a panel of different platelet agonists (figure 26 B) and the relative fluorescence intensity of bound anti-integrin αIIbβ3 antibody was determined by flow cytometry. Several agonists lead to a slight decrease of active integrin αIIbβ3 in Munc13-4 KO platelets compared to wild-type platelets (0.1 U/ml thrombin, U46619+ADP, CRP) but only the small reduction in JON/A fluorescence intensity evoked by the snake venom rhodocytin was significant (figure 26 B).
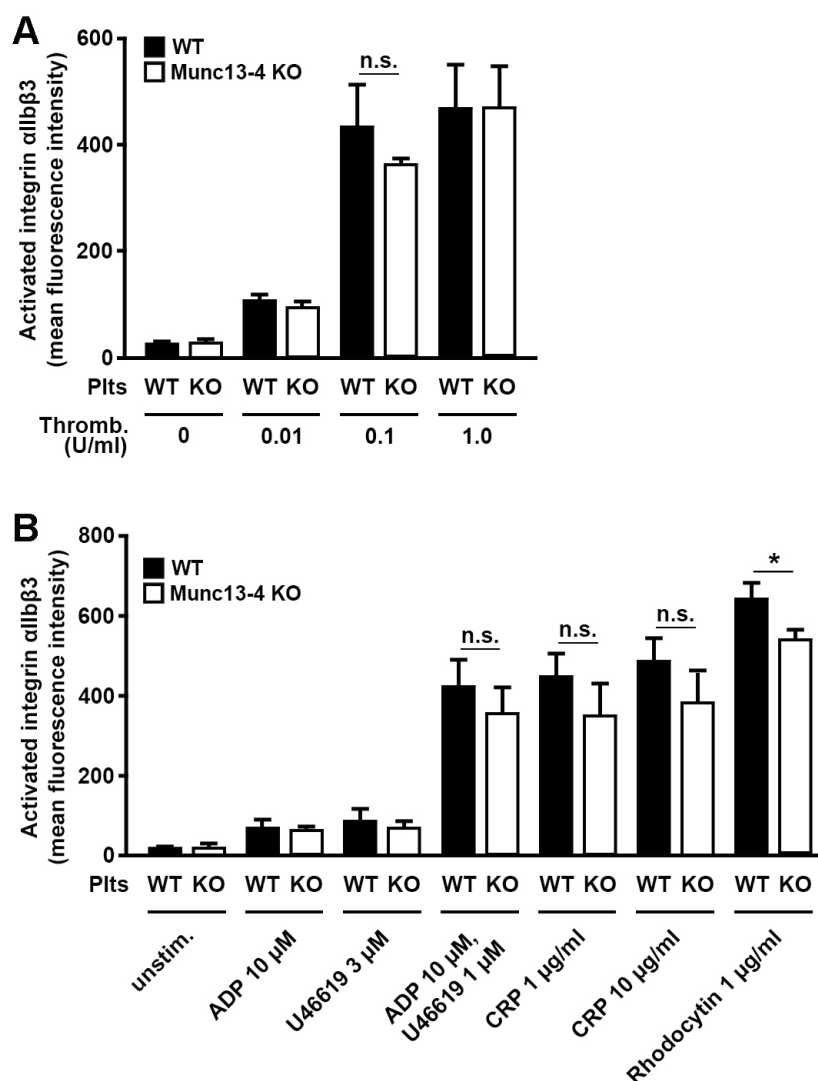
Figure 26: **Activation of surface integrin αIIbβ3 in Munc13-4 KO platelets.** (A,B) Washed platelets from wild-type (WT) and Munc-13-4-deficient mice (KO) were activated with thrombin (A) or the indicated agonists (B) for 15 min, subsequentially stained with a labeled antibody against the active conformation of integrin αIIbβ3 (JON/A) and quantified by flow cytometry (n = 3). U46619, thromboxane A_2 analogue; CRP, collagen-related peptide. Shown are mean values ± S.D.; *, P<0.05; n.s., not significant.

Platelet alpha granules contain multiple proteins and there are an increasing number of publications reporting regulated release of specific proteins (Sehgal and Storrie 2007; Italiano, Richardson et al. 2008; Battinelli, Markens et al. 2011). We therefore chose two different proteins as representative markers for alpha granule release: PF4 and vWF. We assessed PF4 (figure 27 A) and vWF (figure 27 B) levels of supernatants from wild-type and Munc13-4 KO platelets after thrombin stimulation with specific ELISA assays. There was no difference in the secretion of both alpha granule proteins at sub-maximal and maximal platelet stimulation (figure 27 A and B).
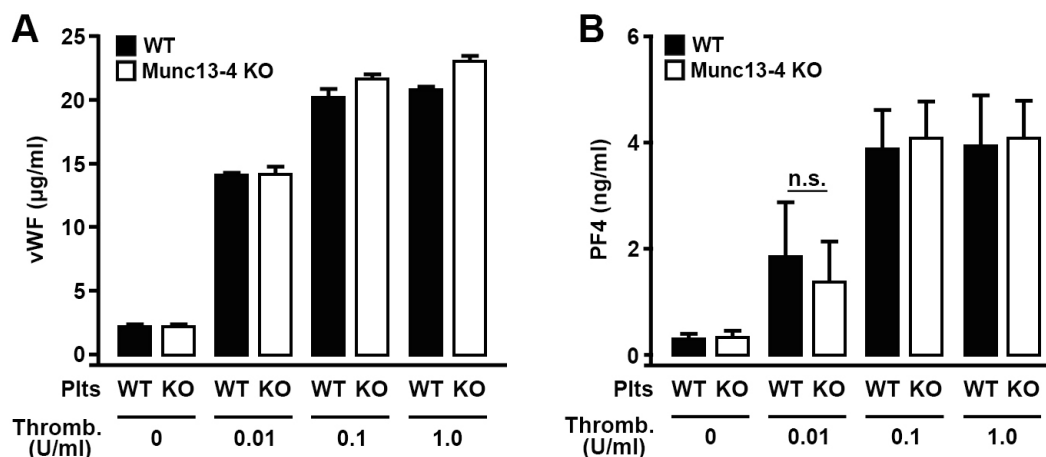
Figure 27: **Munc13-4 KO platelets exhibit normal alpha granule protein release.** (A,B) Effect of increasing concentrations of thrombin on release of platelet factor 4 (PF4) (A) or von Willebrand factor (vWF) (B) from wild-type (WT) or Munc13-4-deficient platelets (KO) (n = 3-5) measured in ELISA assays. Shown are mean values ± S.D.; n.s., not significant.

Platelet alpha granule membranes contain P-selectin (Stenberg, McEver et al. 1985) but P-selectin was also shown to be associated with dense granule membranes (Israels, Gerrard et al. 1992; Youssefian, Masse et al. 1997). Upon activation and granule secretion, granule membranes get integrated into the outer platelet membrane and P-selectin is exposed and serves as a binding receptor for various cell types (Zarbock, Polanowska-Grabowska et al. 2007; van Gils, Zwaginga et al. 2009). P-selectin exposure on the surface of wild-type and Munc-13-4 deficient platelets was determined via flow cytometry in response to increasing thrombin concentrations (figure 28 A) or a panel of other platelet agonists (figure 28 B). There was a trend toward lower P-selectin exposure in Munc13-4 KO platelets compared to wild-type platelets but a significant reduction in P-selectin signal was only observed for the two highest thrombin concentrations (figure 28 A), the combination of U46619 and ADP and rhodocytin (figure 28 B).
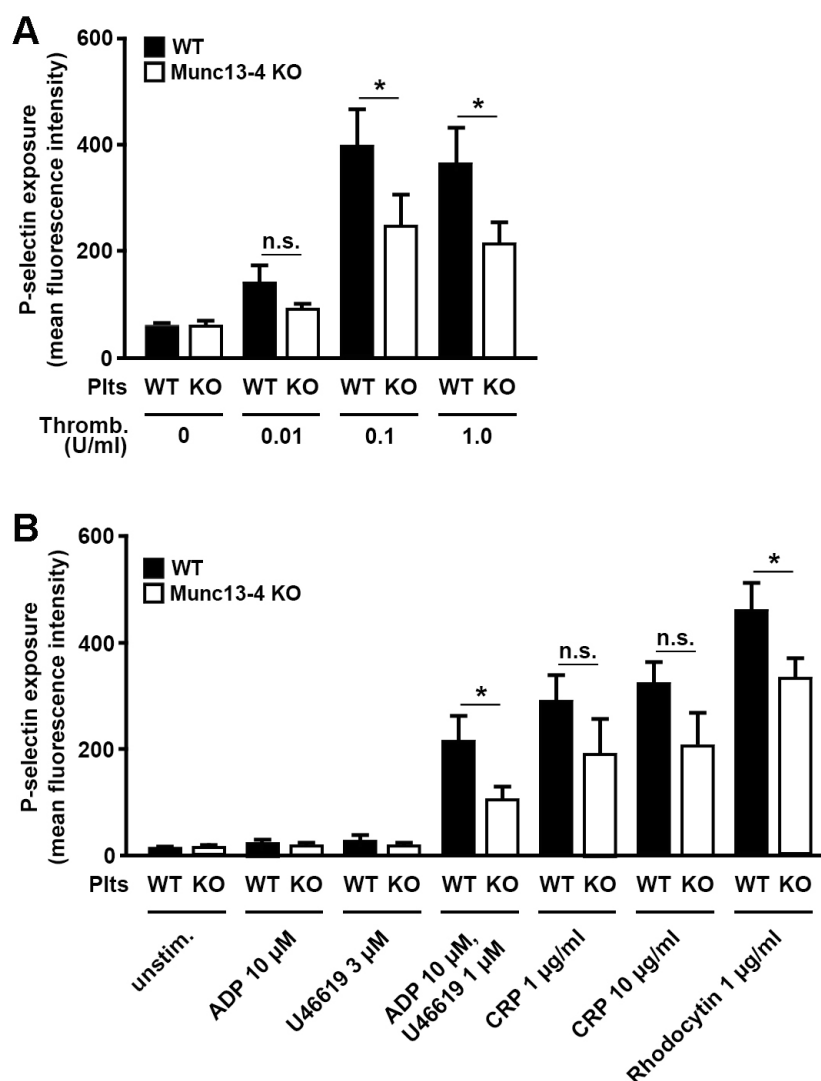
Figure 28: Exposure of P-selectin on platelet outer membranes. (A,B) Washed platelets from wild-type (WT) and Munc-13-4-deficient mice (KO) were activated with thrombin (A) or the indicated agonists (B) for 15 min, subsequentially stained with a labeled anti-P-selectin antibody and quantified by flow cytometry (n = 3). U46619, thromboxane A_2 analogue; CRP, collagen-related peptide. Shown are mean values ± S.D.; *, P<0.05; n.s., not significant.

We measured ATP secretion as a parameter to investigate dense granule secretion in Munc13-4-deficient platelets. Virtually no ATP secretion was detected in platelets isolated from mice lacking Munc13-4 in response to increasing doses of thrombin (figure 29 A), the thromboxane A_2 analogue U46619 (figure 29 B) and collagen (figure 29 C).
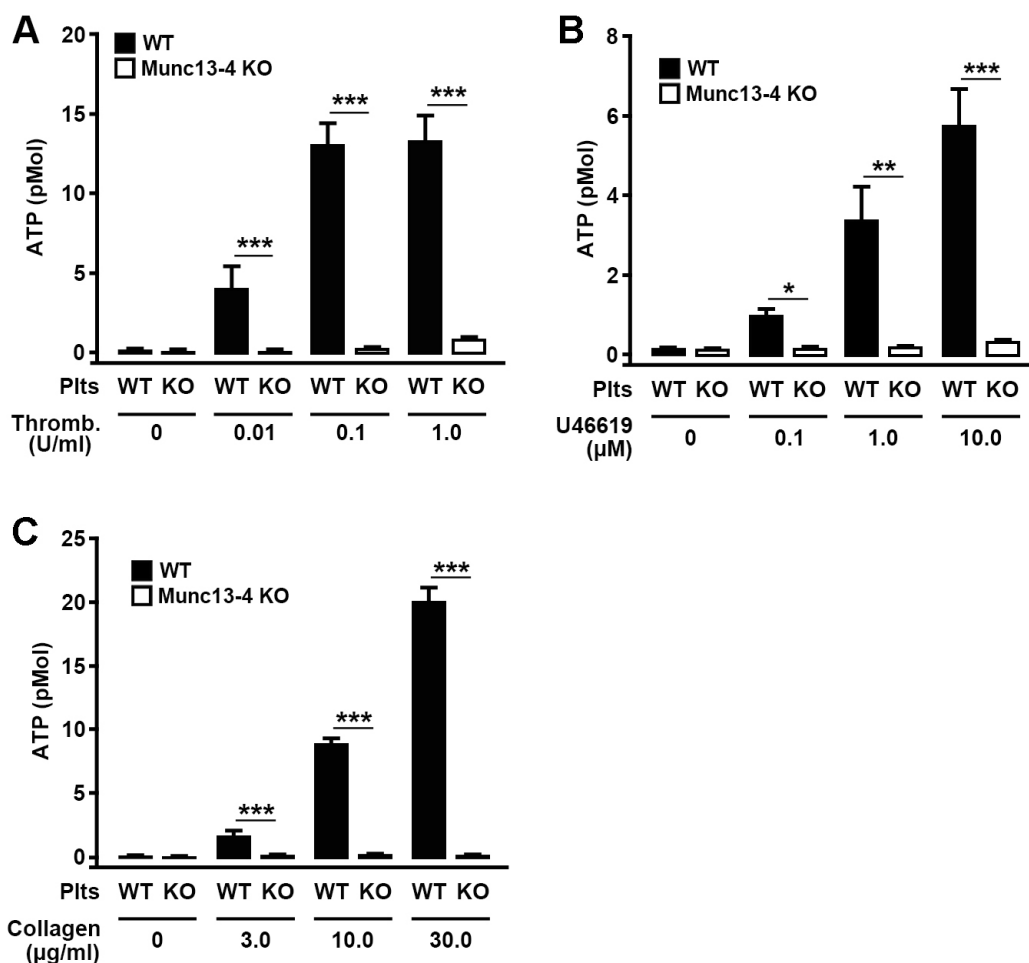
Figure 29: **Impaired dense granule secretion in Munc-13-4-deficient mice.** (A,B,C) Effect of thrombin (A), the thromboxane A2-analogue U46619 (B) or fibrillar collagen (C) on release of ATP from wild-type platelets (WT) or Munc13-4-deficient platelets (KO) (n = 3-5). Shown are mean values ± S.D.; *, P<0.05; **, P<0.001; ***, P<0.001.

Adhesion to collagen under static conditions requires binding of platelet receptor GVI and may be supported by binding to integrin α2β1 (Nieswandt, Pleines et al. 2011). We let washed platelets of wild-type and Munc13-4-deficient mice adhere to coverslips previously coated with fibrillar collagen, washed the coverslips and analyzed the area covered by platelets (figure 30 A). Quantification (figure 30 B) reveals no difference in static adhesion to collagen between both genotypes.
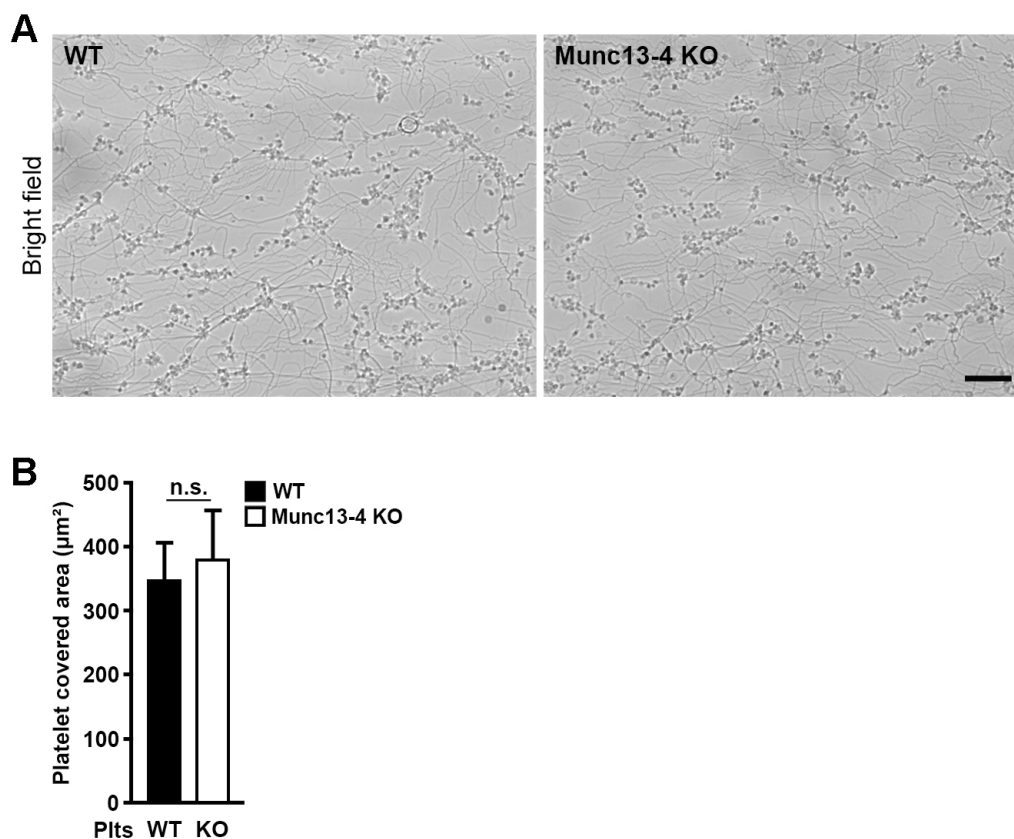
Figure 30: Munc13-4 KO platelets show normal adhesion to collagen. (A,B) Collagen-coated coverslips incubated with platelet suspensions of wild-type (WT) and Munc-13-4-deficient mice (KO). Coverslips were washed and representative brightfield images are shown (A). Bar length: 20 µm. Five randomly chosen areas per genotype (n = 3) were quantified (B). Shown are mean values ± S.D.; n.s., not significant.

Platelet aggregation is an important tool in analysis of platelet function and is influenced by both alpha and dense granule secretion. The impact of secondary mediators in aggregation responses depends on the platelet agonist and the concentration applied to the platelet suspensions. Strong agonists like thrombin are less suitable to assess secretion defects because through stirring and diffusion, they reach every platelet very fast and lead to an immediate formation of pseudopodia (filopodia) and aggregation, in high concentrations even without measurable shape change. No substantial difference between aggregation curves of Munc13-4-deficient platelets and wild-type platelets was observed after stimulation with thrombin (data not shown). In contrast to thrombin, collagen type I fibers only activate the platelets in their immediate vicinity by binding to GPVI and platelet aggregation is supported by activation of neighboring cells via secondary mediators like ADP and thromboxane A_2. Figure displays representative light transmission curves of wild-type platelets and Munc13-4 KO platelets stimulated with 30 µg/ml (figure 31 A), 10 µg/ml (figure 31 B), 3 µg/ml (figure 31 C) and 0.3 µg/ml collagen (figure 31 D). A right-shift of Munc13-4 platelet aggregation compared to wild-type curves is observed in all

concentrations tested, showing a delayed onset of shape change and aggregation which is expected for a defect in dense granule secretion. Once aggregation is initiated, platelet secretion plays only a minor role in reaching plateau aggregation levels but the strong defect in dense granule secretion still leads to a marked decrease in plateau-phase aggregation in Munc13-4 KO platelets compared to wild-type platelets (figure 31 A-D).
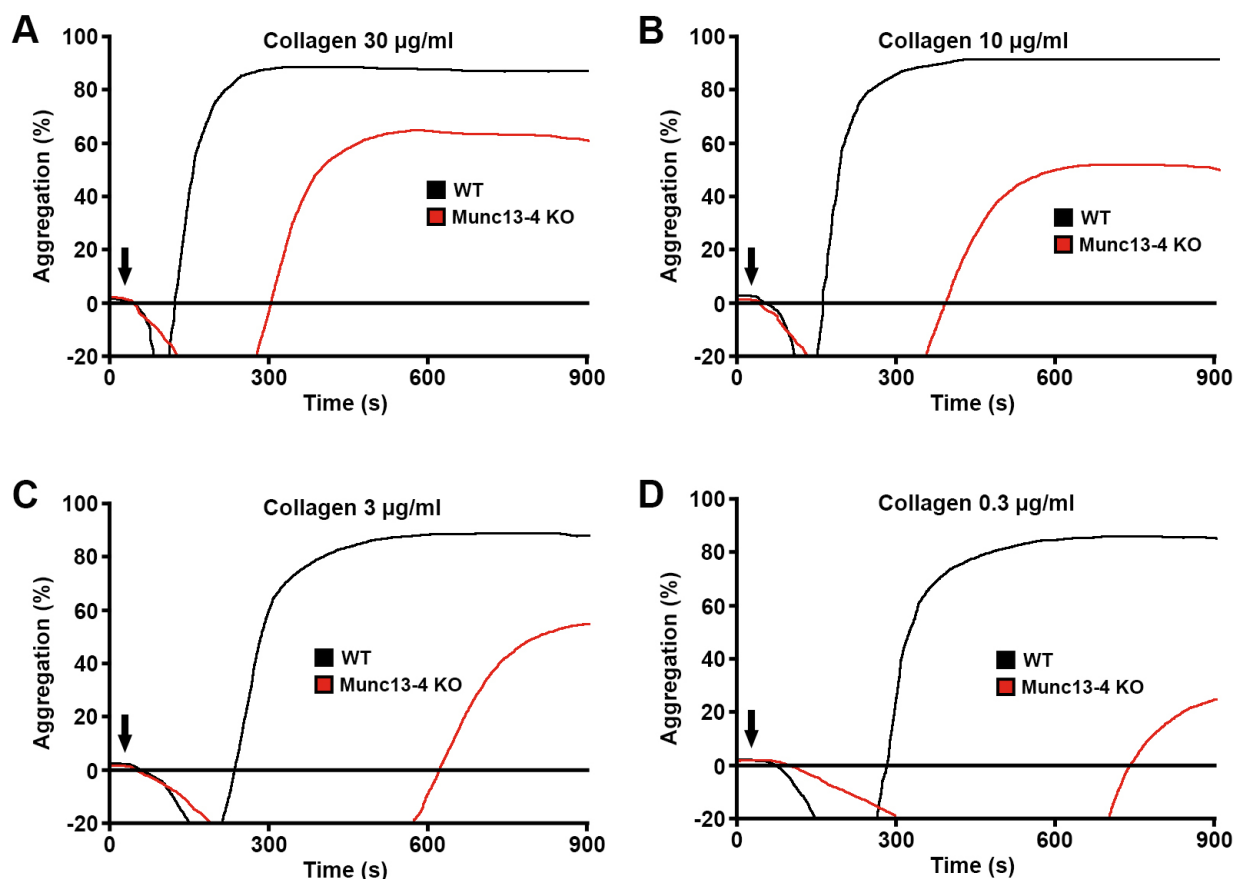

Figure 31: **Aggregation of Munc13-4 KO platelets is impaired in response to collagen.** (A-D) Representative light transmission curves from at least 3 independent experiments of washed platelet suspensions (3×10^8/ml) from wild-type (WT) or Munc13-4-deficient (Munc13-4 KO) mice were measured in an aggregometer. The x-axis shows the time from start of measurement to 900 s, the y-axis shows percentage of aggregation. The arrow indicates application of collagen at a final concentration of 30 µg/ml (A), 10 µg/ml (B), 3 µg/ml (C) or 0.3 µg/ml (D).

Even when isolated Munc13-4 KO platelets were stimulated with intermediate to low doses of the thromboxane A_2 analogue U46619, the delay in onset of aggregation and the decrease in plateau aggregation level reached were obvious compared to wild-type platelets (figure 32 A-C).
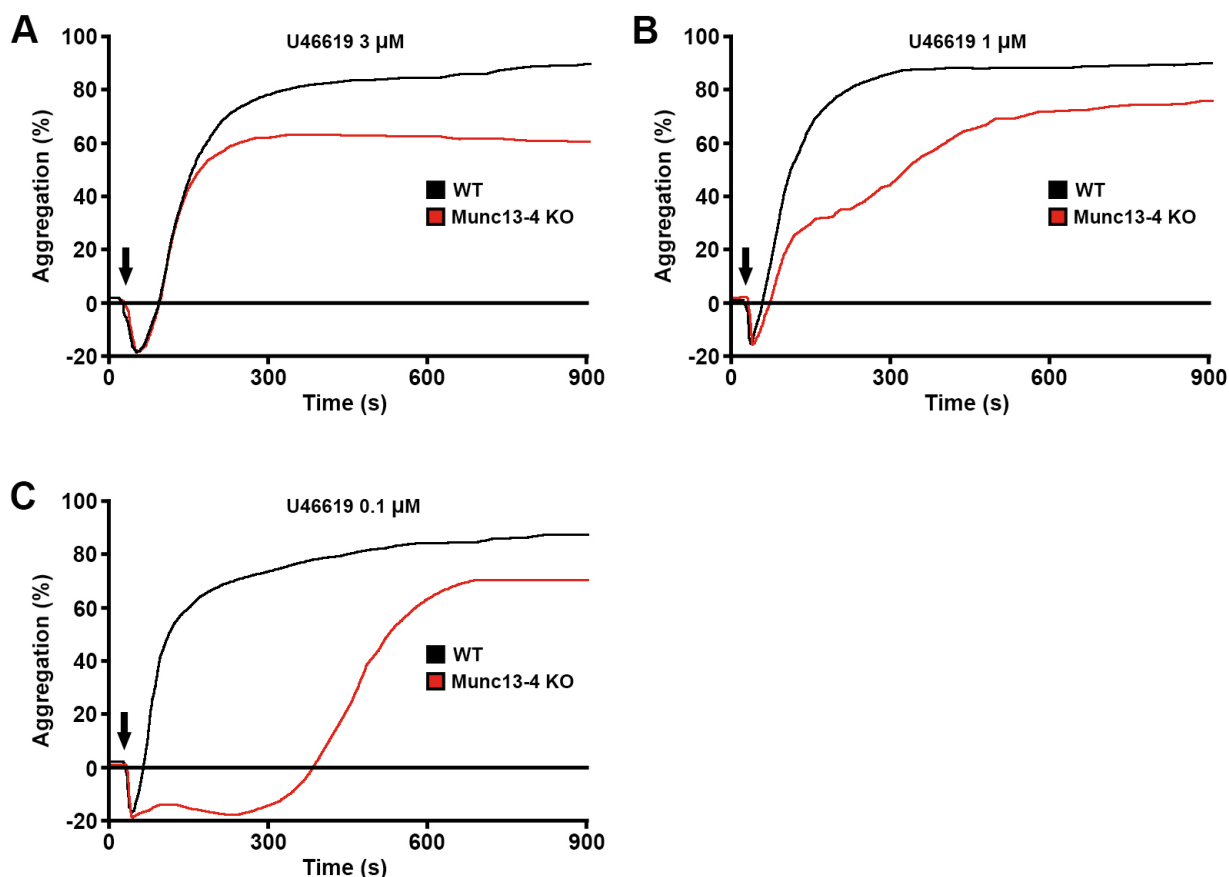
Figure 32: **Aggregation of Munc13-4 KO platelets is impaired in response to U46619.**
(A-C) Representative light transmission curves from at least 3 independent experiments of washed platelet suspensions (3×10^8/ml) from wild-type (WT) or Munc13-4-deficient (Munc13-4 KO) mice were measured in an aggregometer. The x-axis shows the time from start of measurement to 900 s, the y-axis shows percentage of aggregation. The arrow indicates application of the thromboxane A_2 analogue U46619 at a final concentration of 3 µM (A), 1 µM (B) or 0.1 µM (C).

Application of whole blood samples to a flow chamber device is a more complex method to assess platelet function in vitro. This assay involves platelet activation, rolling and binding of single platelets, recruitment of platelets via secondary mediators, formation of aggregates and aggregate stability. Binding of the platelet GPIb-V-IX complex to collagen-bound vWF initiates rolling and adhesion of platelets, then the low-affinity receptor GPVI can bind to collagen and activate the platelets. Aggregate stability is supported by many mediators, especially integrin α2β1 and αIIbβ3, CLEC-2, Gas6 and CD40L (Nieswandt, Pleines et al. 2011). Heparinized mouse blood is transported through a tube-like chamber containing a collagen-coated coverslip at a defined shear rate (1000 s^{-1}) and coverslips are analyzed microscopically for bound platelet aggregates. Munc13-4 KO platelets form smaller aggregates than wild-type platelets (figure 33 A) and a size distribution chart makes this defect even more obvious (figure 33 C). In contrast, quantification of the total area

covered by platelets is approximately the same for both genotypes (figure 33 B), indicating again that adhesion to collagen is not perturbed in Munc13-4 platelets.
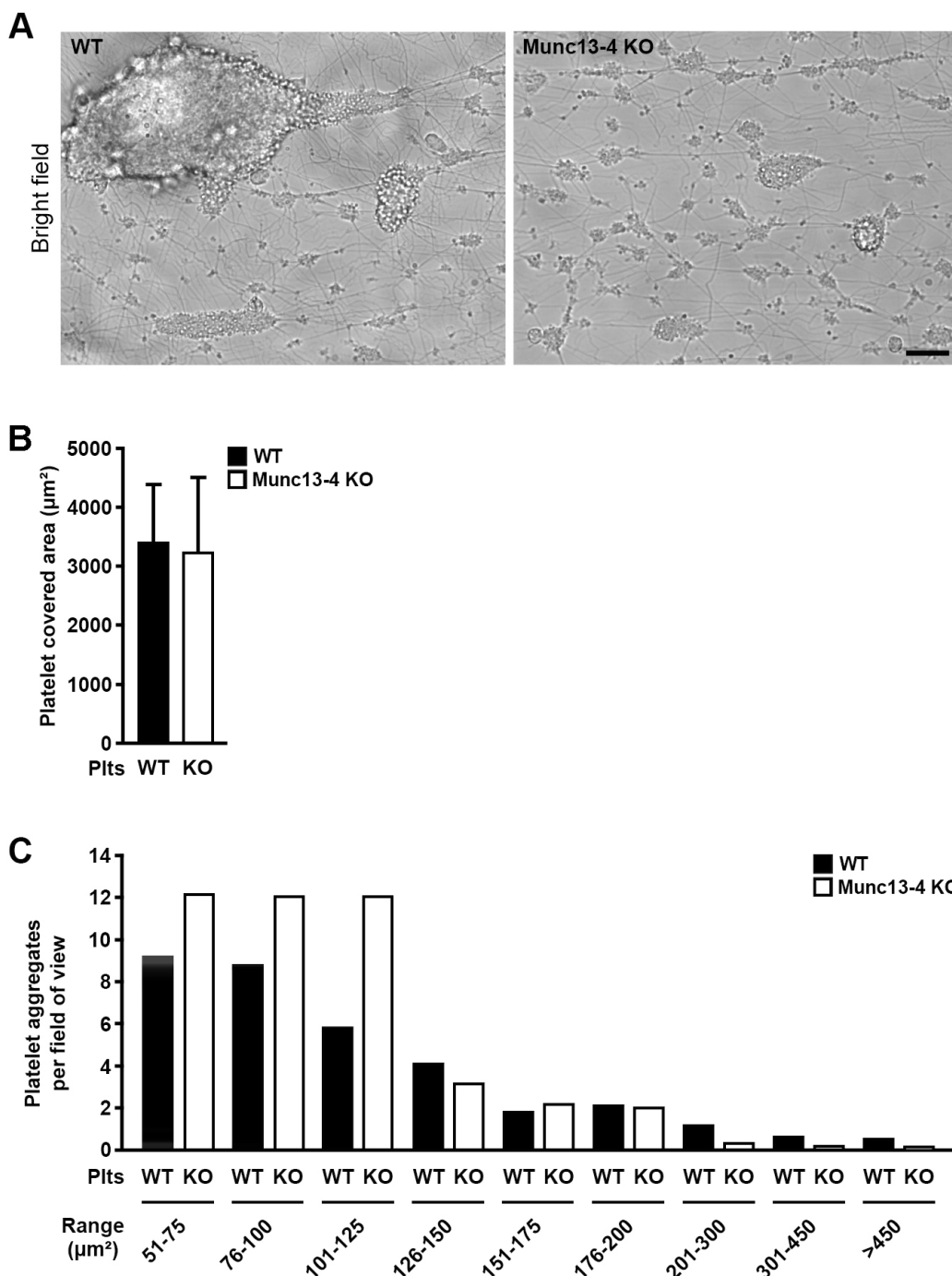

Figure 33: Munc13-4 KO platelets show impaired formation of large aggregates in flow chamber assays. (A-C) Collagen-coated coverslips were fixed in a flow chamber device which was then perfused at a defined shear rate (1000^{-s}) with heparinized blood freshly drawn from wild-type (WT) or Munc-13-4-deficient mice (KO) for 5 min. Coverslips were washed and representative brightfield images are shown (A). Bar length: 20 µm. Three randomly chosen areas per mouse (n = 6) were quantified for total area covered with platelets per field of view (B). To visualize the apparent inability of Munc13-4 KO platelets to form large aggregates despite

intact activation by collagen, the aggregates were split up in size categories (C). Shown are mean values ± S.D. where applicable (B).

Dysfunctional platelet responses often lead to an increase in bleeding time. Mice were anesthetized and tails were cut by 2 mm. Immediately afterwards, tails were submerged into saline and kept at 37°C until bleeding ceased for more than 1 min or until the experiment was stopped after 20 min. Wild-type animals had an average bleeding time of approximately 2 min whereas Munc13-4-deficient animals showed no sign of decrease in blood flow until the experiment was terminated 20 min after tail cut to avoid critical loss of blood (figure 34).
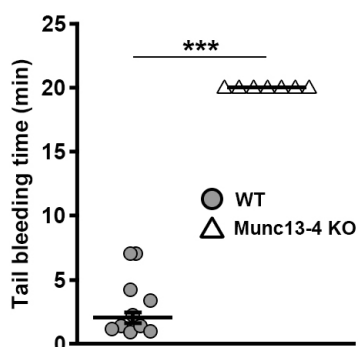

Figure 34: Prolonged tail bleeding time in Munc13-4 KO mice. Mice were kept under isoflurane anesthesia throughout the experiment. Tails of wild-type (WT; gray circles) and Munc13-4 KO mice (Munc13-4 KO; white triangles) were cut 2 mm, the tail was immediately submerged into pre-warmed (37°C) saline. Time was measured until bleeding stopped for more than 1 min. Experiment was terminated after 20 min to avoid critical loss of blood (n = 7-9). Shown are mean values ± S.D.; ***, P<0.001.

Denudation of mesenteric arteries with ferric chloride is a commonly used mouse model for arterial thrombosis. Exposure of extracellular matrix proteins like collagen leads to platelet activation, secretion and finally to occlusion of the vessel by a platelet-rich plug which is almost devoid of red blood cells and lymphocytes. This model strongly depends on platelet granule secretion and there is evidence that dense granules play a major role in thrombus formation (King, McNamee et al. 2009). Munc13-4 KO mice showed only minor platelet aggregate formation and no occlusion during the follow-up time of the experiment (60 min). In wild-type vessels, stable plugs began to form after 2-4 min and after approximately 10 min, no cellular transport through the occluded vessel was observed any more (figure 35 A-D).
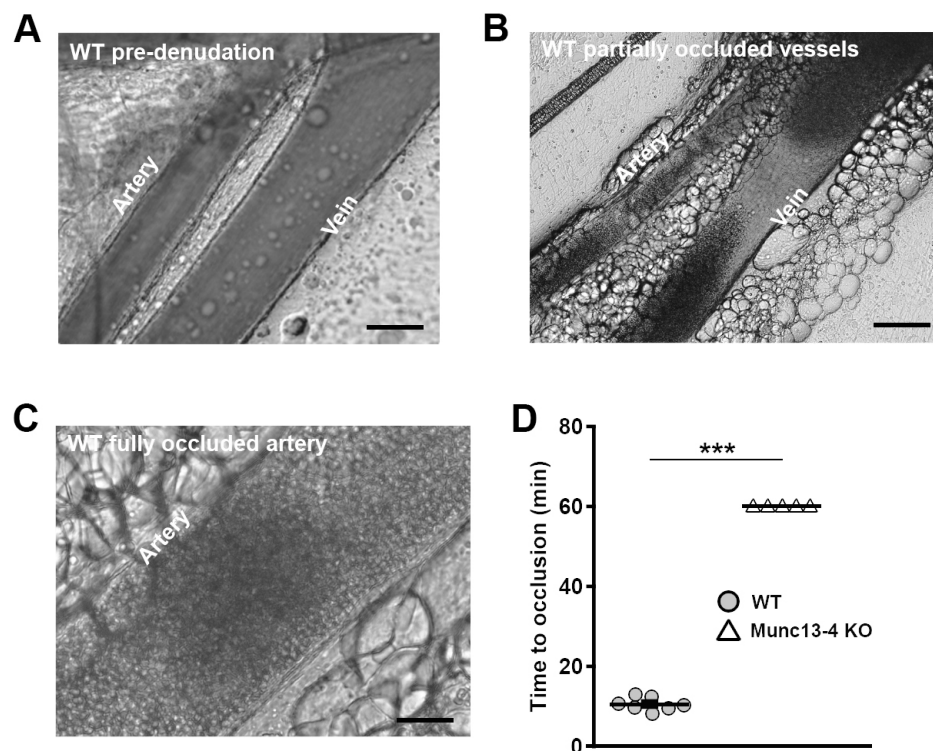
Figure 35: Severely perturbed thrombus formation in Munc13-4 KO mice in vivo.
Three-weeks-old wild-type (WT; gray circles) and Munc13-4 KO mice (Munc13-4 KO; white triangles) were anesthetized with ketamine/xylazine. Through an abdominal incision, the mesenteric bed was carefully pulled out and spread on a heated (37 °C) stage. One artery per animal was denuded with ferric chloride and flow constantly monitored for 60 min. Time was measured until flow stopped completely for more than 1 min. (A-C) Representative brightfield images of wild-type arteries before denudation with ferric chloride (A), partially occluded vessels after denudation (B) and after complete occlusion of the artery (C) (bar length: 1 mm (A,B); 0,25 mm (C)). (D) Quantification of time to occlusion (n = 5-7). Shown are mean values ± S.D.; ***, P<0.001.

Together, these data show that Munc13-4 deficient platelets have normal morphology, granule numbers and contents. Dense granule secretion is abrogated while alpha granule secretion seems mostly unaffected. This secretion defect has major impact on platelet in vivo function in mice as demonstrated in tail bleeding time and thrombosis experiments.

5.2.2 Applying Munc13-4 KO mice to study the impact of dense granule secretion on the progression of atherosclerosis in a mouse model

Having analyzed the secretion properties of Munc13-4 mice in detail, we could now use these mice to assess the progression of atherosclerotic plaque formation compared to control mice. For that purpose, we performed bone marrow transplantation of Munc13-4-deficient and wild-type bone marrow into lethally irradiated LDL receptor knockout mice,

one of the two long-established mouse models of atherosclerosis. Unlike Apolipoprotein E knockout mice, the other commonly used atherosclerosis model in mice, LDLR KO mice only develop atherosclerotic plaques after being fed with a fat- and cholesterol-rich diet. Mice were left on normal chow to recover from irradiation for four weeks. After that time, mice were fed a high-fat, high-cholesterol diet for 16 weeks and body weight was monitored once a week (data not shown). Mice were sacrificed and aortas were excised and carefully prepared for en face staining with Oil Red O, which stains the lipid droplets in atherosclerotic plaques. After staining, aortas were photographed (figure 36 A) and Oil Red O-stained areas were quantified (figure 36 B). There was a slight increase of plaque area in Munc13-4 KO mice but this difference between genotypes was not statistically significant.
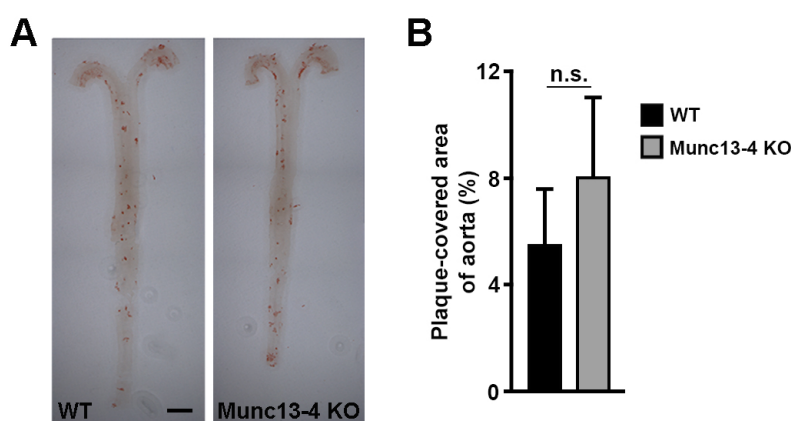

Figure 36: Munc13-4 KO mice have unaltered aortic plaque formation in LDLR KO atherosclerosis model. En face preparations of aortas from LDL receptor knockout mice, which were lethally irradiated and transplanted with bone marrow from either wild-type (WT) or Munc13-4 KO mice (Munc13-4 KO) and fed a high-fat, high-cholesterol diet for 16 weeks were stained with Oil Red O (bar length: 0.5 cm) (A). Plaque area was quantified relative to area of whole aorta (n = 6) (B). Shown are mean values ± S.D.; n.s., not significant.

5.2.3 Studying the role of platelet dense granule secretion in tumor metastasis with Munc13-4-deficient mice

For a long time, evidence has been gathering that platelets are not only activated by tumor cells and are thus responsible for the increased risk of thrombosis in cancer patients (Armand Trousseau, Phlegmasia alba dolens, in: Clinique Medicale de l'Hotel-Dieu de Paris, Vol 3, 2nd Edition, Ballière, Paris, 1865, pp 654-712) but also influence tumor cells in the circulation and the formation of metastasis (Joyce and Pollard 2009; Erpenbeck and Schon 2010; Gay and Felding-Habermann 2011). In experimental settings where platelets were depleted by antibodies, the number of lung metastasis in mouse models was strongly reduced (Erpenbeck and Schon 2010). The mechanisms underlying this effect are still elusive. Since it has been shown that platelets can be directly activated by and bind to tumor cells (Nieswandt, Hafner et al. 1999), we hypothesized that the presence of platelets and possibly platelet secretion could influence properties of tumor cells. We tested this by

applying platelets in a classic transmigration assay where tumor cells transmigrate through an endothelial cell layer in vitro. We added isolated platelets to the top chamber of a transwell plate together with B16 mouse melanoma and Lewis lung mouse carcinoma (LLC1) cells. The tumor cells were stained with calcein prior to the experiment and tumor cell transmigration through a monolayer of Mile Sven I (MS1) microvascular mouse endothelial cells was assessed 15 hours later by counting the tumor cells in the lower chamber. The presence of platelets significantly increased transmigration of tumor cells two- to three-fold compared to tumor cells alone (figure 37 A and B). This increase in tumor cell transmigration was dependent on the presence of endothelial cells, since tumor cell transmigration per se was not altered (figure 37 C).
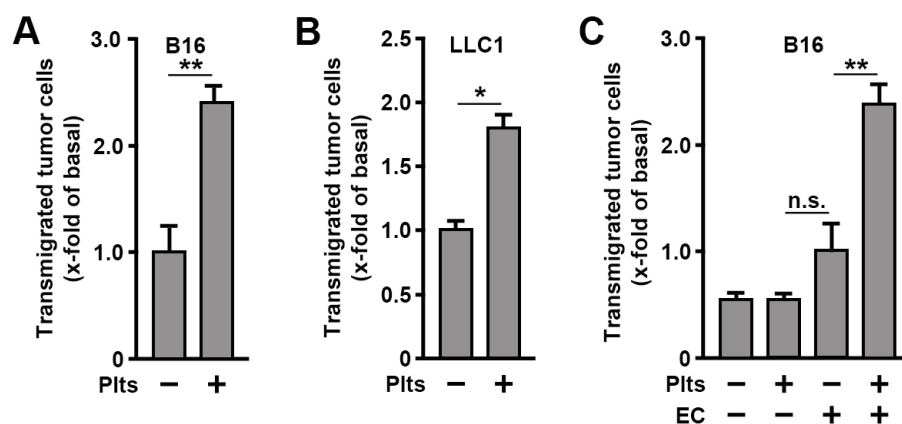

Figure 37: Wild-type platelets enhance B16 and LLC1 tumor cell transmigration through an endothelial layer. (A-C) The indicated murine tumor cells were seeded on murine MS1 microvascular endothelial cells, and tumor cell transmigration was determined in the absence or presence of platelets (-/+ Plts) (A,B) or in absence and presence of endothelial cells (-/+ EC) (C) (n = 5). Shown are mean values ± S.E.M.; *P < 0.05; **P < 0.01; n.s., not significant.

Platelet supernatant from platelets previously stimulated with tumor cells alone was sufficient to induce a boost in tumor cell transmigration while supernatant from unstimulated platelets was without effect (figure 38 A), suggesting that the tumor cell-induced platelet secretion stimulates tumor cell transmigration through an endothelial layer. To test whether soluble mediators of platelet activation were involved, we added the cyclooxygenase inhibitor flurbiprofen to inhibit formation of thromboxane A_2 and the ATP/ADP-dephosphorylating enzyme apyrase to scavenge these nucleotide platelet agonists. Addition of flurbiprofen did not influence the platelet-mediated increase in tumor cell transmigration, but apyrase completely inhibited this increase (figure 38 B). To investigate whether tumor cells induce platelet ATP secretion, we performed luciferase ATP assay on supernatants of platelets alone, B16 tumor cells alone and platelets incubated with tumor cells (figure 38 C). We observed a low basal ATP secretion by tumor cells. High amounts of ATP were released when platelets were incubated with tumor cells, and this ATP secretion was suppressed when apyrase was present in addition (figure 38 C).
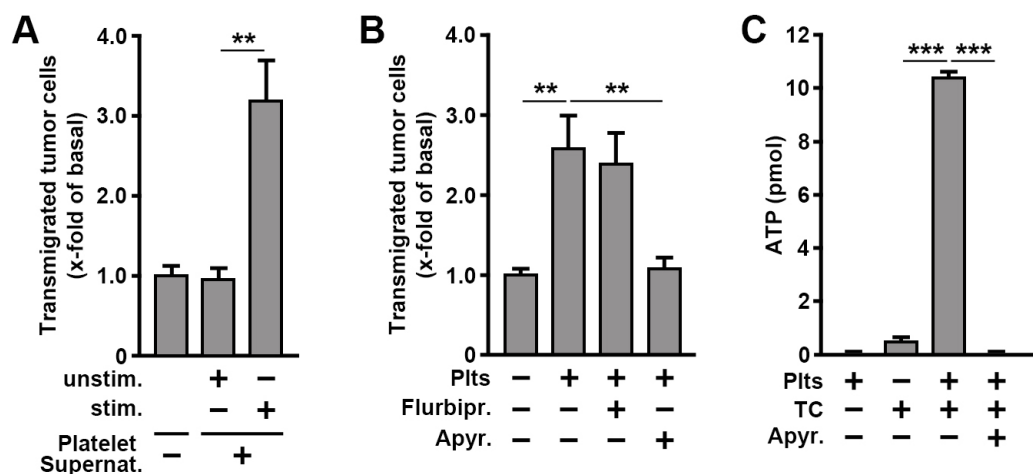
Figure 38: Wild-type platelet releasates enhance B16 tumor cell transmigration, this effect can be reversed by apyrase. B16 melanoma cells were seeded on murine MS1 endothelial cells, and tumor cell transmigration was determined in the absence or presence of supernatants (supernat.) of platelets preincubated in the absence (- stim.) or presence of tumor cells (+ stim.) (A) (n = 5). (B) Effect of the COX-inhibitor flurbiprofen (Flurbipr., 100 nM) or the ATP/ADP degrading enzyme apyrase (Apyr., 20 U/ml) on platelet (Plts)-dependent stimulation of B16 cell transendothelial migration (n = 5). (C) Release of ATP from platelets (Plts) alone, B16 tumor cells (TC) alone or a mixture of tumor cells and platelets (1:100) in the absence or presence of apyrase (-/+ Apyr.; 20 U/ml). Shown are mean values ± S.E.M. (A,B) or S.D. (C); **P<0.01; ***, P<0.001.

We thus investigated if ATP itself influences tumor cell transmigration. Addition of the stable analogue ATPγS (figure 39 A) or increasing concentrations of ATP alone (figure 39 B) indeed evoked a strong increase in transendothelial tumor cell transmigration, indicating that ATP secreted from tumor-cell-activated platelets interferes directly with the transmigration of tumor cells through an endothelial layer.
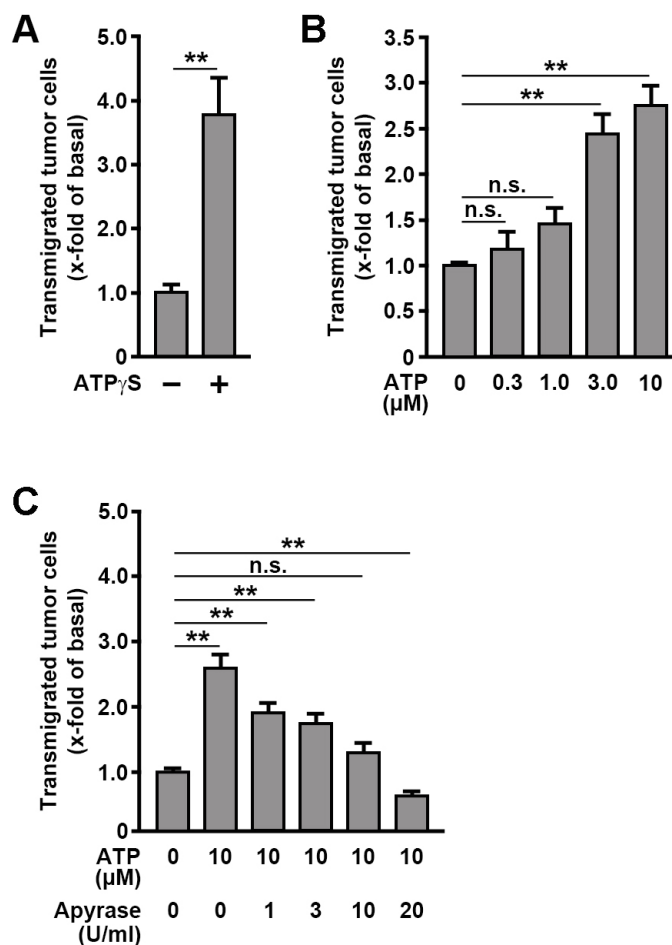
Figure 39: Exogenous addition ATP or its stable analogue ATPγS stimulate tumor cell transmigration. (A-C) B16 melanoma cells were seeded on murine MS1 endothelial cells, and tumor cell transmigration was determined. Effect of ATPγS (10 µM) (A) or increasing concentrations of ATP (B) on tumor cell transmigration (n = 5). (C) Effect of increasing concentrations of apyrase on the ATP-dependent stimulation of B16 tumor cell transmigration. Shown are mean values ± S.E.M.; **, P<0.01; n.s., not significant.

This observation lead us to investigate whether ATP released from platelets acts on endothelial cells and thereby influences tumor cell transmigration. We used FITC-labeled dextran added to the upper chamber of a transwell assay to monitor changes in permeability of an endothelial monolayer upon addition of supernatant from platelets alone, B16 tumor cells alone and platelets incubated with rumor cells in the absence or presence of apyrase (figure 40). Only the supernatant of tumor-cell-stimulated platelets lead to a marked increase in endothelial permeability when FITC-dextran levels on the bottom of the lower well were measured and this effect was completely inhibited by the presence of apyrase.
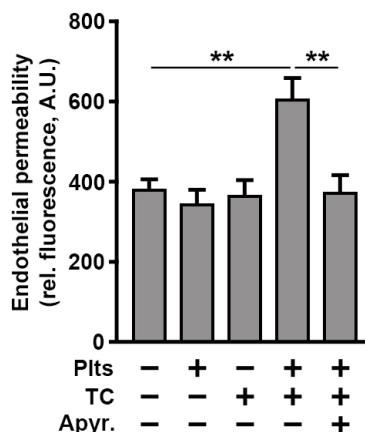
Figure 40: Supernatant from platelets stimulated with tumor cells increases endothelial permeability, an effect, which can be abrogated by addition of apyrase. MS1 endothelial cells were grown to a monolayer and buffer; supernatants from platelets alone (+ Plts), B16 tumor cells alone (+ TC) or platelets stimulated with tumor cells in the absence or presence of apyrase (20 U/ml; -/+ Apyr.) were added to the upper chamber together with FITC-labeled dextran 70,000 kDa. Diffusion of FITC-dextran through the endothelial layer to the lower chamber was measured after 90 min. Shown are mean values ± S.D.; **, $P<0.01$.

Endothelial permeability is mediated by endothelial barrier function, so we visualized the effect of supernatants of platelets alone, tumor cells alone, platelets stimulated with tumor cells and platelets stimulated with tumor cells together with apyrase on MS1 endothelial cell morphology by immunocytochemistry (figure 41). A marker for endothelial adherens junctions (VE cadherin) together with staining for f-actin revealed a significant increase in discontinuous endothelial junctions in MS1 cells incubated with supernatant from tumor-cell stimulated platelets. This effect was inhibited by addition of apyrase to the platelet-tumor cell suspension (figure 41 A). Quantification of two independent experiments is shown in figure 41 B.
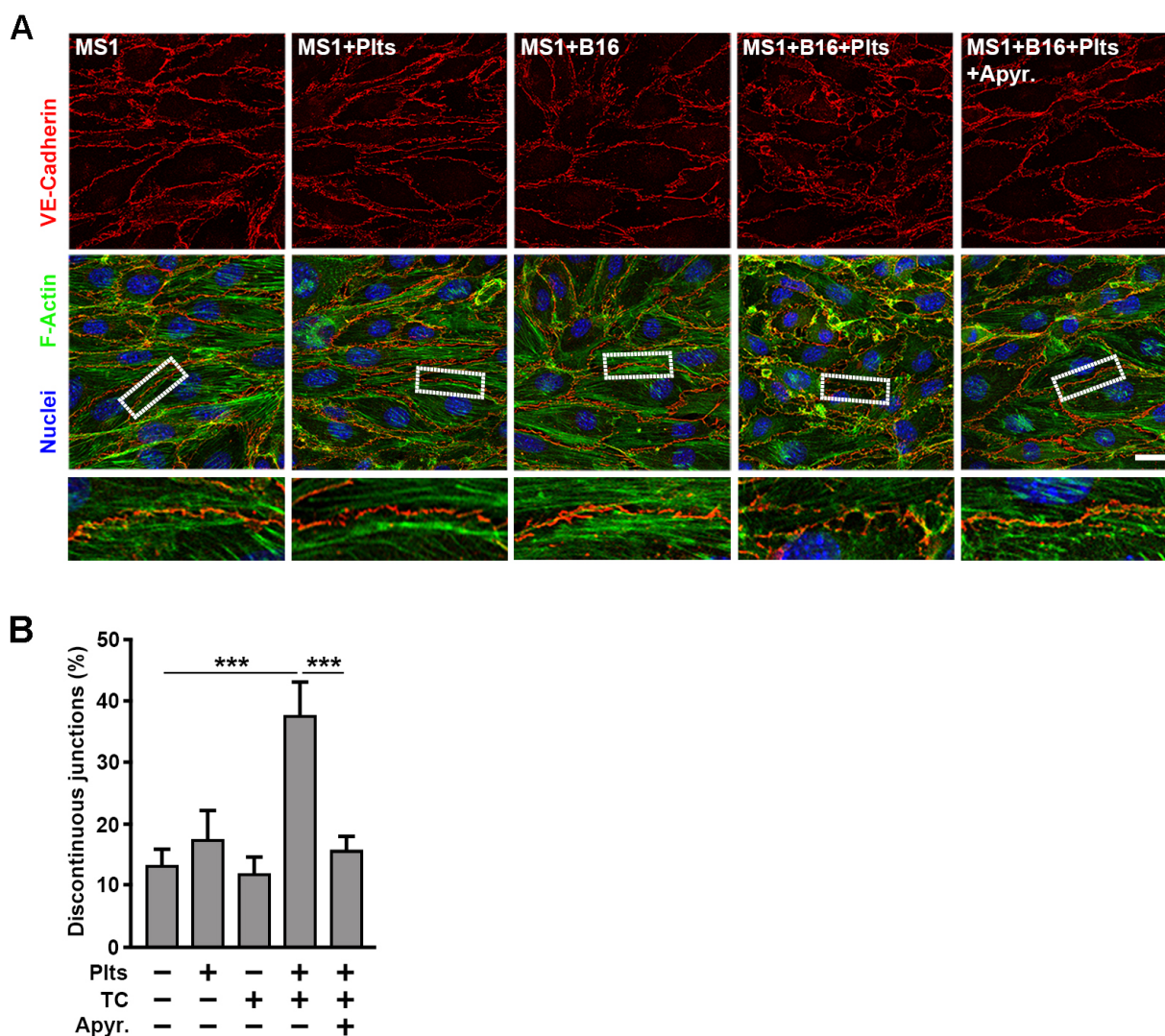
Figure 41: Supernatant from platelets stimulated with tumor cells destabilizes endothelial barriers, an effect, which can be abrogated by addition of apyrase. (A,B) MS1 endothelial cells were grown to a monolayer and buffer, supernatants from platelets alone (+ Plts), B16 tumor cells alone (+ TC) or platelets stimulated with tumor cells in the absence or presence of apyrase (-/+ Apyr.) were added for 90 min. MS1 cells were then fixed and stained for the adherens junction marker VE-cadherin (red) and f-actin (green), nuclei were stained with DAPI (blue). Representative confocal images are shown in (A), white boxes are enlarged at the bottom. Discontinuous junctions were quantified in (B) (n = 6). Shown are mean values ± S.D.; ***, P<0.001.

Together, these findings indicate that release of nucleotides from platelets enhances tumor cell transmigration trough an endothelial cell layer by modifying endothelial barriers in vitro. These observations translate to a human cell set-up where human tumor cells transmigrate trough Human umbilical vein endothelial cells (HUVECs) in the presence and absence of isolated human platelets. The number of transmigrated pancreatic carcinoma (CFPAC-1) (figure 42 A) and neuroblastoma (SH-SY5Y) (figure 42 B) cells was approximately two to

three-fold higher when supernatant from tumor cell-stimulated platelets was present compared to tumor cells alone. Various human tumor cell lines were able to induce ATP release in human platelets (figure 42 C). Permeability of monolayer of HUVEC was strongly increased after addition of tumor-cell-stimulated platelets and apyrase completely blocked this increase (figure 42 D).
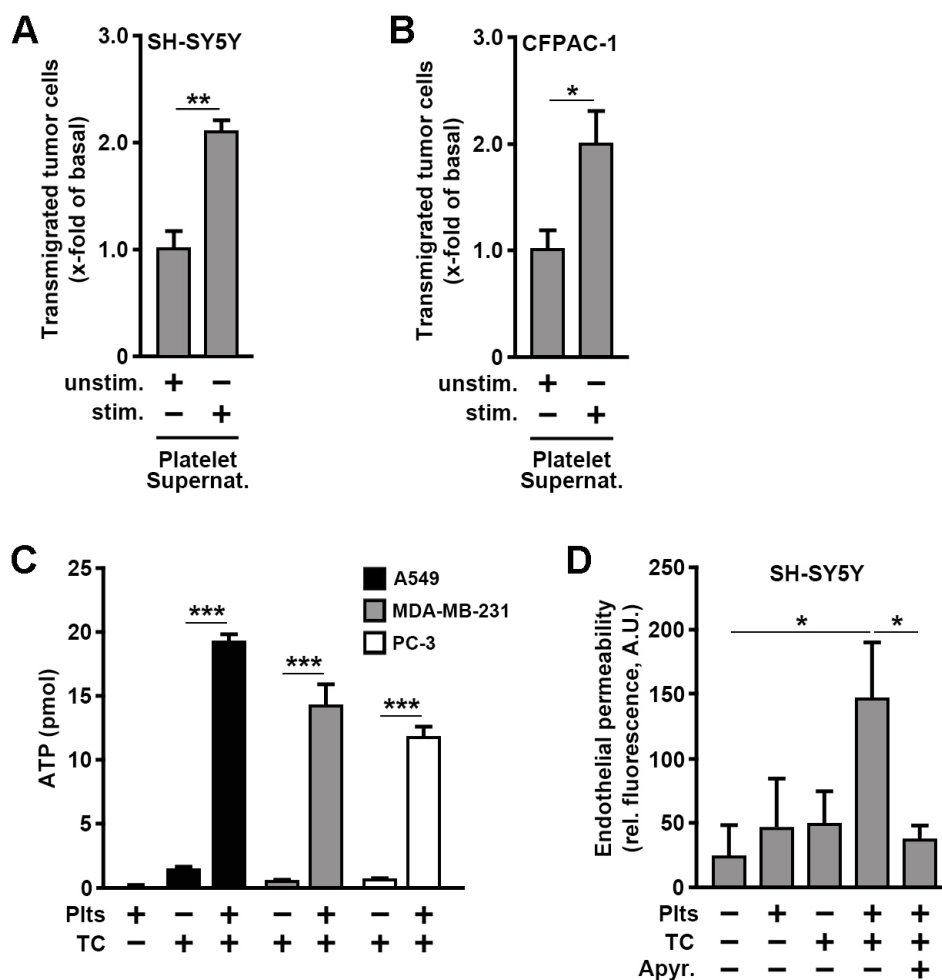

Figure 42: Human platelets enhance tumor cell transmigration through a HUVEC monolayer via release of ATP and disruption of endothelial barriers. Supernatants of human platelets preincubated in the absence (- stim.) or presence (+ stim.) of SH-SY5Y human neuroblastoma (A) or CFPAC-1 human pancreatic carcinoma cells were added to a monolayer of umbilical vein endothelial cells (HUVEC). Transmigration of the respective tumor cells through the endothelial cell layer was determined (n = 5). (C) Release of ATP from platelets (Plts) alone, A549 human lung carcinoma (A549; black bars), MDA-MB-231 breast adenocarcinoma (MDA-MB 231; grey bars) or PC-3 prostate adenocarcinoma (PC-3, white bars) cells (TC) alone or a mixture of tumor cells and platelets (1:100) incubated for 10 min (n = 5). (D) HUVEC were grown to a monolayer and buffer, supernatants from platelets alone (+ Plts), SH-SY5Y tumor cells alone (+ TC) or platelets stimulated with tumor cells in the absence or presence of apyrase (20 U/ml; -/+ Apyr.) were added to the upper chamber together with FITC-labeled dextran 70,000 kDa. Diffusion of FITC-dextran

through the endothelial layer to the lower chamber was measured after 90 min (n = 5). Shown are mean values± S.D. (C,D) or ± S.E.M. (A,B); *P < 0.05; **P < 0.01; ***, P<0.001.

There is evidence for a number of potential mechanisms how tumor cells interact directly with platelets, notably through platelet P-selectin and integrin αIIbβ3 (Erpenbeck and Schon 2010; Gay and Felding-Habermann 2011). B16 tumor cells have been shown to expose tissue factor on their surface (Amarzguioui, Peng et al. 2006; Niers, Bruggemann et al. 2009) and potential thrombin generation on the surface of B16 cell could activate platelets. We used hirudin to inhibit thrombin formation, antibodies against most known platelet surface receptors or pre-incubation of tumor cells with anti-podoplanin antibody to inhibit binding to platelet CLEC-2 to study their impact on platelet-dependent enhancement of tumor cell transmigration (figure 43 A). The addition of thrombin inhibitor hirudin to tumor cells prior to addition to the transmigration assay and lead to a partial but significant reduction in the stimulating effect of platelets on tumor cell transmigration, but there was substantial variation between experiments (data not shown). Blocking of P-selectin on platelets reduced the transmigration of tumor cells and this slight reduction was reproducible in independent experiments (data not shown) but not significant, whereas the reduction of GPIbα was very variable. None of the tested antibodies and inhibitors decreased platelet-mediated B16 tumor cell transmigration to basal levels. Addition of hirudin as well as addition of the antibody against P-selectin to platelets prior to incubation with tumor cells also lead to lower levels of ATP secretion compared to wild-type platelets and B16 tumor cells alone, although this was not significant (figure 43 B).
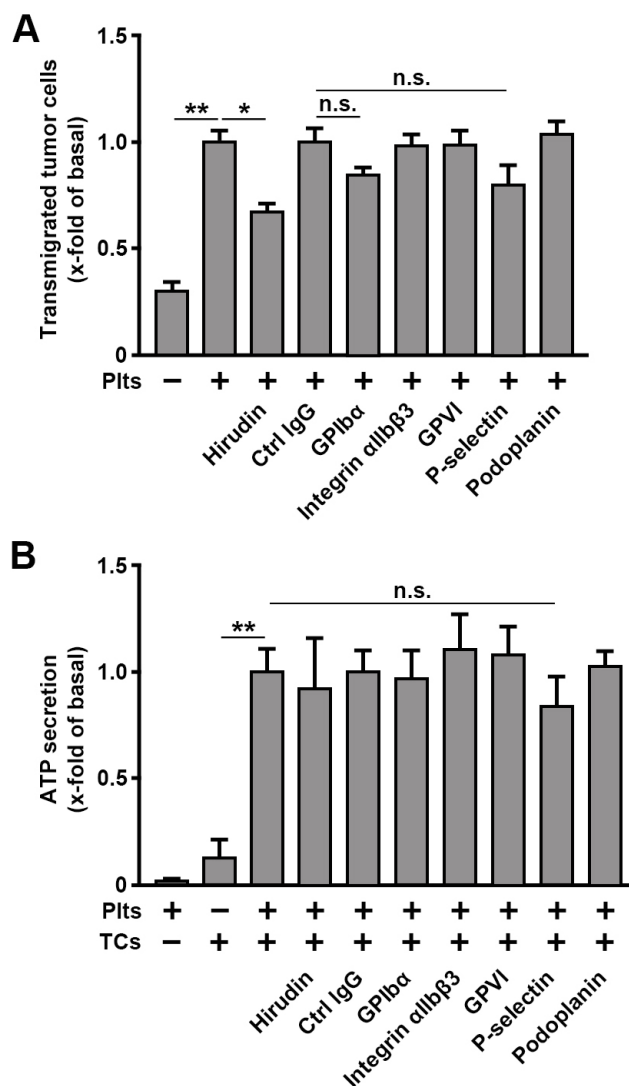
Figure 43: Platelet-mediated enhancement of tumor cell transmigration and tumor-cell-induced platelet ATP release are not influenced by a panel of blocking agents. (A) B16 tumor cells were seeded on murine MS1 microvascular endothelial cells, and tumor cell transmigration was determined in the presence of platelet supernatants of unstimulated platelets (- Plts) or platelets incubated with the thrombin inactivator hirudin, blocking antibodies against the indicated platelet surface proteins or the tumor cell surface protein podoplanin and stimulated with B16 tumor cells (+ Plts) (n = 5). (B) Release of ATP from platelets (Plts) alone, B16 tumor cells (TC) alone or a mixture of tumor cells and platelets (1:100) in the absence or presence of the same blocking agents as in (A). Shown are mean values ± S.E.M. (A) or S.D. (B);); *P < 0.05; **P < 0.01; n.s., not significant.

The fact that none of the inhibitors of receptors and mediators known or suspected to influence platelet-tumor cell interactions (Erpenbeck and Schon 2010; Gay and Felding-Habermann 2011) showed a strong effect in our in vitro transmigration assay indicates that it is either a combination of several factors or a yet unknown mechanism by which tumor cells elicit platelet secretion in our transmigration set-up.

To further investigate whether nucleotides released from platelet dense granules mediate the increase in tumor cell transmigration, we employed Munc13-4 KO platelets as a suitable tool since extensive analysis proved that Munc13-4 KO platelets have a specific deficit in dense granule secretion (see above). We compared the number of transmigrated B16 (figure 44 A) and LLC1 (figure 44 B) tumor cells upon the addition of wild-type and Munc13-4-deficient platelets to the upper chamber. Munc13-4 KO platelets in addition to both tumor cell lines showed the same amount of transmigrated tumor cells as tumor cells alone (figure 44), further indicating that release of dense granule contents from tumor-cell-activated platelets is the source of increased transendothelial migration of tumor cells.
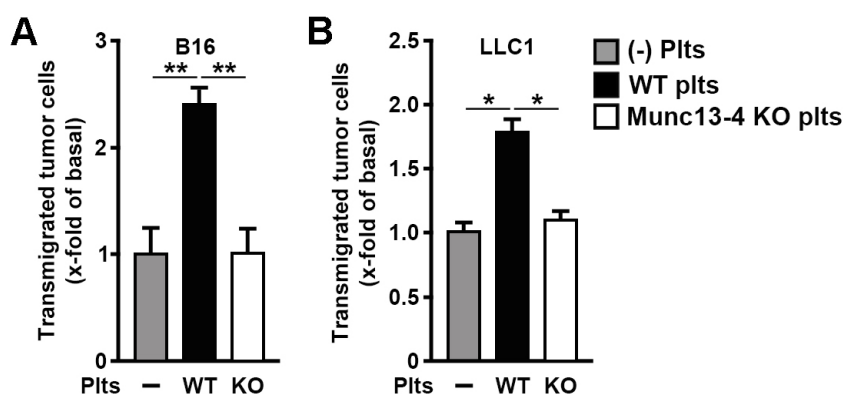
Figure 44: Platelets with defective ATP secretion impede platelet-mediated enhancement of tumor cell transmigration. (A,B) B16 (A) and LLC1 (B) tumor cell transmigration in the absence (- Plts) or presence of wild-type (WT) or Munc13-4 KO (KO) platelets through an MS1 endothelial layer (n = 5). Shown are mean values ± S.E.M.; *P < 0.05; **P < 0.01.

To exclude that activation of platelets by tumor cells uses mechanisms which elicit a different secretion pattern in platelets than the agonists used above, we repeated vWF (figure 45 A) and PF4 (figure 45 B) ELISAs and ATP luciferase assay (figure 45 C) applying B16 and LLC1 tumor cells as stimuli. In line with the results for the classical platelet agonists, we observed similar levels of PF4 and vWF secretion in wild-type and Munc13-4-deficient platelets whereas no ATP secretion above the levels measured for tumor cells alone was detected for tumor cells incubated with Munc13-4-deficient platelets.
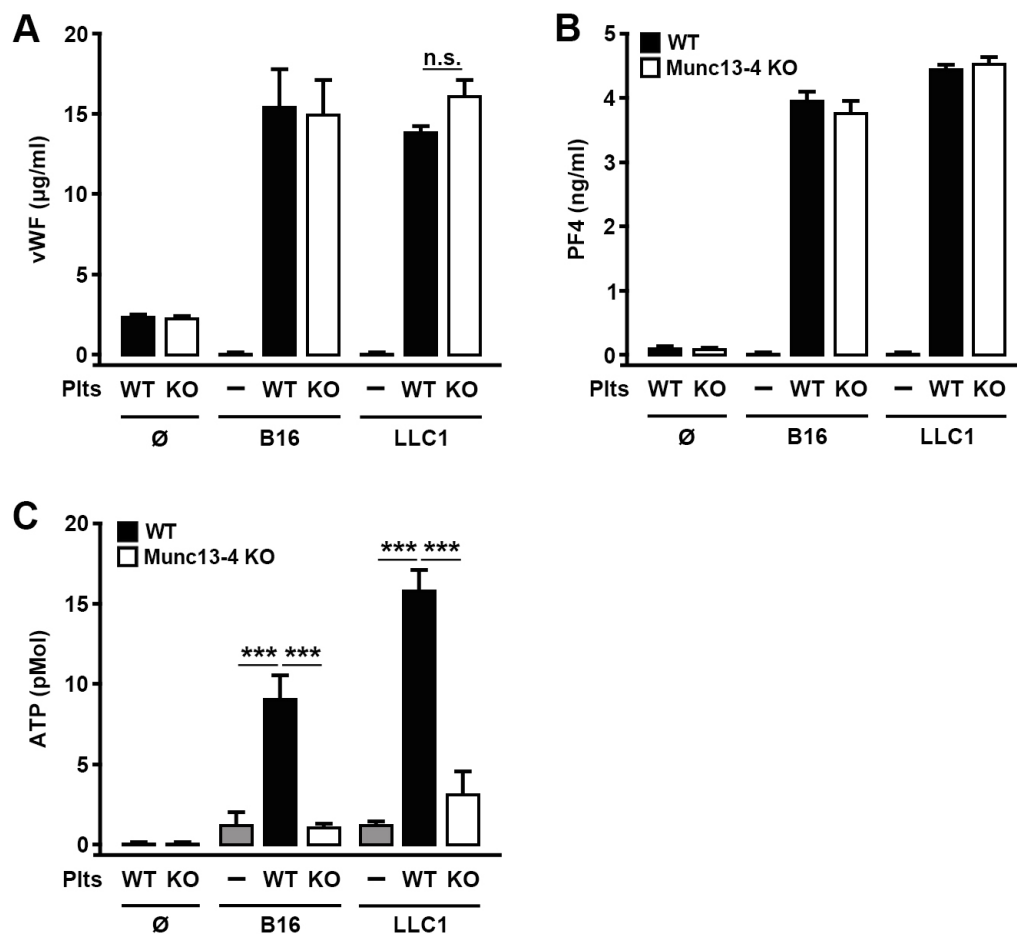
Figure 45: Munc13-4 KO platelets exhibit normal alpha granule protein release but abrogated ATP release in response to tumor cells. (A,B) Effect of increasing concentrations of thrombin on release of platelet factor 4 (PF4) (A), von Willebrand factor (vWF) (B) or ATP (C) from wild-type (WT) or Munc13-4-deficient platelets (KO) (n = 3-5). Shown are mean values ± S.D.; ***, P<0.001; n.s., not significant.

It has been shown that platelets can adhere and stably attach to tumor cells (Nieswandt, Hafner et al. 1999). This property alone could possibly influence activation of platelets by tumor cells or survival of tumor cells in the circulation (Palumbo, Talmage et al. 2005; Gay and Felding-Habermann 2011), so we labeled isolated wild-type and Munc13-4 KO platelets with CFSE and incubated them with B16 melanoma cells. We used confocal microscopy to visualize binding of fluorescent platelets to tumor cells (figure 46 A) and quantified the CFSE signal on tumor cells with flow cytometry (figure 46 B). Munc13-4-deficient platelets equally bound to tumor cells although it appeared as if it was more single platelets, each in contact with the tumor cell. In wild-type platelets, two or more platelets could often be found attached to each other and the tumor cell. Quantification clearly proved that this did not influence total amount of platelets bound to tumor cells since there was no difference between genotypes.
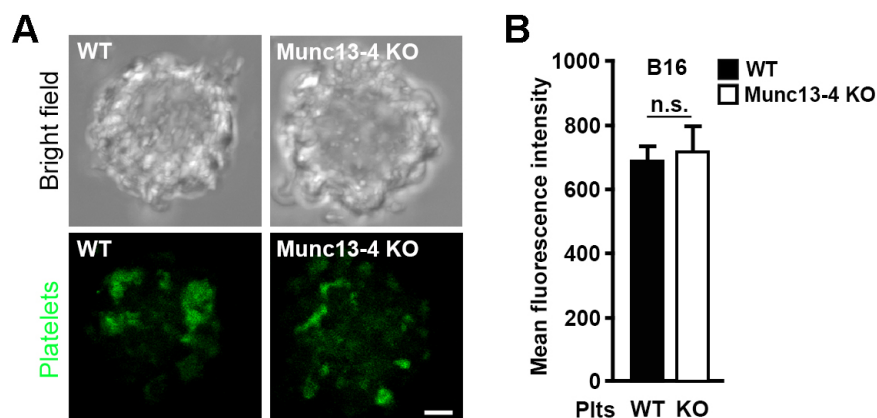
Figure 46: **Munc-13-4 KO platelets show normal adhesion to tumor cells.** (A,B) Washed wild-type (WT) and Munc13-4 KO (KO) platelets were labeled with CFSE (green) and incubated with B16 melanoma cells. (A) Confocal stacks were taken and representative images of maximum projections are displayed (bar length: 2 µm). (B) Quantification was performed by measuring the amount of CFSE-labeling in a gate set on tumor cells in flow cytometry (n = 6). Shown are mean values ± S.D.; n.s., not significant.

The availability of Munc13-4 KO mice with their unique property of defective platelet dense granule secretion provided the means to investigate the significance of platelet nucleotide secretion in in vivo tumor models. Since endothelial secretion of vWF could influence tumor cell adhesion to the vessel wall (Kerk, Strozyk et al. 2010), we determined expression levels of the four Munc13 isoforms (Munc13-1, -2, -3, -4) in the MS1 mouse microvascular endothelial cell line (Figure 47 A) and mouse primary lung endothelial cells (figure 47 B) to exclude a contribution of defective endothelial secretion in Munc13-4 KO mice. Munc13-2 was the only Munc13 isoform detected in mouse endothelial cells.

Figure 47: **The murine microvascular endothelial cell line MS1 and mouse primary lung endothelial cells express the Munc13-2 isoform.** (A,B) Two independent RNA preparations from MS1 (A) and isolated primary lung endothelial (B) cells

were combined and expression of the four known Munc13 isoforms was
determined relative to 18 S rRNA (n = 3). Shown are mean values ± S.D..
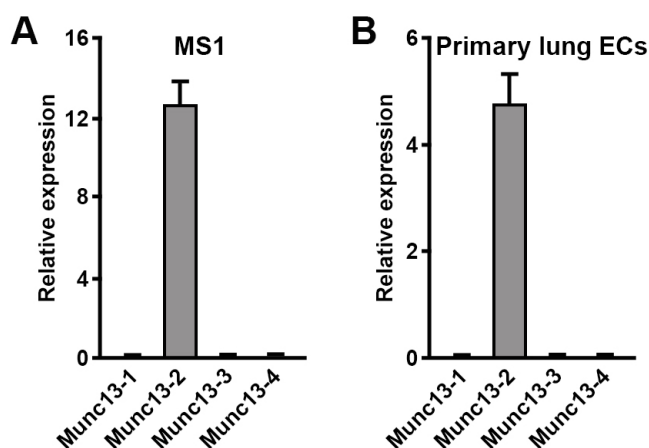
Munc13-4 KO mice are thus a good tool to investigate the role of platelet dense granule
release in B16 and LLC1 tumor models. We therefore employed both primary tumor models
by injecting B16 and LLC1 tumor cells in the flank of mice and intravenous injection of both
C57/Bl6 tumor cell lines to study metastasis formation dependent and independent of a
primary tumor. For the flank tumor model, tumor growth was regularly monitored by caliper
measurement. Mice were sacrificed after 21 days and lungs and primary tumors removed.
Primary tumor weight was determined and tumors were sectioned and analyzed for gross
angiogenesis defects by CD31 staining. B16 primary tumors from wild-type (figure 48 A)
and Munc13-4 KO mice (figure 48 B) showed no difference in CD31 staining. Quantification
of vessel length (Figure 48 C) and diameter (figure 48 D) was also unaltered in Munc13-4-
deficient mice compared to wild-type mice.

Figure 48: **Primary tumors from flank injection of B16 melanoma cells show
comparable vessel formation in wild-type and Munc13-4 KO mice.** (A-D)
Wild-type and Munc13-4 KO mice were injected subcutaneously with 1×10^6 B16
melanoma cells. Mice were sacrificed after 21 days, primary tumors excised and
30 µm cryosections were analyzed with CD31 staining to visualize the endothelial
layer in vessels (red). Representative maximum projections of confocal stacks
from wild-type (A) and Munc13-4 KO (B) animals are shown (bar length: 20 µm).
Quantification of vessel length (C) and diameter (D) of five randomly chosen

areas per animal was done (n = 3). Shown are mean values ± S.D.; n.s., not significant.

Exemplary images of LLC1 tumors derived from wild-type (figure 49 A) and Munc13-4 KO mice (figure 49 B) as well as quantification of vessel length (figure 49 C) and vessel diameter (figure 49 D) revealed that also in this tumor model, the parameters assessed here for tumor angiogenesis are unchanged in Munc13-4 KO mice. Hematoxylin/eosin (H/E) stained sections from both primary tumor models confirmed this finding (data not shown).
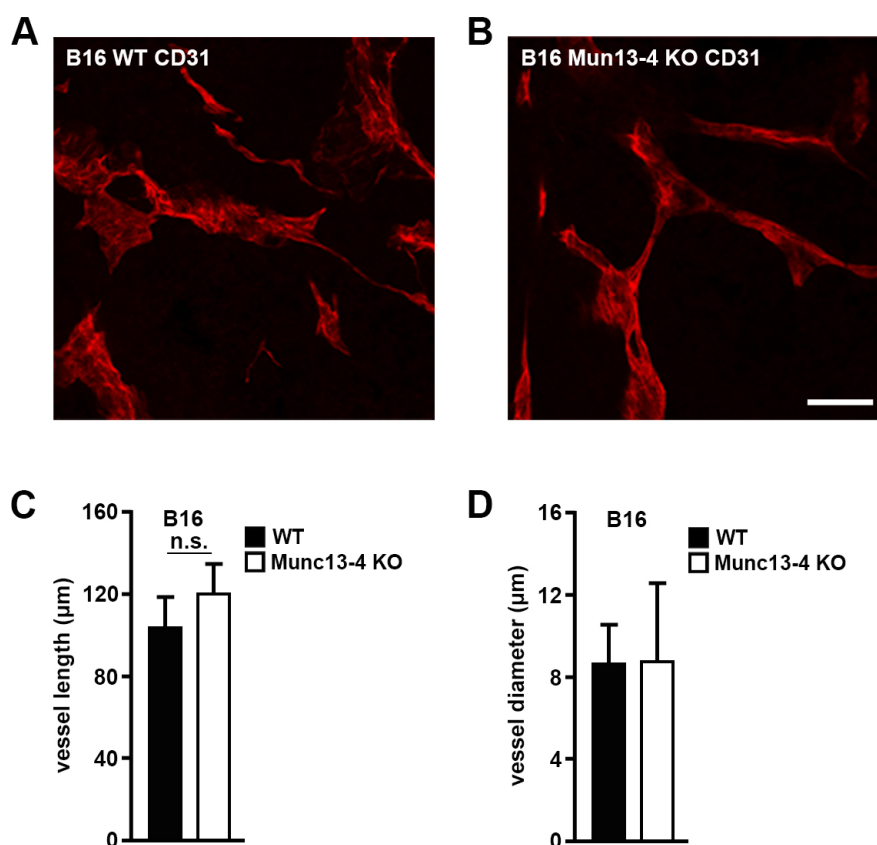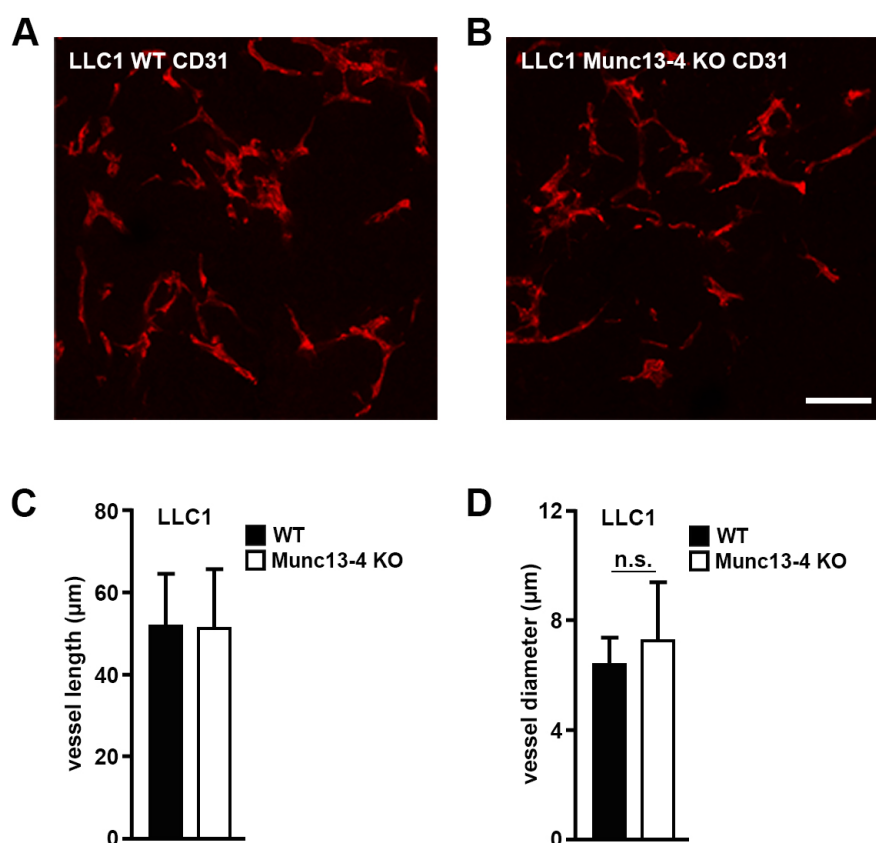

Figure 49: Primary tumors from flank injection of LLC1 carcinoma cells show comparable vessel formation in wild-type and Munc13-4 KO mice. (A-D) Wild-type and Munc13-4 KO mice were injected subcutaneously with 1×10^6 LLC1 cells. Mice were sacrificed after 21 days; primary tumors excised and 30 μm cryosections were analyzed with CD31 staining to visualize the endothelial layer in vessels (red). Representative maximum projections of confocal stacks from wild-type (A) and Munc13-4 KO (B) animals are shown (bar length: 20 μm). Quantification of vessel length (C) and diameter (D) of five randomly chosen areas per animal was done (n = 3). Shown are mean values ± S.D.; n.s., not significant.

There was also no difference in B16 primary tumor growth (data not shown) and tumor weight (figure 50 A) between wild-type and Munc13-4 KO animals. In contrast, formation of metastases in the lung determined by H/E stained sections throughout the lung was

strongly reduced in Munc13-4 deficient mice (figure 50 B). Splitting in size categories revealed that metastases of all sizes were markedly reduced, indicating that growth of metastases, once established, was not affected. Likewise, tumor weight of tumors derived from flank-injected LLC1 cells (figure 50 C) was unchanged in Munc13-4 KO mice compared to wild-type mice and the number of lung metastases was also strongly reduced (figure 50 D) in Munc13-4-deficient animals.
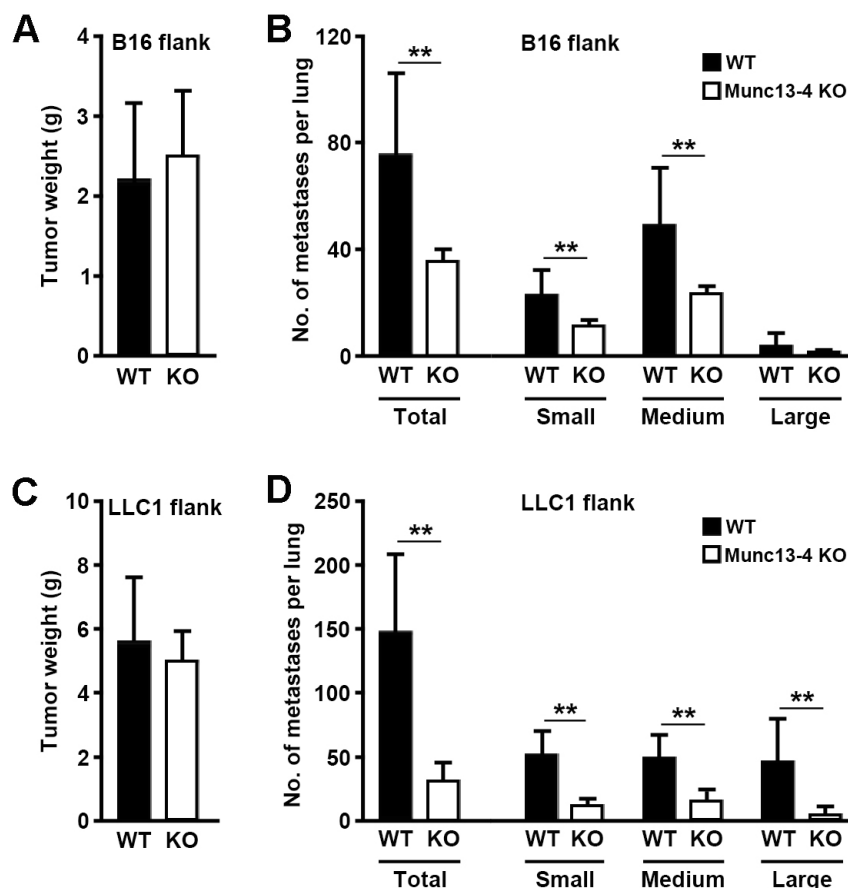
Figure 50: **Primary tumor weight after flank injection of B16 and LLC1 is unchanged but metastasis is strongly impaired in Munc13-4 KO mice compared to wild-type mice.** (A-D) Wild-type and Munc13-4 KO mice were injected subcutaneously with 1×10^{6} B16 (A,B) or LLC1 (C,D) cells. Mice were sacrificed after 21 days, primary tumors excised and weighed (A,C) (n = 6-10). Lungs were cut and metastases counted with H/E staining. Metastases were grouped in small (diameter: <0.1 mm), medium-sized (diameter: 0.1-1.0 mm) or large (diameter: >1.0 mm) metastases (B,D) (n = 6-10). diameter (with CD31 staining to visualize the endothelial layer in vessels (red). Shown are mean values ± S.D.; *, P<0.05; **, P<0.01; n.s., not significant.

I.v. injection of tumor cells is used to study seeding of organs independent of a primary tumor and effects influencing priming of tumor cells for intravasation and intravasation into the circulation. When we injected B16 melanoma (figure 51 A) or LLC1 carcinoma (figure

51 B) cells into the tail vein of mice, we observed strongly diminished formation of metastases in the lungs of Munc13-4 KO mice compared to wild-type mice after 12 days.
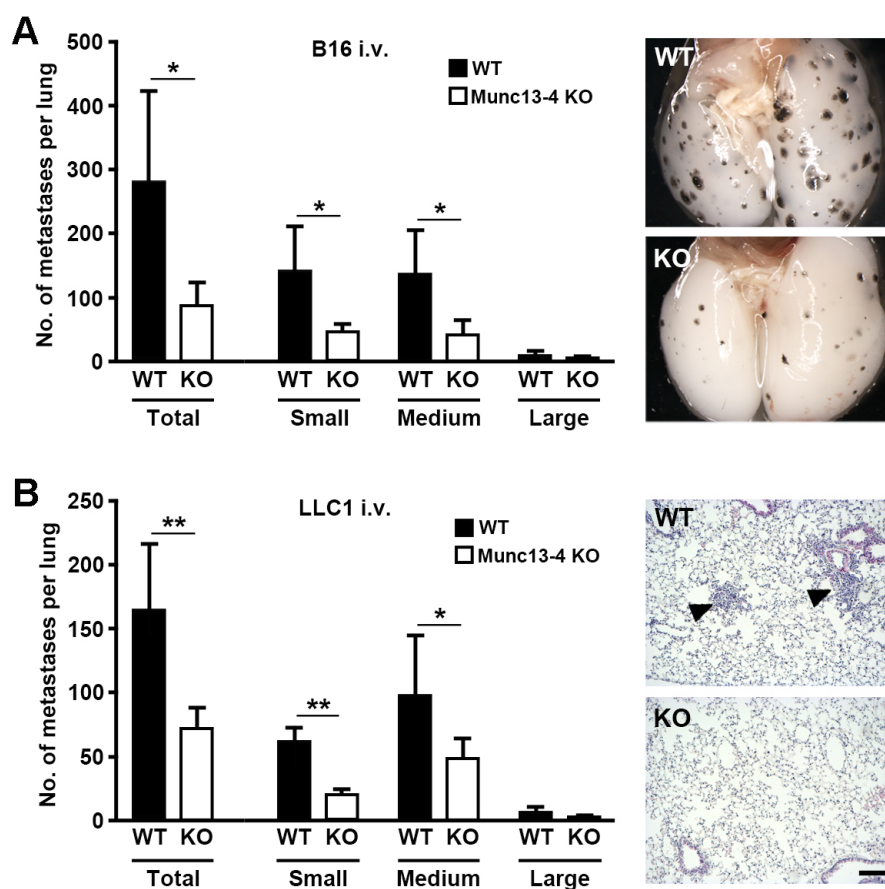
Figure 51: Formation of metastases is strongly reduced in Munc13-4 KO mice compared to wild-type mice after B16 or LLC1 i.v. injection. (A,B) B16 (A) or LLC1 cells (B) were injected i.v. into wild-type (WT) or Munc13-4-deficient mice (KO), and 12 days later, lung metastases were evaluated with H/E staining as in figure (n = 6-10). The images show representative lung surface metastases (A) or stained lung sections (B) from wild-type (WT) or Munc13-4-deficient mice (KO). Bar length: 100 µm. Arrowheads indicate metastases. Shown are mean values ± S.D.; *, P<0.05; **, P<0.01.

These findings suggest that progression of primary tumors and tumor angiogenesis is not affected by the absence of platelet dense granule secretion while dense granule secretion has a strong impact on the occurrence of lung metastasis in the models investigated in this study, possibly by mechanisms which influence tumor cell extravasation as suggested by the enhancement of tumor cell transmigration in the presence of platelets in vitro and strongly reduced metastasis after tumor cell i.v. injection in vivo. Taking into account that tumor cell transmigration in the absence of endothelial cells is unchanged by the addition of platelets and apyrase can block the platelet-mediated transendothelial migration of tumor cells, we hypothesized that molecules released from platelet dense granules upon

stimulation by tumor cells, in particular nucleotides, act on endothelial receptors and modify endothelial junctions, thereby allowing tumor cells a more efficient passage.

To test this hypothesis, we first determined the levels of P2Y metabotropic and P2X ionotropic receptors on the pancreatic microvascular cell line used for the in vitro experiments, MS1 (figure 52 A and B), mouse primary lung endothelial cells (figure 52 C and D), and human umbilical vein endothelial cells (HUVECs) (figure 52 E and F).

Figure 52: P2Y and P2X receptor expression in the murine microvascular endothelial cell line MS1, mouse primary lung endothelial cells and human umbilical vein endothelial cells (HUVEC). (A-F) Two independent RNA preparations from MS1 (A,B), isolated primary lung endothelial cells (C,D) and HUVEC (E,F) were
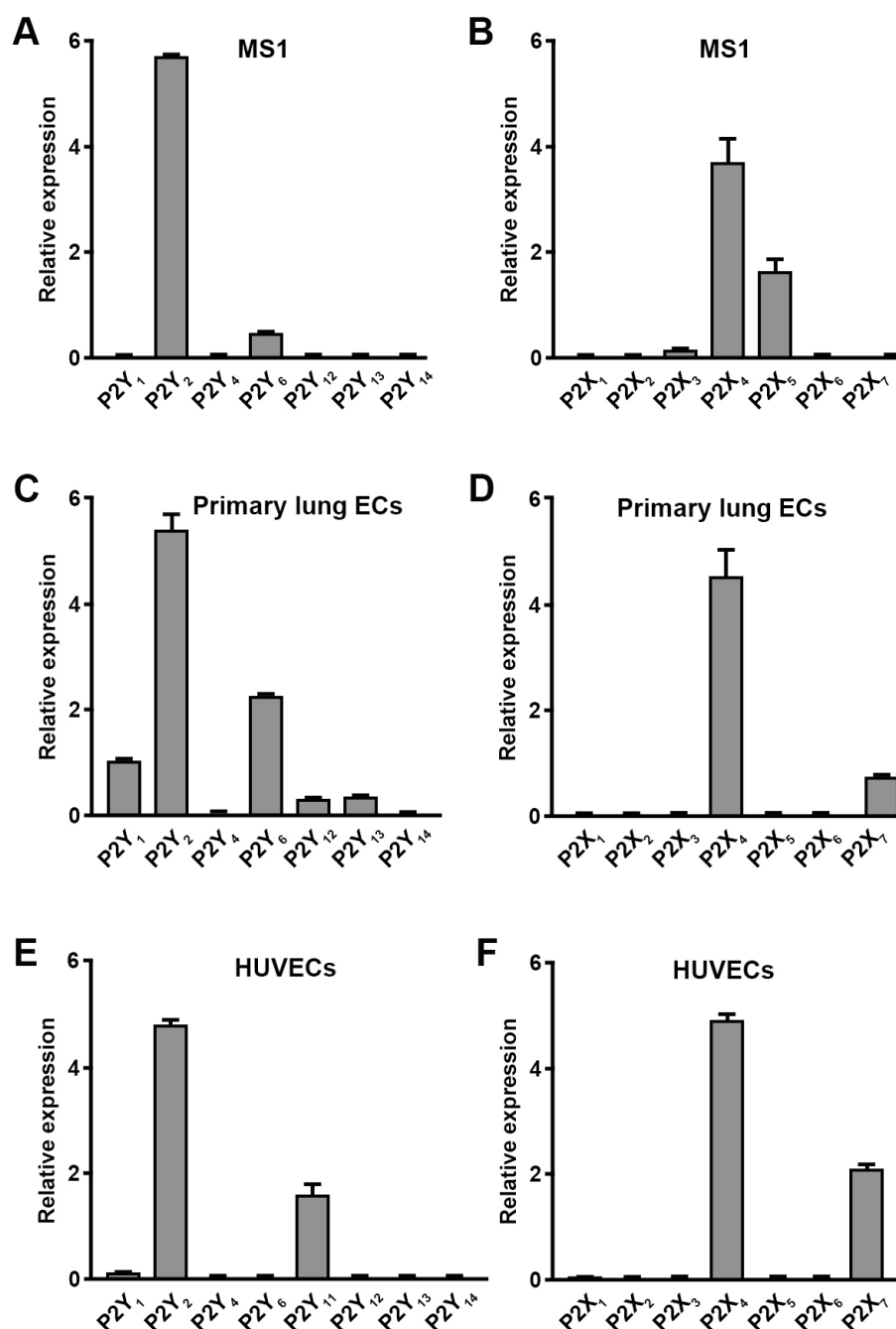
combined and expression of P2Y (A,C,E) and P2X (B,D,F) subtypes was determined relative to 18 S rRNA (n = 3). Shown are mean values ± S.D..

Since ATP alone was sufficient to enhance tumor cell transmigration in vitro, we focused on receptors with great ATP affinity (table 24). This excludes $P2Y_6$ (UDP) and leaves $P2Y_1$, $P2Y_2$ and $P2X_4$ as the most likely candidates mediating the ATP effects on endothelial cells.

Receptor	Agonist	Organism	Mode of action	Unit	Affinity
P2Y1	ATP	Human	Partial agonist	pIC_{50}	6.1 - 7.8
	ADP	Human	Full agonist	pIC_{50}	6.2 - 7.2
P2Y2	UTP	Human	Full agonist	pEC_{50}	8.1
	ATP	Human	Full agonist	pEC_{50}	7.07
P2Y4	UTP	Human	Full agonist	pEC_{50}	6.3
	ATP	Rat	Partial agonist	pEC_{50}	5.7 - 6.3
P2Y6	UDP	Human	Full agonist	pEC_{50}	6.5
	UTP	Human	Partial agonist	pEC_{50}	5.2
	ADP	Human	Partial agonist	pEC_{50}	4.5
P2Y11	UTP	Human	Full agonist	pEC_{50}	5.2
	ATP	Human	Full agonist	pEC_{50}	4.2 - 5.6
P2Y12	ADP	Human	Full agonist	pK_i	5.9
	ATP	Human	Full agonist	pK_i	5.2
P2Y13	ADP	Human	Full agonist	pIC_{50}	6.5
	ATP	Human	Full agonist	pIC_{50}	5.4
P2Y14	UDP-glucose	Mouse	Full agonist	pEC_{50}	7.7
	UDP-glucose	Rat	Full agonist	pEC_{50}	7.6
	UDP-glucose	Human	Full agonist	pIC_{50}	7.1

Table 24: **Affinities of P2Y receptor subtypes for their natural ligands.** Affinities for ATP and ADP were highlighted with red letters. $P2Y_2$ receptor has the highest affinity for ATP, this is marked with grey background. Source: IUPHAR database (www.iuphar.org), July 5th 2012.

To test if blockade of any of the ATP receptor found to be expressed on endothelial cells has an impact on platelet-induced transmigration of tumor cells through an endothelial layer, we used specific antagonists against $P2Y_1$ and $P2X_4$ (figure 53 A) and knockdown of $P2Y_1$, $P2Y_2$ and $P2X_4$ mRNAs (figure 53 B). Platelet-dependent tumor cell transmigration was not influenced by inhibition or knockdown of $P2Y_1$ and $P2X_4$, but knockdown of $P2Y_2$ mRNA, for which no selective antagonist is available, strongly reduced enhancement of tumor cell transmigration by platelets compared to control siRNA-transfected MS1 cells. Results are normalized to transmigration of B16 tumor cells alone through a monolayer of endothelial cells transfected with control siRNA.
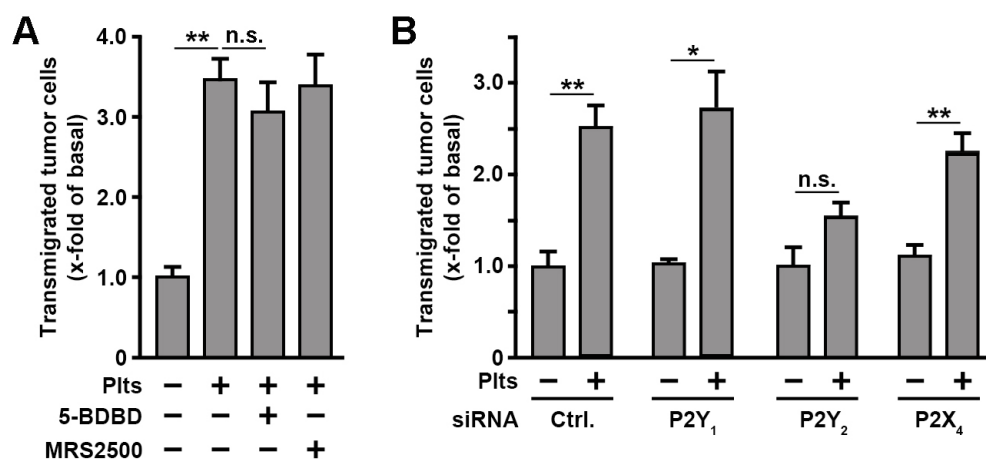
Figure 53: Platelet-mediated facilitation of tumor cell transmigration involves P2Y$_2$ receptors. (A) Effect of the P2X$_4$ receptor antagonist 5-BDBD (1 µM) and of the P2Y$_1$ antagonist MRS2500 (100 nM) on platelet-stimulated transendothelial migration of B16 cells (n = 5). (B) Endothelial cells were transfected with control siRNA or with siRNAs directed against the mRNAs encoding P2Y$_1$, P2Y$_2$ or P2X$_4$. Thereafter, transmigration of B16 cells was determined in the absence or presence of platelets (-/+ Plts) (n = 5). Shown are mean values ± S.E.M; *P < 0.05; **P < 0.01; n.s., not significant.

Knockdown efficiencies of siRNA against P2Y$_1$ (figure 54 A), P2Y$_2$ (figure 54 B) and P2X$_4$ (figure 54 C) were determined by qPCR with and normalized to 18S rRNA and H3F3A. Efficiencies ranged from roughly 80 % (P2X$_4$) to approximately 90 % (P2Y$_1$).
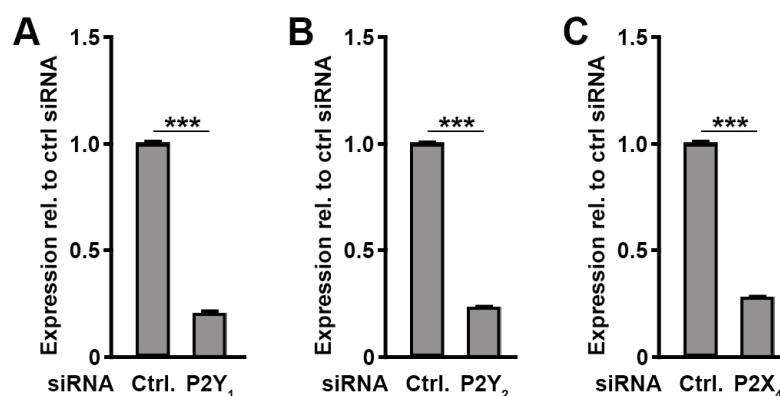
Figure 54: Knockdown efficiencies in MS1 cells for siRNAs against P2Y$_1$, P2Y$_2$ or P2X$_4$. (A-C) MS1 endothelial cells were transfected with control siRNA or with siRNAs directed against the mRNAs encoding P2Y$_1$ (A), P2Y$_2$ (B) or P2X$_4$ (C) in parallel to the MS1 cells used for the transmigration experiments shown in figure. After 48 hours, when the transmigration assay was started, RNA was isolated and qPCR performed. Results are normalized to 18S rRNA and H3F3A levels (n = 4). Shown are mean values ± S.D.; ***P < 0.001.

For the siRNA against P2Y$_2$, functional effects of the knockdown were assessed in a Fluo4-based Calcium assay (figure 55 A and B) showing decrease of approximately 85 % in

maximum mobilization of intracellular Calcium upon addition of the specific P2Y$_2$ agonist UTP.
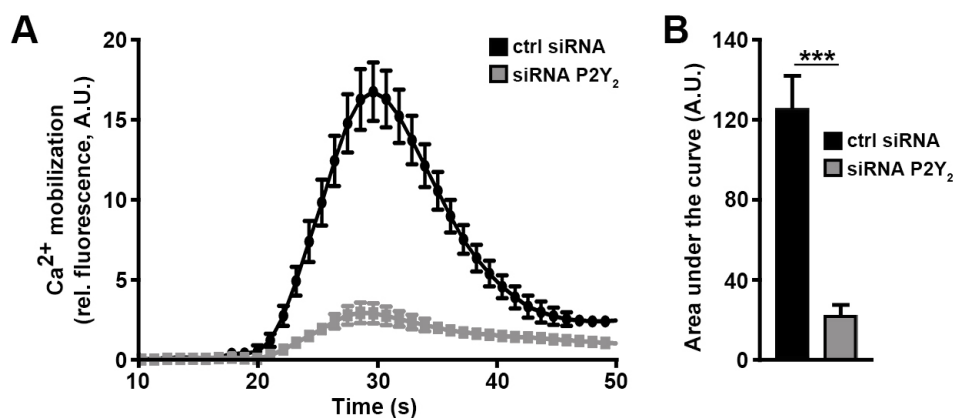
Figure 55: Functional analysis of knockdown of P2Y$_2$ mRNA in MS1 cells. (A,B) MS1 endothelial cells were transfected with control siRNA or with siRNA directed against the mRNA encoding P2Y$_2$ (as in figure and figure). 48 hours later, UTP effects (10 µM) on free intracellular [Ca2+]$_i$ in Fluo4-loaded cells (n = 5) were determined. Graphs of control siRNA-treated (ctrl siRNA) and transfected with siRNA against P2Y$_2$ mRNA (siRNA P2Y$_2$) are shown (A) and area under the curve was calculated for the interval 20 - 50 s (B). Shown are mean values ± S.D.; ***P < 0.001.

The results obtained for P2Y$_2$ receptor mRNA knockdown in endothelial cells in transmigrations assays employing B16 melanoma cells could be confirmed under the same conditions with transmigrating LLC1 carcinoma cells (figure 56). The number of transmigrated LLC1 cells upon addition of platelets was reduced to the level of tumor cell transmigration in the absence of platelets, when endothelial cells were transfected with siRNA against P2Y$_2$.
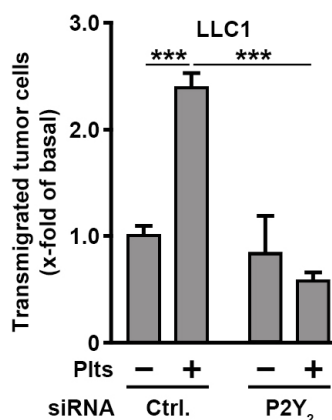
Figure 56: Knockdown of P2Y$_2$ receptor mRNA leads to reversal of platelet-enhanced tumor cell transmigration. Endothelial cells were transfected with control siRNA or with siRNA directed against the mRNA encoding P2Y$_2$. Thereafter,

transmigration of LLC1 cells was determined in the absence or presence of platelets (-/+ Plts) (n = 5). Shown are mean values ± S.E.M***P < 0.001.

We also determined whether P2Y receptors are expressed in the mouse tumor cell lines used in this study, B16 melanoma and LLC1 carcinoma, and did not find any of the seven known mouse P2Y receptors expressed (data not shown) on these tumor cell lines. This is in accordance with the unresponsiveness of both B16 and LLC1 cells to platelets in the transmigration assay without endothelial monolayer (figure 37 C and data not shown) despite the fact that high levels of ATP and ADP released from platelets must be present (figure 38 C).

Collectively, the in vitro data suggest that platelets are activated by tumor cells (figures 38 C, 42 C, 45 A-C), secrete large amounts of ATP (figures 38 C, 42 C, 45 C) which act locally on endothelial $P2Y_2$ receptors (figures 53 B, 56), open endothelial barriers (figures 40, 41, 42 D) and lead to an increase in transmigrated tumor cells. We next investigated whether similar mechanisms cause the major reduction in primary tumor and i.v. metastasis models observed in Munc13-4-deficient mice which lack ATP secretion (figure 51). Therefore, we injected a 70'000 kDa FITC-labeled dextran solution one minute before tail vein injection of 100'000 B16 melanoma cells in wild-type, Munc13-4 KO and $P2Y_2$ KO mice, sacrificed the animals after 3 hours and immediately collected the lungs in para-formaldehyde. Immunostaining of the endothelial marker PECAM-1 (CD31) and DAPI for visualization of nuclei revealed spots of FITC-dextran in extraluminal sites of wild-type lungs injected with FITC-dextran and B16 tumor cells (figure 57 A, quantification in 57 B). Leakage of FITC-dextran into the parenchyma was only minimal in wild-type mice that were not injected with B16 tumor cells (control condition), Munc13-4 KO and $P2Y_2$ KO lungs, suggesting that indeed, wild-type platelets facilitate tumor cell-dependent vascular leakage of the lung endothelium and either inhibition of dense granule secretion or deletion of the $P2Y_2$ receptor reverses this effect.
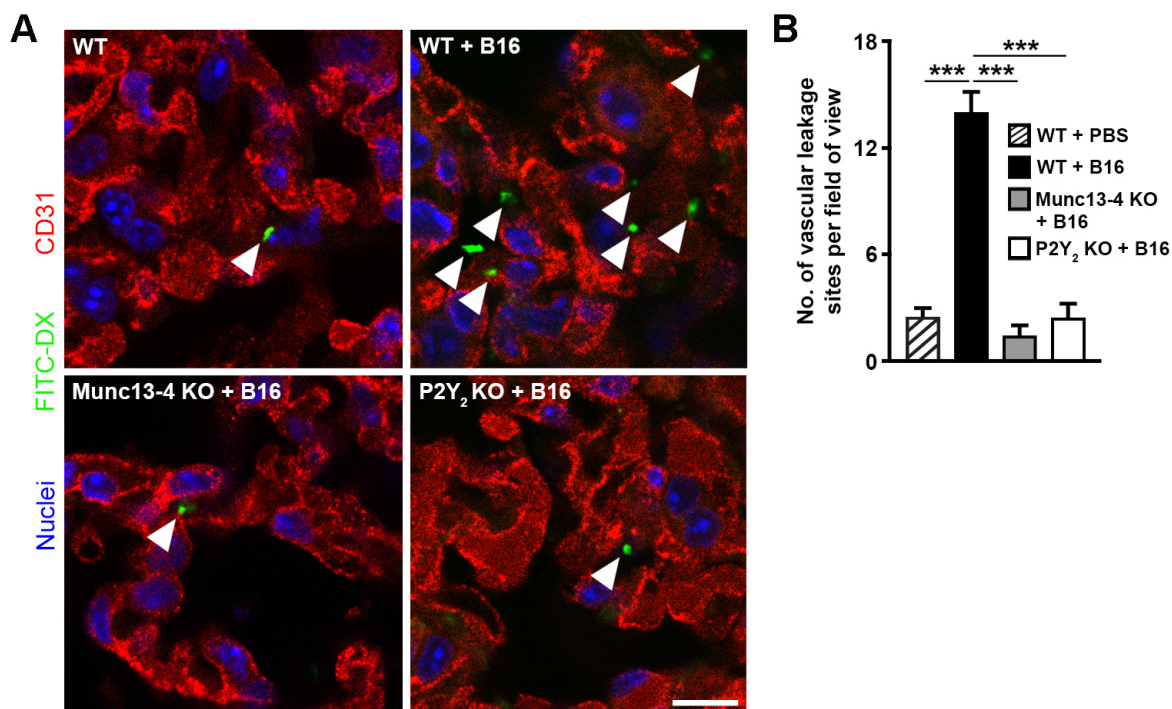
Figure 57: **Platelet-mediated enhancement of tumor cell-dependent FITC-dextran vascular leakage in the lung is abrogated in mice with defective ATP secretion and in P2Y$_2$ receptor knockout mice.** FITC-dextran (70,000 kDa) was injected i.v. 30 s before B16 tumor cells (1x10^5) or buffer into wild-type (WT), Munc13-4-deficient (Munc13-4 KO) or P2Y$_2$-deficient (P2Y$_2$ KO) mice. 3 hours after injection, lungs were excised and cryosections stained for CD31 (red) or cell nuclei (blue). Representative images are displayed in (A), extravasation sites of FITC-dextran (FITC-DX; green) are indicated by arrowheads (bar length: 10 μm). The bar diagram (B) shows a quantification of extraluminal FITC-positive sites (n = 4). Shown are mean values ± S.D; ***P < 0.001.

To test whether reduced vascular leakage in Munc13-4 KO and P2Y$_2$ KO corresponds to less extravasation of tumor cells at early time points after tumor cell injection, we labeled B16 tumor cells with CFSE, excised the lungs 6 hours post-injection and analyzed lung sections. We found markedly reduced numbers of extravasating B16 tumor cells in Munc13-4 KO and P2Y$_2$ KO lungs compared to wild-type lungs. Extravasating tumor cells were identified by protrusions and cell parts reaching out of the lumen (figure 58 A). Quantification is shown in figure 58 B.
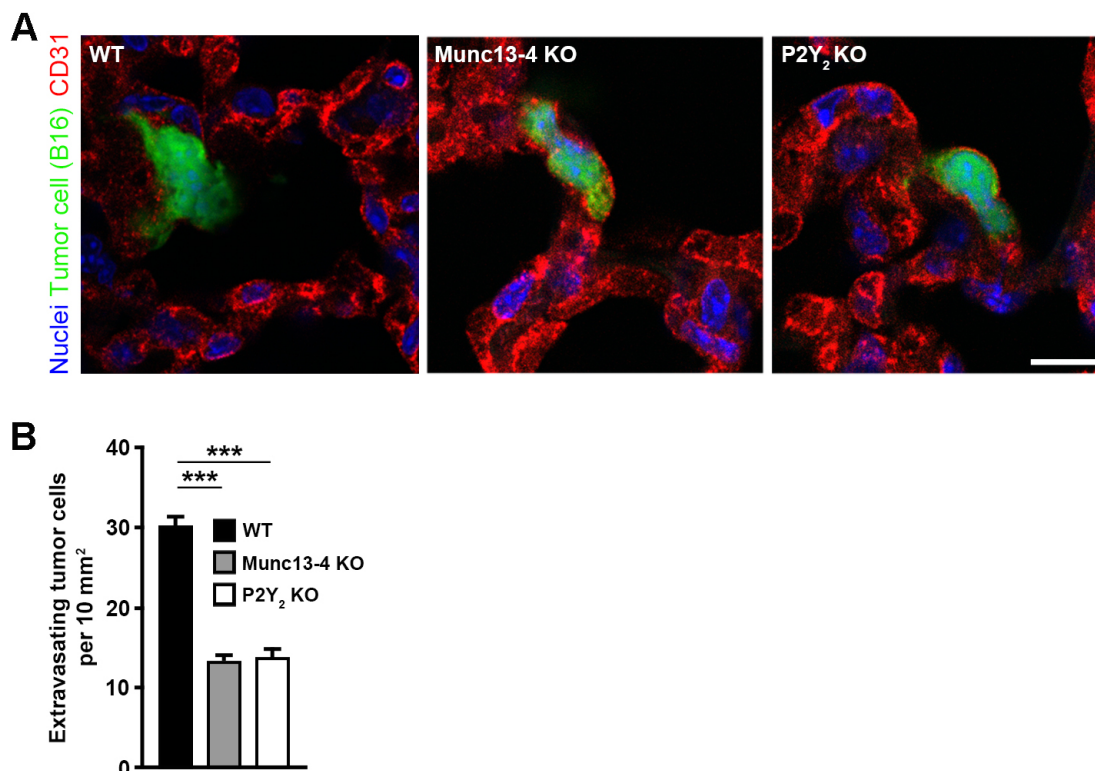
Figure 58: Platelet-mediated facilitation of tumor cell extravasation and metastasis involves ATP secretion from platelets and P2Y$_2$ receptors. (A,B) Extravasation of CFSE-labeled B16 cells in the lungs of wild-type (WT), Munc13-4-deficient (Munc14-3 KO) or P2Y$_2$-deficient (P2Y$_2$ KO) mice 6 hours after i.v.-injection. Shown in (A) are representative images of lung sections stained for CD31 (red) or cell nuclei (blue), B16 cells are in green (bar length: 10 μm). The numbers of extravasating tumor cells per 10 mm^2 lung area are quantified in (B) (n = 9-10). Shown are mean values ± S.D.; ***P < 0.001.

We next determined whether less vascular permeability of FITC-dextran in P2Y$_2$ KO mice and reduced numbers of extravasating tumor cells in these animals a few hours after tumor cell injection translates to less metastasis after 12 days post-injection. Indeed, we observed strongly reduced formation of pulmonary metastases after tail vein injection of B16 melanoma (figure 59 A) and LLC1 carcinoma (figure 59 B) cells in P2Y$_2$ KO mice compared to wild-type controls. The level of reduction in metastasis in P2Y$_2$ KO mice (figure 59) corresponded to the level of reduction observed in Munc13-4 KO mice (figure 51), ranging between 60-75%. These findings further support the concept that ATP released by platelets modifies endothelial junctions through P2Y$_2$ receptors and facilitates tumor cell passage through the endothelial layer.
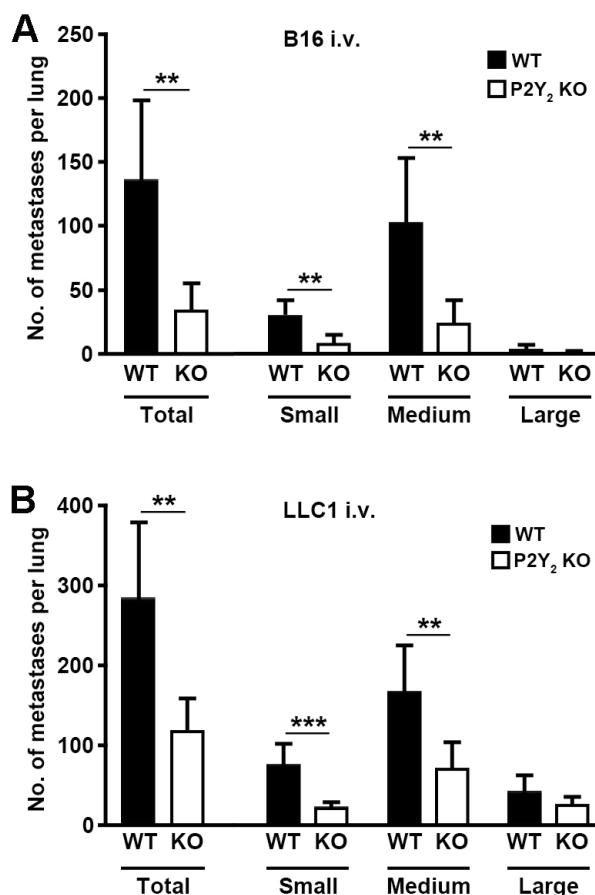
Figure 59: Formation of metastases involves the ATP receptor $P2Y_2$. (A,B) B16 (A) and LLC1 cells (B) were injected i.v. in wild-type (WT) and $P2Y_2$-deficient mice (KO), and 12 days later, lung metastases were analyzed histologically (n = 7-10). Shown are mean values ± S.D.; **P < 0.01; ***P < 0.001.

NK cells lead host defense against circulating tumor cells and have been shown to strongly influence metastasis (Nieswandt, Hafner et al. 1999; Palumbo, Talmage et al. 2005). NK cell lysis of target cells involves Munc13-4, NK cells lacking Munc13-4 are largely unable to lyse target cells in vitro (Crozat, Hoebe et al. 2007). NK cells from Munc13-4 KO mice should therefore provide less protection from formation of metastases in these mice and rather counteract the lack of platelet dense granule secretion. We assessed the number of metastases in wild-type and Munc13-4 KO mice after i.v. injection of B16 melanoma cells under NK cell-depleted conditions. Repeated injection of anti-asialo GM1 antibody depleted NK cells by more than 90% throughout the experiment (figure 60 A). The reduction of metastasis in Munc13-4-deficient animals compared to wild-type mice was not influenced by NK cell depletion (figure 60 B). A recent publication (Granot, Henke et al. 2011) showed an involvement of neutrophil $P2Y_2$ receptor in metastasis of breast cancer cells. In addition, it was reported that release of tertiary granules of in vitro differentiated human neutrophils was slightly decreased after knock-down of Munc13-4 mRNA (Pivot-Pajot, Varoqueaux et al. 2008), so we tested whether depletion of neutrophils in wild-type, Munc13-4 KO and $P2Y_2$ KO mice had an impact on the metastasis phenotype observed after B16 melanoma

injection into the tail vein. Using an anti-Ly6G antibody, neutrophils could be depleted by roughly 80-90% throughout the experiment (figure 60 C) and formation of metastases in the lung was still strongly reduced in both Munc13-4-deficient and P2Y$_2$-deficient animals compared to wild-types (figure 60 D).
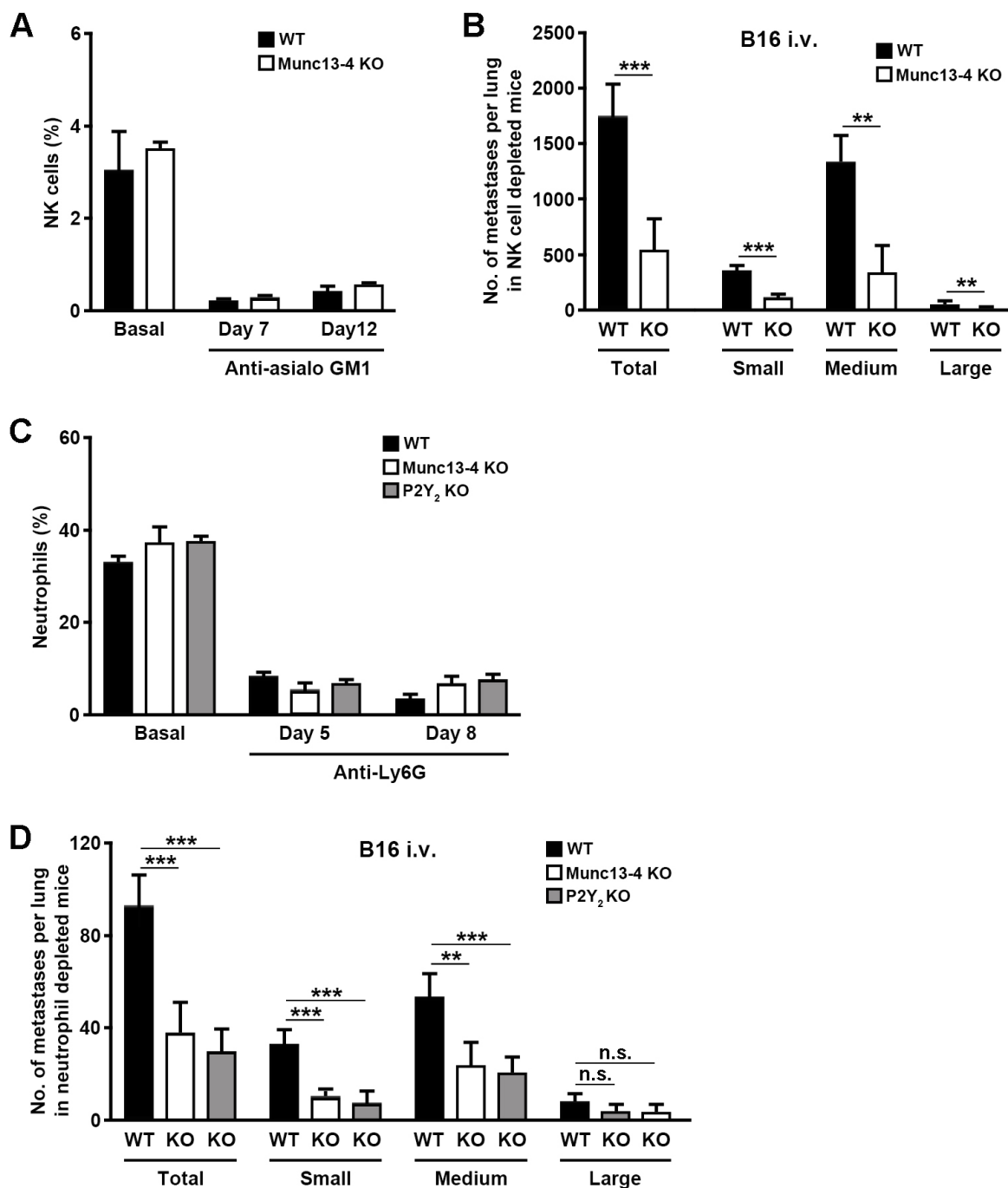
Figure 60: Effect of NK-cell depletion and neutrophil depletion on metastasis of B16 tumor cells in wild-type, Munc13-4-deficient and P2Y$_2$-deficient mice. (A) NK cell counts as identified by NK1.1 and CD3e staining in flow cytometry relative to granulocyte number before antibody injection and on day 7 and 12 after tumor

cell injection (n = 4-5). (B) Number of lung metastases detected in H/E staining in antibody treated wild-type (WT) and Munc13-4-deficient (Munc13-4 KO) mice (n = 4-5). NK cells were depleted using repeated injections of anti-asialo GM1 antibody. (C) Percentage of Ly6G-positive neutrophils relative to granulocyte number before antibody injection and on day 5 and 8 after tumor cell injection (n = 5). (D) Number of lung metastases detected in H/E staining in antibody treated wild-type (WT) Munc13-4-deficient (Munc13-4 KO) and P2Y$_2$-deficient (P2Y$_2$ KO) mice (n = 5). Neutrophils were depleted using repeated injections of anti-Ly6G antibody. Shown are mean values ± S.D.; **, P < 0.01; ***P < 0.001; n.s., not significant.

6 <u>Discussion</u>

As mentioned in the introduction, many studies in recent decades have revealed a role for platelets exceeding their primary function in hemostasis. Considering their ability to secrete two types of vesicles, alpha and dense granules, packed with a multitude of known signaling molecules and intercellular mediators, to interact directly with various other cell types and even show distinct responses in different milieus despite their lack of a nucleus, it is not surprising that evidence is accumulating for a contribution of platelets to such diverse pathophysiological outcomes as atherosclerosis and cancer. Since these two diseases are the leading causes of death in industrial civilizations and there may be therapeutic potential for anti-platelet treatments, we sought to evaluate the role of platelet secretion in mouse models for atherosclerosis and cancer. So far, no genetic tool was available in mice that lead to a defined secretion defect in platelets while keeping morphology and other platelet functions intact. Thus, we first tried to generate and describe mouse lines with an isolated secretion defect in platelets. Subsequently, we were able to study the effect of defective platelet dense granule secretion in LDLR-KO atherosclerosis model and the two tumor mouse models on C57/Bl6 background, B16F10 and LLC1.

6.1 Establishing a mouse line with specific platelet granule secretion defect with heterologous toxin expression

SNARE proteins are indispensable mediators of regulated exocytosis and targeting the respective isoforms in a platelet-specific manner seemed an obvious approach in our attempt to generate mouse lines with a secretion defect in platelets. *Clostridium* toxins represent natural tools to target specific SNARE proteins and make them unavailable for fusion events by cleavage at specific sites. It is well established that botulinum toxins and tetanus toxin can be efficiently applied to interfere with granule secretion in vitro (Schiavo, Matteoli et al. 2000) and it has been shown that expression of tetanus toxin in Sertoli cells leads to severe impairment of spermatogenesis (Eisel, Reynolds et al. 1993) or to suppression of glutamatergic signaling in cerebellar granule cells (Yamamoto, Wada et al. 2003) in vivo. The level of cleavage of the respective SNARE family member had to be substantial, especially when other proteins may be able to compensate the loss of one isoform. In our transgenic constructs, compensatory action was conceivable after BoNT-C cleavage of syntaxin-2 in mouse platelets, which could be replaced by syntaxin-4 in fusion events or TeNT cleavage of VAMP-3, where VAMP-8 could compensate, although these two VAMP isoforms present in mouse platelets seem to have a more specialized function (Ren, Ye et al. 2008). The PF4 promotor seemed to be a suitable driver of toxin expression in platelets since it is a platelet-specific protein and is highly abundant in platelet alpha granules (Brandt, Petersen et al. 2000; Blair and Flaumenhaft 2009). Still, it is conceivable that important regulatory domains lying further upstream or downstream than the area

covered by the PF4 gene-carrying BAC used in this study (approximately 100,000 bp upstream and downstream of the PF4 gene) were missing in our constructs. There are occasional reports of regulatory elements lying more than 100,000 bp apart from the gene they control (Yuasa, Takeda et al. 2012). Another critical parameter for efficient transcription into mRNA is organism-specific codon usage (Gustafsson, Govindarajan et al. 2004). We had the *Clostridial* sequences of BoNT-C and -E optimized for *Mus musculus* codon usage, potential splice sites removed and synthetized by experts (Entelechon). It was thus unexpected that even after repeated injection of the thoroughly verified constructs into mouse oocytes, the best reduction of the respective SNARE protein in transgenic founder animals of the PF4-BoNT-C line was approximately 40% of wild-type syntaxin-2 levels; in the PF4-BoNT-E line, it was approximately 60% of wild-type SNAP-23 levels and cleavage of VAMP-3 by PF4-TeNT constructs was uncertain. These results from Western blot analysis of isolated platelets were not promising with regard to functional defects in platelet granule release. The mouse line with the best potential for functional impact on platelet release was the PF4-BoNT-E line with a maximum of 40% of SNAP-23 cleaved since SNAP-23 is the only SNAP isoform described in platelets (Flaumenhaft, Croce et al. 1999). However, none of the founder mice and their offspring, even after breeding homozygous mice and double-transgene-positives for PF4-BoNT-C and PF4-BoNT-E, showed impaired platelet function as determined by aggregometry, P-selectin exposure in flow cytometry and flow chamber assays. One group (Foran, Mohammed et al. 2003) observed that BoNT-A caused a complete abrogation of neuromuscular transmission but only cleaved 6% of SNAP-25 in nerve endings. They hypothesized that the toxin specifically cleaves a subpopulation of SNAP-25 in the active zone directly involved in transmitter release. Another report (Meunier, Lisk et al. 2003) found only 11.7% cleavage of SNAP-25 by BoNT-E and 6.5% cleavage by BoNT-A in completely paralyzed muscles mediating the toe spread reflex after minimal dose hind leg injection of the toxins in mice. In contrast to our mouse lines which only expressed the light chain capable of SNARE cleavage but not of entering a cell, these authors used the full-length toxin. Maybe the full-length toxin is capable not only to bind to membrane receptors and mediate its own uptake into the endocyctotic pathway (Schiavo, Matteoli et al. 2000) but also to relocate to the active zone and recognize a subset of its target SNARE protein which is activated and ready to mediate granule fusion. This ability may be lost when the heavy chain is not present or secondary structure is affected when only the light chain is translated.

6.2 Establishing a mouse line with specific platelet granule secretion defect with expression of dominant-negative SNAP-23 mutants

With the two dominant-negative constructs, one lacking the last eight amino acids of SNAP-23 and one with three alanine mutations at important positions for interaction with the exocytotic SNARE complex, we sought to overcome the problems encountered with the

toxin constructs. We amplified SNAP-23 cDNA from freshly isolated primary mouse RNA and optimized expression with the insertion of two short introns known to increase expression (Lacy-Hulbert, Thomas et al. 2001) in vivo. We added a triple myc tag to be able to trace expression of the construct. However, as experienced with the toxin constructs discussed earlier, our results suggest that the level of expression of the dominant-negative constructs was too low to cause functional defects in exocytosis. The constructs were carefully checked for integrity and correct sequence and expression of the construct in vivo could be confirmed at least for the PF4-SNAP-23 Ala construct, albeit at low levels compared to endogenous SNAP-23 protein levels. A possible explanation for the failure of the three toxin and the two SNAP-23 constructs could be the backbone sequence they have in common: the PF4 BAC RP24-98A4. This BAC seemed to be the best choice available since it is the only commercially available BAC that covers large areas upstream and downstream of the PF4 gene, but again, as mentioned in section 4.1, it is always possible that important regulatory sequences were missing.

6.3 Analysis of the Jinx mouse line, a genetically modified null-mutant of the Munc13-4 gene

6.3.1 Basal analysis

Our Western blot analysis of Munc13-4 levels in platelets isolated from Unc13d^{Jinx} mice showed no detectable Munc13-4 protein, which corresponds well with the in silico prediction that the premature stop codon caused by the *Jinx* mutation leads to an unstable mRNA product and subsequent decay (Crozat, Hoebe et al. 2007). Loss of the Munc13 isoforms has been shown to cause severe defects in vesicle release in many secretory cell types. Lack of Munc13-1 causes abrogation of vesicle release in glutamatergic hippocampal neurons (Augustin, Rosenmund et al. 1999), mice deficient for the mainly cerebellar isoform Munc13-3 are unable to learn complex motor tasks due to impairment in signaling in parallel fiber-Purkinje cell synapses (Augustin, Korte et al. 2001). Insulin secretion from mouse pancreatic beta cells deficient in Munc13-1 is reduced, causing glucose intolerance (Kwan, Xie et al. 2007). Mutations in the Munc13-4 gene in humans are associated with type 3 Familial hemophagocytic lymphohisiocytosis (FHL3) which is caused by severe defects in exocytosis of lytic granules of lymphocytes. Crozat et al. show that the *Jinx* mutation leads to severe impairment of NK cells to lyse target cells (Crozat, Hoebe et al. 2007). We found Munc13-4 to be the only Munc13 isoform expressed in platelets and thus hypothezised that loss of Munc13-4 would interfere with granule secretion without affecting other platelet functions or morphology. Accordingly, we detected normal platelet numbers and normal levels of the platelet surface receptors GPIb, GPV, GPVI, GPIX, integrin α2, integrin β1, integrin αIIbβ3. CD9 levels were approximately 15% lower in Munc13-4 KO platelets compared to wild-type platelets and surface CLEC-2 was reduced by approximately 35%. Activation of integrin αIIbβ3 is termed the "final common pathway" of

platelet activation (Nieswandt, Varga-Szabo et al. 2009). Agonist stimulation results in PLC activation and formation of IP_3 and DAG, which leads to a rise in intracellular calcium levels and in the end, triggers the switch of a "low-affinity state" of integrin αIIbβ3 to a "high-affinity state". Therefore, the level of integrin αIIbβ3 in active conformation of agonist-stimulated platelets is a cumulative measure of several signaling cascades in platelets including activation by agonists, efficient intracellular signal transduction and efficient modification of integrin αIIbβ3 itself. It also predicts the efficiency of integrin αIIbβ3 to bind to its ligand fibrinogen, which influences platelet aggregation and further "outside-in" signaling of integrin αIIbβ3 to stabilize aggregates. We saw a roughly 20% reduction in active integrin αIIbβ3 in Munc13-4-deficient platelets with all agonists tested (thrombin, ADP, U46619, CRP and rhodocytin) but only with the snake venom rhodocytin, this difference was statistically significant. This slight reduction may be secondary to the dense granule secretion defect found in these platelets since the lack of ADP as a secondary mediator of autocrine and paracrine positive feedback loops certainly influences overall activation of platelets, even if they are diluted 1:100 in flow cytometry compared to aggregation assays. The fact that in high concentrations of the strong platelet agonist thrombin, the difference in integrin αIIbβ3 activation in Munc13-4 KO platelets and wild-type platelets no longer observed, also supports this notion.

We chose the two functionally important alpha granule proteins PF4 and vWF as representative markers of alpha granule release. The platelet-specific chemokine PF4 and the adhesive molecule vWF are synthetized in megakaryocytes during thrombopoiesis (Harrison and Cramer 1993) and contribute to hemostatic as well as pathophysiological functions of platelets (Terraube, Marx et al. 2007; Kasper and Petersen 2011; Nieswandt, Pleines et al. 2011). There was no difference in PF4 or vWF secretion between Munc13-4 KO platelets and wild-type platelets in response to low, intermediate and high concentrations of thrombin. The small, but not significant decrease in PF4 release after stimulation with low-dose thrombin could be reversed by the addition of a selective antagonist against $P2Y_{12}$ receptor (data not shown), indicating that this difference is caused by a lack of ADP secretion from dense granules in Munc13-4-deficient platelets. U46619 and collagen only evoked minor release of PF4 under the conditions assessed here and there was no difference between Munc13-4 KO and wild-type platelets (data not shown). Another common marker of platelet granule release is exposure of P-selectin on the surface of activated platelets. P-selectin is absent from the outer membranes of resting platelets and can be found associated with membranes of alpha and dense granules (Israels, Gerrard et al. 1992; Youssefian, Masse et al. 1997). Upon granule fusion, P-selectin is integrated into the outer membrane and mediates interaction with leukocytes in hemostasis but is also involved in atherogenesis and neointima formation (Smyth, McEver et al. 2009). We observed a reduction of 20-40% in P-selectin exposure on the surface of Munc13-4-deficient platelets compared to wild-type platelets upon stimulation with thrombin, ADP, U46619, CRP or rhodocytin, not always statistically significant but reproducible. It is

currently unknown how much of total P-selectin is found associated with dense granule membranes and it is technically challenging to obtain reliable results. The total number of dense granules per platelet is also hard to determine in electron microscopy (White 2008) but is estimated to be approximately 10 times lower than the number of alpha granules per platelet (Holmsen and Weiss 1979). On the other hand, upon maximal stimulation with thrombin, up to 90% of platelet dense granules are released but only about 60% of alpha granules (Ren, Barber et al. 2007). The observed reduction of surface P-selectin in Munc13-4 KO platelets could thus be caused by the portion of P-selectin associated with dense granules that are not released in Munc13-4 KO platelets or by a subpopulation of alpha granules containing P-selectin, but not PF4 or vWF, which is released in a Munc13-4-dependent manner.

In contrast to alpha granule secretion, we found no detectable ATP secretion from dense granules of isolated Munc13-4-deficient platelets upon stimulation with thrombin, U46619 or collagen, suggesting that platelet dense granule release in these platelets is completely abrogated. To our knowledge, this is the first genetically modified mouse line with a specific dense granule secretion defect without affecting granule formation or contents.

The ability of washed Munc13-4 KO platelets to adhere to collagen, which mainly requires binding of platelet GPVI receptor (Nieswandt, Pleines et al. 2011), is unaltered, whereas in the more complex setting of the flow chamber assay, Munc13-4 platelets can form smaller aggregates but fail to produce stable, large, three-dimensional structures as observed for wild-type platelets. Under high shear stress as in the flow chamber (1000^{-s}), initial contact with collagen is mainly mediated by interaction of the GPIb-V-IX complex with collagen-bound vWF, subsequent binding of GPVI together with its non-covalently associated co-receptor FcR γ-chain activates platelets, leads to secretion of secondary mediators like ADP, recruitment of more platelets and leukocytes into the thrombus. Binding of integrins to vWF and fibrinogen and less well-defined mediators like CLEC-2, Gas6 and CD40L support bridging between platelets (Nieswandt, Pleines et al. 2011). The lack of large, three-dimensional aggregates in Munc13-4 KO platelets in flow chamber assays is probably due to reduced numbers of platelets recruited through local ADP secretion to already activated and collagen-bound platelets. Blood flow is very fast at a shear rate of 1000^{-s} and platelets only have the length of a coverslip to get in contact with collagen or secondary mediators, decelerate and attach to collagen or other platelets. This may require very efficient signal amplification and a loss of ADP as autocrine and paracrine messenger cannot be compensated. This notion is supported by reports showing that blocking the platelet ADP receptors leads to impaired aggregation in vitro (Hechler, Cattaneo et al. 2005). Serotonin (Nishihira, Yamashita et al. 2006), polyphosphates (Ruiz, Lea et al. 2004; Smith, Mutch et al. 2006) and calcium (Rendu, Brohard-Bohn 2001) released from platelet dense granules may play supportive roles in aggregate and thrombus stabilization.

Secondary mediators, mainly ADP and thromboxane A$_2$, influence platelet aggregation in response to weak agonists. Aggregometry is used routinely as a diagnostic tool for human platelet disorders. Storage pool disorders of dense granules are rare but patients with Hermansky Pudlak syndrome or Chediak Higashi syndrome mostly have intact alpha granule content and function but reduced amounts of dense granules and reduced nucleotide levels. Aggregation responses of platelet-rich plasma of patients with these syndromes in response to collagen are usually decreased (Kottke-Marchant and Corcoran 2002), and in response to thromboxane analogues show reduced maximum aggregation levels (Weiss and Lages 1988). We found delayed and decreased plateau levels of platelet aggregation in platelets isolated from Munc13-4 KO mice compared to wild-type platelets in response to collagen and reduced maximal aggregation in these platelets upon stimulation with U46619. These findings maybe show a more pronounced defect in Munc13-4-deficient platelets but in general correspond well to the clinical data on patients with dense granule storage pool diseases and defects in dense granule secretion. In the storage pool diseases described so far, ADP secretion from dense granules is only strongly decreased (Kottke-Marchant and Corcoran 2002), so the consequences of a complete shutdown of dense granule secretion as observed for Munc13-4 KO mice are expected to be more severe.

The lack of stable, large aggregates found in flow chamber assay and the impaired aggregation responses of Munc13-4 KO platelets have dramatic correlates in these mice in tail bleeding and ferric chloride thrombosis models in vivo. Tail bleeding in Munc13-4 KO has to be stopped by outside intervention to prevent critical loss of blood in Munc13-4 KO animals. Some small, mural thrombi are formed in Munc13-4 KO mice when mesenteric arteries are denuded with ferric chloride, but no larger aggregates build up and eventually occlude the vessel as seen after approximately 10 min in wild-type animals. These results correlate well with the observation that mice lacking Hermansky-Pudlak syndrome 3 (HPS3) gene, which have impaired platelet dense-granule secretion due to defects in dense granule biogenesis (Novak, Sweet et al. 1988; Suzuki, Li et al. 2001), have negligible reduction of arterial blood flow after treatment with ferric chloride (King, McNamee et al. 2009). In another mouse model of Hermansky Pudlak syndrome, ruby eye mice, animals were shown to have strongly diminished amounts of aggregate formation after laser injury of cremaster arterioles (Graham, Ren et al. 2009), a model which depends more on formation of thrombin than exposure of ECM (Sachs and Nieswandt 2007). Blocking P2Y receptors is sufficient to inhibit thrombus formation in vivo (Oury, Toth-Zsamboki et al. 2006) and in clinical applications (Secco, G. G., R. Parisi, et al. 2012), lack of ADP secretion in Munc13-4-deficient animals is thus probably the major factor causing the protection from thrombosis in these mice. As in aggregate formation under flow, addiotional lack of serotonin, polyphosphates and calcium may further contribute to the inhibition of thrombus formation in Munc13-4 KO mice.

In summary, our basal analysis of Munc13-4-deficient platelet function reveals a selective abrogation of dense granule secretion, while morphology, platelet count, granule

constituents and basal surface glycoprotein receptor levels as well as alpha granule secretion are intact. The lack of dense granule secretion leads to severe phenotypes in tail bleeding and thrombosis models, emphasizing the contribution of dense granule contents, mainly secondary activation of platelets via ADP, to these pathophysiological conditions. Our results are largely confirmed by a report from Ren et al. describing platelet responses of the same mouse line (Unc13d^{Jinx}) with regard to morphology, platelet count, activation, level of granule contents, and, importantly, complete lack of dense granule secretion (Ren, Wimmer et al. 2010).

6.3.2 Applying Munc13-4 KO mice to study the impact of dense granule secretion on the progression of atherosclerosis in a mouse model

A previous report showing reduced atherosclerotic plaque formation in mice with a strong reduction in dense granule formation during thrombopoiesis (Graham, Ren et al. 2009) could not be confirmed in this study in two independent experiments with LDL receptor knockout mice transplanted with Munc13-4-deficient or wild-type bone marrow. LDLR KO mice are prone to develop atherosclerotic lesions after being exposed to high blood levels of fat and cholesterol and are one of two well-established murine models for atherosclerosis. There was no difference in aortic plaque formation after 16 weeks of high fat, high cholesterol diet in LDLR KO mice reconstituted with Munc13-4-deficient or wild-type bone marrow.

Several molecules released from platelet dense granules have been implicated in inflammation and atherogenesis. Dense-granule-derived polyphosphates have been shown to upregulate bradykinin production, which in turn stimulates the generation of the pro-inflammatory cytokines IL1β and TNFα (Muller, Mutch et al. 2009). The protein 14-3-3ζ was identified in dense granules from human platelets with a proteomics approach and shown to be present in atherosclerotic plaques from patients' samples with aneurysms (Hernandez-Ruiz, Valverde et al. 2007). Serotonin has mitogenic effects on endothelial cells (Pakala, Willerson et al. 1994) and smooth muscle cells (Hodivala-Dilke, McHugh et al. 1999) in vitro and could contribute to the proliferation of these cell types characteristic for atherosclerotic plaque formation in vivo. In summary, there is some indirect evidence that molecules released from dense granules could be involved in atherogenesis but the contributions of alpha granule proteins like PF4, RANTES, CD40L are much more well-established. It is thus not surprising that we do not see a reduction of plaque formation in LDLR KO mice lacking platelet dense granule secretion but with largely normal alpha granule secretion.

6.3.3 Studying the role of platelet dense granule secretion in tumor metastasis with Munc13-4-deficient mice

Platelets have been shown to be associated with tumor cells early after vascular arrest (Crissman, Hatfield et al. 1988; Im, Fu et al. 2004) and to be able to closely interact with

tumor cells (Nieswandt, Hafner et al. 1999; Borsig, Wong et al. 2001). Together with the observation that chemical or genetic depletion of platelets strongly suppresses metastasis in mouse models (Pearlstein, Ambrogio et al. 1984; Camerer, Qazi et al. 2004), we hypothesized that platelets could influence the important step after vascular arrest of tumor cells in the metastatic cascade, leaving the circulation through extravasation to reach the organ parenchyma. The first barrier for tumor cells to overcome in extravasation is the endothelial layer. Transmigration assays represent a simplified and well-controlled in vitro model for this step, so we investigated the impact of platelets on the ability of tumor cells to transmigrate through an endothelial layer. We found a 2-4-fold increase in tumor cell transmigration upon the addition of platelets, depending on the tumor cell line used. These results are consistent with studies describing a supporting role of platelets in diapedesis of neutrophils (Lam, Burns et al. 2011; Badrnya, Butler et al. 2012) and monocytes (da Costa Martins, van Gils et al. 2006; van Gils, Zwaginga et al. 2009) in vitro and in vivo. It is conceivable that platelets facilitate direct contact of tumor cells through their multitude of surface receptors known to interact with endothelial cells and many other cell types (Stokes and Granger 2012) and also tumor cells (Jain, Harris et al. 2010; Gay and Felding-Habermann 2011), or that secondary to their ability to connect directly with tumor cells, they become activated and release mediators that influence tumor cells or endothelial cells. We found that the enhancement of tumor cells transmigration was strictly dependent on the presence of endothelial cells. Since tumor cells are very heterogeneous in many of their properties, this may be different in other cell lines, but none of the two mouse or the two human tumor cell lines tested here showed an increase in basal tumor cell transmigration in the presence of platelets or supernatants from resting platelets. We could show that tumor cell-stimulated supernatants of platelets were sufficient to induce the platelet-mediated fraction of tumor cell transendothelial migration and that apyrase, an enzyme, which quickly dephosphorylates ATP and ADP, was able to block this effect completely, suggesting that nucleotides secreted from activated platelets enable tumor cells to transmigrate more efficiently. This was confirmed by applying Munc13-4-deficient platelets, which lack nucleotide secretion, to the transmigration assay, as here again, the enhancing effects of wild-type platelets on tumor cell transmigration through an endothelial layer were completely inhibited. Wild-type platelets showed a strong, tumor cell-induced ATP secretion, an effect, which also abrogated in Munc13-4 KO platelets. At the same time, we could show that the ability of Munc13-4 KO platelets to attach to tumor cells or the ability of tumor cells to elicit alpha granule secretion in these platelets was normal. These unique properties make Munc13-4-deficient mice an ideal tool to investigate whether nucleotide secretion from platelets plays a role in metastatic events in vivo. Indeed, we saw a strong reduction in formation of metastases in the lungs of Munc13-4 KO animals compared to wild-type mice in the two homotypic tumor models available for C57/Bl6 background, B16 melanoma and LLC1 lung carcinoma. The reduction in metastasis was also observed upon i.v. injection of B16 and LLC1 cells and the size distribution of metastases showed

reduction in metastases of all sizes in Munc13-4-deficient animals, implying that this effect is independent of a primary tumor and growth of metastases is not affected. This notion, at least for larger, structured metastases, is supported by the fact that analysis of primary tumors showed no signs of leakage or gross differences in tumor structure in H/E staining (data not shown) or abnormal angiogenesis in Munc13-4 KO animals. These data indicate that release of nucleotides from platelets promotes tumor cell metastasis in vivo and provide a possible mechanism for observations that the metastatic potential of tumor cells correlates with their ability to activate platelets (Pearlstein, Salk et al. 1980; Camerer, Qazi et al. 2004). To elucidate the down-stream signaling pathways mediating this effect, we studied the impact of tumor cells in combination with platelets on endothelial morphology and permeability and saw a nucleotide-dependent disruption of endothelial barriers and parallel increase in endothelial permeability, confirming that nucleotides released from tumor cell-stimulated platelets act on endothelial receptors, facilitating tumor cell passage. Of the seven known metabotropic and seven ionotropic nucleotide receptors in mice, we found predominant expression of the UTP/ATP receptor $P2Y_2$ and the ion-channel $P2X_4$ in mouse endothelial cells. This corresponds to the fact that addition of exogenous ATP alone was sufficient to increase tumor cell transmigration through an endothelial layer, since $P2Y_2$ is the P2Y-type receptor with the highest affinity to ATP (Lazarowski, Watt et al. 1995; Kim, Ravi et al. 2002). Blockade and knockdown of $P2X_4$ in endothelial cells prior to transmigration did not influence platelet-facilitated transmigration of tumor cells, but knockdown of $P2Y_2$, for which no selective antagonist is available, prevented this effect in transmigration of both B16 and LLC1 cells. These data indicate that ATP secreted from platelets in large amounts upon stimulation by tumor cells binds to endothelial $P2Y_2$ receptors to facilitate tumor cell transmigration and is in line with a report demonstrating that endothelial $P2Y_2$ receptor mediates neutrophil transendothelial migration (Kukulski, Ben Yebdri et al. 2010). The downstream effects of $P2Y_2$ activation are rise of intracellular calcium through coupling to G-proteins G_q/G_{11} (Abbracchio, Burnstock et al. 2006) and activation of protein kinase C, which has been shown to destabilize the endothelial barrier (Gavard and Gutkind 2008; Knezevic, Tauseef et al. 2009; Korhonen, Fisslthaler et al. 2009), specifically by disassembling VE-cadherin adherens junction, which leads to an increase endothelial permeability (Tiruppathi, Ahmmed et al. 2006; Vandenbroucke St Amant, Tauseef et al. 2012). Our finding that $P2Y_2$ is the major ATP receptor in this context is supported by a study showing that selective agonists and antagonists of P2X receptors could not reproduce or block the intracellular effects of ATP on HUVECs but the selective $P2Y_2$ agonist UTP evoked intracellular calcium mobilization with similar EC_{50} values as ATP and knockdown of $P2Y_2$ blunted calcium responses (Raqeeb, Sheng et al. 2011). Another pathway induced by endothelial $P2Y_2$ shown to contribute to melanoma metastasis is activation of vascular endothelial growth factor receptor-2 (VEGFR-2/KDR/Flk-1) through rapid tyrosine phosphorylation (Seye, Yu et al. 2003; Seye, Yu et al. 2004) and subsequent

upregulation of vascular cell adhesion molecule-1 (VCAM-1) (Vidal-Vanaclocha, Fantuzzi et al. 2000; Langley, Carlisle et al. 2001; Seye, Yu et al. 2004).

In the in vivo situation, we could show that tumor cells injected i.v. increase endothelial permeability in the lung at one to approximately three hours after injection and that this increase is mediated by platelet nucleotides and $P2Y_2$ receptors, since Munc13-4 KO and $P2Y_2$ KO mice showed almost no vascular leakage under these conditions. Less vascular leakage translated to lower numbers of extravasating tumor cells in these animals compared to wild-type controls six hours after tumor cell injection, implying that the strong reduction in metastases observed in the lungs of Munc13-4 KO animals 12 days after injection is caused by a lower number of tumor cells that pave their way through the endothelial layer to the organ parenchyma. Consequently, $P2Y_2$ KO animals also showed a strong decrease in metastases in the lung after i.v. injection of B16 melanoma or LLC1 carcinoma cells, confirming the concept established in this study.

In summary, these results suggest that in accordance with the in vitro data, tumor cells locally activate platelets, platelets subsequently secrete high amounts of ATP which bind to the endothelial $P2Y_2$ receptor, destabilize endothelial barriers and thus allow a more efficient extravasation of tumor cells into the target organ parenchyma. Figure 61 shows a model describing this mechanism.
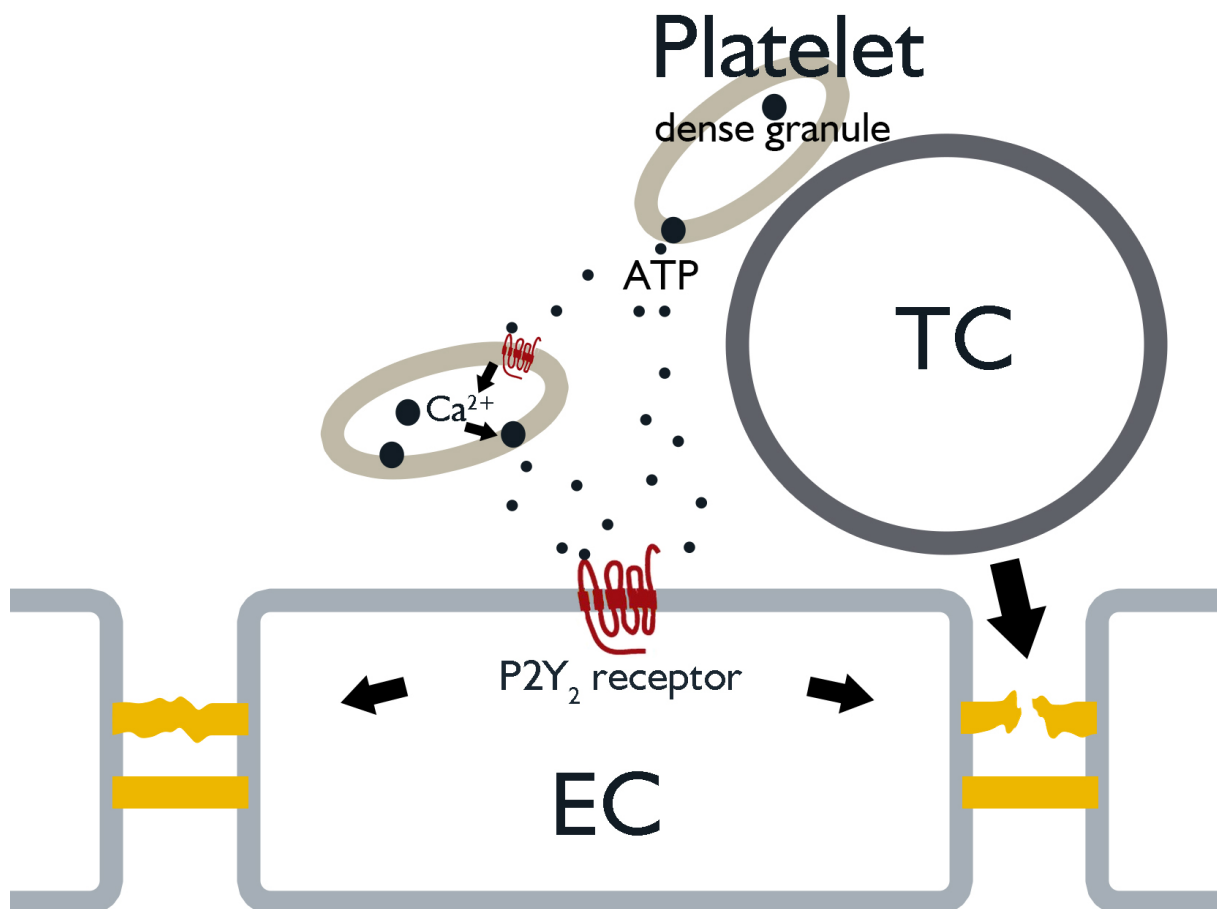
Figure 61: **Model of platelet-mediated facilitation of tumor cell transmigration.** Tumor cells (TC) activate platelets, which in turn secrete ATP from dense granules. ATP binds to platelet P2Y receptors to induce autocrine and paracrine positive feedback loops and to endothelial ATP receptor $P2Y_2$. This destabilizes endothelial barriers and thus allows tumor cells to transmigrate more efficiently.

This mechanism represents a promising target for anti-metastatic therapies avoiding bleeding complications that arise from application of classical anti-platelet drugs (Erpenbeck and Schon 2010; Gay and Felding-Habermann 2011) and proves that platelets are major players in the metastatic cascade. The benefits of low-dose aspirin, which is sufficient to inhibit platelet function, in the prevention of metastatic events was pointed out in a recent post-hoc analysis of large randomized cardiovascular trials (Rothwell, Wilson et al. 2012). We hereby provide evidence for a new downstream mechanism in platelet-mediated tumor metastasis besides evasion of NK cell lysis in the circulation (Nieswandt, Hafner et al. 1999; Palumbo, Talmage et al. 2005) and release of mitogenic (Labelle, Begum et al. 2011) or angiogenic factors (Boucharaba, Serre et al. 2004; Italiano, Richardson et al. 2008). Targeting endothelial $P2Y_2$ receptor to inhibit nucleotide signaling from tumor cell-activated platelets may be a successful approach to prevent tumor cell metastasis and avoiding side effects of anti-platelet drugs.

7   <u>Summary</u>

7.1   Introduction

The involvement of platelets in various diseases has been increasingly recognized in the recent decades. This contribution is believed to involve platelet secretion and formation of reactive microparticles. Platelets contain two functionally important forms of vesicles, alpha and dense granules, which are secreted upon activation of platelets. Alpha granules incorporate larger molecules such as adhesive proteins, e.g. P-selectin, vWF and fibrinogen; chemokines like PF4 and RANTES and growth hormones like VEGF and PDGF are among the most important proteins attributed to the involvement of platelets in pathological conditions. In contrast, dense granules contain small molecules like ADP, ATP, serotonin and histamine, and they are more rapidly and completely secreted than alpha granules. Like in all secreting cells, regulated exocytosis in platelets is mediated by "zippering" of three different classes of SNARE proteins. The subtypes of these proteins found to be involved in platelet secretion are SNAP-23, syntaxin-2 and -4 and VAMP-3 and -8. Apart from SNARE proteins, other conserved proteins influencing exocytosis by e.g. acting on SNARE proteins have been described, one of the most important ones being Munc13.

Platelets contribute to the progression of atherosclerosis by local deposition of inflammatory mediators like PF4, RANTES and CD40L, which leads to enhanced leukocyte recruitment and plaque formation. In 1865, Armand Trousseau first described the correlation between cancer and thrombotic events. Since the 1960s, an increasing number of studies have found an involvement of platelets also in the progression of cancer, especially in the formation of metastases. Platelets bind to circulating tumor cells and may shield them from NK cell attacks and shear stress. Platelets may also facilitate the interaction of tumor cells with other cell types and the vessel wall. Lastly, they may secrete molecules that influence the tumor cell phenotype and invasiveness.

7.2   Aims of this study

We sought to generate and describe genetically modified mouse lines with defective platelet secretion and to employ these mouse lines in murine models of atherosclerosis and tumor progression to study the role of platelet secretion under pathological in vivo conditions.

7.3   Results

Clostridial toxins cleave members of the SNARE protein family and can thus completely block exocytosis of neuronal and other cells. We generated three transgenic mouse lines expressing tetanus, botulinum-E or -C light chains and two transgenic mouse lines with dominant-negative mutations of SNAP-23 under the control of the platelet-specific PF4 promotor. None of these constructs was able to interfere with platelet secretion despite expression of the transgene.

A functional null mutant of the only Munc13 isoform expressed in platelets, Munc13-4, showed complete lack of dense granule secretion, measured by ATP release, while alpha granule release as determined by PF4 and vWF secretion, was unaltered. Morphology, composition and adhesion of these platelets were also normal. Aggregation in response to U46619 and collagen and formation of large aggregates in flow chamber assays was attenuated. Munc13-4-deficient mice showed a severe defect in bleeding time and no formation of stable aggregates in $FeCl_3$ thrombosis model.

In response to B16 melanoma and LLC1 carcinoma cells, Munc13-4 KO platelets also showed complete abrogation of dense granule secretion, whereas alpha granule secretion and binding of platelets to tumor cells was unchanged. Interestingly, wild-type platelets, but not Munc13-4 KO platelets, enhanced transmigration of B16 and LLC1 cells through an endothelial cell layer. Exogenous ATP was able to mimic the effect of wild-type platelets and the ATP-degrading enzyme apyrase blocked platelet-mediated tumor cell transmigration. Platelets incubated with tumor cells secreted large amounts of ATP. Murine endothelial cells showed perturbed adherens junctions identified by irregular VE-cadherin staining and gap formation when incubated with supernatants from tumor cell-activated platelets as well as increased permeability under the same conditions. Addition of apyrase preserved normal endothelial morphology and function. In vivo, primary tumor growth and weight was comparable in wild-type and Munc13-4 KO mice upon B16 or LLC1 flank injection but formation of lung metastases was strongly reduced. Number, but not size of metastases was also reduced upon i.v. injection of B16 and LLC1 cells. We found $P2Y_2$ and $P2X_4$ receptors to be the most abundantly expressed endothelial metabotropic and ionotropic ATP receptors, respectively. Neither knock-down nor inhibition of $P2X_4$ in endothelial cells influenced platelet-mediated transendothelial migration of B16 cells, but knock-down of $P2Y_2$, for which no specific antagonist is available, strongly reduced platelet-dependent tumor cell transmigration. When B16 melanoma cells were injected i.v. shortly after FITC-dextran (70 kDa) into wild-type mice, prominent leakage of FITC-dextran was observed three hours post-injection at extraluminal sites in the lung. In contrast, leakage into the lung parenchyma was at basal levels in Munc13-4 KO and $P2Y_2$ KO mice after B16 cell injection. Marginal vascular leakage in Munc13-4 KO mice lacking platelet ATP secretion and in $P2Y_2$ KO mice lacking the main endothelial ATP receptor correlated with strongly reduced extravasation of CFSE-labeled B16 melanoma cells 6 hours post-injection in these mice. Consistently, $P2Y_2$ KO mice showed strongly reduced formation of metastases in the lung after i.v. injection of B16 or LLC1 tumor cells.

Bone marrow-transplanted LDLR KO mice reconstituted with Munc13-4-deficient or wild-type bone marrow and subjected to 16 weeks of high fat diet showed no significant difference in atherosclerotic plaque formation in the aorta.

7.4   Discussion

We hereby provide a thorough analysis of a mouse line with an exclusive defect in platelet dense granule secretion, thus representing a unique genetic tool to study the role of dense

granule secretion in various contexts without interfering with other platelet functions. We also provide evidence how extravasation of circulating tumor cells is facilitated by tumor cell-induced ATP release from platelets. This ATP release destabilizes endothelial barriers and facilitates tumor cell extravasation and formation of metastases in the target organ. Since metastasis is the leading cause of cancer death, pharmacological interference with endothelial P2Y$_2$ receptor function may represent a promising therapeutic strategy.

8   References

Abbracchio, M. P., G. Burnstock, et al. (2006). "International Union of Pharmacology LVIII: update on the P2Y G protein-coupled nucleotide receptors: from molecular mechanisms and pathophysiology to therapy." Pharmacol Rev **58**(3): 281-341.

Abdullah, L. H., J. T. Bundy, et al. (2003). "Mucin secretion and PKC isoforms in SPOC1 goblet cells: differential activation by purinergic agonist and PMA." Am J Physiol Lung Cell Mol Physiol **285**(1): L149-160.

Amarzguioui, M., Q. Peng, et al. (2006). "Ex vivo and in vivo delivery of anti-tissue factor short interfering RNA inhibits mouse pulmonary metastasis of B16 melanoma cells." Clin Cancer Res **12**(13): 4055-4061.

Ashery, U., F. Varoqueaux, et al. (2000). "Munc13-1 acts as a priming factor for large dense-core vesicles in bovine chromaffin cells." EMBO J **19**(14): 3586-3596.

Augustin, I., S. Korte, et al. (2001). "The cerebellum-specific Munc13 isoform Munc13-3 regulates cerebellar synaptic transmission and motor learning in mice." J Neurosci **21**(1): 10-17.

Augustin, I., C. Rosenmund, et al. (1999). "Munc13-1 is essential for fusion competence of glutamatergic synaptic vesicles." Nature **400**(6743): 457-461.

Auton, M., C. Zhu, et al. (2010). "The mechanism of VWF-mediated platelet GPIbalpha binding." Biophys J **99**(4): 1192-1201.

Badrnya, S., L. M. Butler, et al. (2012). "Platelets directly enhance neutrophil transmigration in response to oxidised low-density lipoprotein." Thromb Haemost **108**(4).

Bambace, N. M., J. E. Levis, et al. (2010). "The effect of P2Y-mediated platelet activation on the release of VEGF and endostatin from platelets." Platelets **21**(2): 85-93.

Bastida, E., L. Almirall, et al. (1987). "Tumor-cell-induced platelet aggregation is a glycoprotein-dependent and lipoxygenase-associated process." Int J Cancer **39**(6): 760-763.

Basu, J., A. Betz, et al. (2007). "Munc13-1 C1 domain activation lowers the energy barrier for synaptic vesicle fusion." J Neurosci **27**(5): 1200-1210.

Battinelli, E. M., B. A. Markens, et al. (2011). "Release of angiogenesis regulatory proteins from platelet alpha granules: modulation of physiologic and pathologic angiogenesis." Blood **118**(5): 1359-1369.

Bender, M., S. Hofmann, et al. (2010). "Differentially regulated GPVI ectodomain shedding by multiple platelet-expressed proteinases." Blood **116**(17): 3347-3355.

Bergmeier, W., K. Rackebrandt, et al. (2000). "Structural and functional characterization of the mouse von Willebrand factor receptor GPIb-IX with novel monoclonal antibodies." Blood **95**(3): 886-893.

Blair, P. and R. Flaumenhaft (2009). "Platelet alpha-granules: basic biology and clinical correlates." Blood Rev **23**(4): 177-189.

Blostein, M. D., I. Rajotte, et al. (2011). "Elevated plasma gas6 levels are associated with venous thromboembolic disease." J Thromb Thrombolysis **32**(3): 272-278.

Borsig, L., R. Wong, et al. (2001). "Heparin and cancer revisited: mechanistic connections involving platelets, P-selectin, carcinoma mucins, and tumor metastasis." Proc Natl Acad Sci U S A **98**(6): 3352-3357.

Boucharaba, A., C. M. Serre, et al. (2004). "Platelet-derived lysophosphatidic acid supports the progression of osteolytic bone metastases in breast cancer." J Clin Invest **114**(12): 1714-1725.

Brandt, E., F. Petersen, et al. (2000). "The beta-thromboglobulins and platelet factor 4: blood platelet-derived CXC chemokines with divergent roles in early neutrophil regulation." J Leukoc Biol **67**(4): 471-478.

Brzezinska, A. A., J. L. Johnson, et al. (2008). "The Rab27a effectors JFC1/Slp1 and Munc13-4 regulate exocytosis of neutrophil granules." Traffic **9**(12): 2151-2164.

Camerer, E., A. A. Qazi, et al. (2004). "Platelets, protease-activated receptors, and fibrinogen in hematogenous metastasis." Blood **104**(2): 397-401.

Chaffer, C. L. and R. A. Weinberg (2011). "A perspective on cancer cell metastasis." Science **331**(6024): 1559-1564.

Chaineau, M., L. Danglot, et al. (2009). "Multiple roles of the vesicular-SNARE TI-VAMP in post-Golgi and endosomal trafficking." FEBS Lett **583**(23): 3817-3826.

Chatterjee, M., Z. Huang, et al. (2011). "Distinct platelet packaging, release, and surface expression of proangiogenic and antiangiogenic factors on different platelet stimuli." Blood **117**(14): 3907-3911.

Chen, D., A. M. Bernstein, et al. (2000). "Molecular mechanisms of platelet exocytosis: role of SNAP-23 and syntaxin 2 in dense core granule release." Blood **95**(3): 921-929.

Chen, D., P. P. Lemons, et al. (2000). "Molecular mechanisms of platelet exocytosis: role of SNAP-23 and syntaxin 2 and 4 in lysosome release." Blood **96**(5): 1782-1788.

Chen, S. and J. T. Barbieri (2006). "Unique substrate recognition by botulinum neurotoxins serotypes A and E." J Biol Chem **281**(16): 10906-10911.

Chen, S. and J. T. Barbieri (2007). "Multiple pocket recognition of SNAP25 by botulinum neurotoxin serotype E." J Biol Chem **282**(35): 25540-25547.

Chen, Y. A., R. H. Scheller (2001). "SNARE-mediated membrane fusion." Nature Reviews Molecular Cell Biology **2**: 98-106.

Ciferri, S., C. Emiliani, et al. (2000). "Platelets release their lysosomal content in vivo in humans upon activation." Thromb Haemost **83**(1): 157-164.

Claesson-Welsh, L. (2012). "Blood vessels as targets in tumor therapy." Ups J Med Sci **117**(2): 178-186.

Coller, B. S. (2011). "Historical perspective and future directions in platelet research." J Thromb Haemost **9 Suppl 1**: 374-395.

Coupland, L. A., B. H. Chong, et al. (2012). "Platelets and P-selectin control tumor cell metastasis in an organ-specific manner and independently of NK cells." Cancer Res.

Covic, L., A. L. Gresser, et al. (2000). "Biphasic kinetics of activation and signaling for PAR1 and PAR4 thrombin receptors in platelets." Biochemistry 39(18): 5458-5467.

Crissman, J. D., J. S. Hatfield, et al. (1988). "Morphological study of the interaction of intravascular tumor cells with endothelial cells and subendothelial matrix." Cancer Res 48(14): 4065-4072.

Crozat, K., P. Georgel, et al. (2006). "Analysis of the MCMV resistome by ENU mutagenesis." Mamm Genome 17(5): 398-406.

Crozat, K., K. Hoebe, et al. (2007). "Jinx, an MCMV susceptibility phenotype caused by disruption of Unc13d: a mouse model of type 3 familial hemophagocytic lymphohistiocytosis." J Exp Med 204(4): 853-863.

da Costa Martins, P. A., J. M. van Gils, et al. (2006). "Platelet binding to monocytes increases the adhesive properties of monocytes by up-regulating the expression and functionality of beta1 and beta2 integrins." J Leukoc Biol 79(3): 499-507.

Dangel, O., E. Mergia, et al. (2010). "Nitric oxide-sensitive guanylyl cyclase is the only nitric oxide receptor mediating platelet inhibition." J Thromb Haemost 8(6): 1343-1352.

Dolly, J. O. and K. R. Aoki (2006). "The structure and mode of action of different botulinum toxins." Eur J Neurol 13(Suppl 4): 1-9.

Eisel, U., K. Reynolds, et al. (1993). "Tetanus toxin light chain expression in Sertoli cells of transgenic mice causes alterations of the actin cytoskeleton and disrupts spermatogenesis." EMBO J 12(9): 3365-3372.

Erpenbeck, L. and M. P. Schon (2010). "Deadly allies: the fatal interplay between platelets and metastasizing cancer cells." Blood 115(17): 3427-3436.

Feldmann, J., I. Callebaut, et al. (2003). "Munc13-4 is essential for cytolytic granules fusion and is mutated in a form of familial hemophagocytic lymphohistiocytosis (FHL3)." Cell 115(4): 461-473.

Feng, D., K. Crane, et al. (2002). "Subcellular distribution of 3 functional platelet SNARE proteins: human cellubrevin, SNAP-23, and syntaxin 2." Blood 99(11): 4006-4014.

Flaumenhaft, R., K. Croce, et al. (1999). "Proteins of the exocytotic core complex mediate platelet alpha-granule secretion. Roles of vesicle-associated membrane protein, SNAP-23, and syntaxin 4." J Biol Chem 274(4): 2492-2501.

Flaumenhaft, R., N. Rozenvayn, et al. (2007). "SNAP-23 and syntaxin-2 localize to the extracellular surface of the platelet plasma membrane." Blood 110(5): 1492-1501.

Foran, P. G., N. Mohammed, et al. (2003). "Evaluation of the therapeutic usefulness of botulinum neurotoxin B, C1, E, and F compared with the long lasting type A. Basis for distinct durations of inhibition of exocytosis in central neurons." J Biol Chem 278(2): 1363-1371.

Gader, A. G., A. K. Ghumlas, et al. (2008). "The ultrastructure of camel blood platelets: a comparative study with human, bovine, and equine cells." Platelets **19**(1): 51-58.

Gasic, G. J., T. B. Gasic, et al. (1973). "Platelet-tumor-cell interactions in mice. The role of platelets in the spread of malignant disease." Int J Cancer **11**(3): 704-718.

Gasic, G. J., T. B. Gasic, et al. (1968). "Antimetastatic effects associated with platelet reduction." Proc Natl Acad Sci U S A **61**(1): 46-52.

Gavard, J. and J. S. Gutkind (2008). "Protein kinase C-related kinase and ROCK are required for thrombin-induced endothelial cell permeability downstream from Galpha12/13 and Galpha11/q." J Biol Chem **283**(44): 29888-29896.

Gay, L. J. and B. Felding-Habermann (2011). "Contribution of platelets to tumour metastasis." Nat Rev Cancer **11**(2): 123-134.

Ge, S., J. G. White, et al. (2012). "Cytoskeletal F-actin, not the circumferential coil of microtubules, regulates platelet dense-body granule secretion." Platelets **23**(4): 259-263.

Ge, S., J. G. White, et al. (2009) "Quantal release of serotonin from platelets." Anal Chem **81**(8): 2935-2943.

Ge, S., Woo E, et al. (2011). "Electrochemical measurement of endogenous serotonin release from human blood platelets." Anal Chem **83**(7): 2598-604.

Gerdes, N., L. Zhu, et al. (2011). "Platelets regulate CD4(+) T-cell differentiation via multiple chemokines in humans." Thromb Haemost **106**(2): 353-362.

Gillitzer, A., M. Peluso, et al. (2008). "Effect of dominant negative SNAP-23 expression on platelet function." J Thromb Haemost **6**(10): 1757-1763.

Gleissner, C. A. (2012). "Macrophage Phenotype Modulation by CXCL4 in Atherosclerosis." Front Physiol **3**: 1.

Gleissner, C. A., I. Shaked, et al. (2010). "CXC chemokine ligand 4 induces a unique transcriptome in monocyte-derived macrophages." J Immunol **184**(9): 4810-4818.

Gong, L., H. J. Mi, et al. (2012). "P-selectin-mediated platelet activation promotes adhesion of non-small cell lung carcinoma cells on vascular endothelial cells under flow." Mol Med Report **5**(4): 935-942.

Gorelik, E., R. H. Wiltrout, et al. (1982). "Role of NK cells in the control of metastatic spread and growth of tumor cells in mice." Int J Cancer **30**(1): 107-112.

Graham, G. J., Q. Ren, et al. (2009). "Endobrevin/VAMP-8-dependent dense granule release mediates thrombus formation in vivo." Blood **114**(5): 1083-1090.

Granot, Z., E. Henke, et al. (2011). "Tumor entrained neutrophils inhibit seeding in the premetastatic lung." Cancer Cell **20**(3): 300-314.

Griffiths, G. M. (1997). "Protein sorting and secretion during CTL killing." Semin Immunol **9**(2): 109-115.

Grossi, I. M., L. A. Fitzgerald, et al. (1987). "Inhibition of human tumor cell induced platelet aggregation by antibodies to platelet glycoproteins Ib and IIb/IIIa." Proc Soc Exp Biol Med **186**(3): 378-383.

Gustafsson, C., S. Govindarajan, et al. (2004). "Codon bias and heterologous protein expression." Trends Biotechnol **22**(7): 346-353.

Hanna, N. (1985). "The role of natural killer cells in the control of tumor growth and metastasis." Biochim Biophys Acta **780**(3): 213-226.

Harrison, P. and E. M. Cramer (1993). "Platelet alpha-granules." Blood Rev **7**(1): 52-62.

Hechler, B., M. Cattaneo, et al. (2005). "The P2 receptors in platelet function." Semin Thromb Hemost **1**(2): 150-161.

Hernandez-Ruiz, L., F. Valverde, et al. (2007). "Organellar proteomics of human platelet dense granules reveals that 14-3-3zeta is a granule protein related to atherosclerosis." J Proteome Res **6**(11): 4449-4457.

Ho-Tin-Noe, B., T. Goerge, et al. (2008). "Platelet granule secretion continuously prevents intratumor hemorrhage." Cancer Res **68**(16): 6851-6858.

Hodivala-Dilke, K. M., K. P. McHugh, et al. (1999). "Beta3-integrin-deficient mice are a model for Glanzmann thrombasthenia showing placental defects and reduced survival." J Clin Invest **103**(2): 229-238.

Holmsen, H. and H. J. Weiss (1979). "Secretable storage pools in platelets." Annu Rev Med **30**: 119-134.

Hong, W. (2005). "SNAREs and traffic." Biochim Biophys Acta **1744**(3): 493-517.

Huang, X., L. Sheu, et al. (2001). "Cholecystokinin-regulated exocytosis in rat pancreatic acinar cells is inhibited by a C-terminus truncated mutant of SNAP-23." Pancreas **23**(2): 125-133.

Humeau, Y., F. Doussau, et al. (2000). "How botulinum and tetanus neurotoxins block neurotransmitter release." Biochimie **82**(5): 427-46.

Im, J. H., W. Fu, et al. (2004). "Coagulation facilitates tumor cell spreading in the pulmonary vasculature during early metastatic colony formation." Cancer Res **64**(23): 8613-8619.

Israels, S. J., J. M. Gerrard, et al. (1992). "Platelet dense granule membranes contain both granulophysin and P-selectin (GMP-140)." Blood **80**(1): 143-152.

Italiano, J. E., Jr. and E. M. Battinelli (2009). "Selective sorting of alpha-granule proteins." J Thromb Haemost **7 Suppl 1**: 173-176.

Italiano, J. E., Jr., J. L. Richardson, et al. (2008). "Angiogenesis is regulated by a novel mechanism: pro- and antiangiogenic proteins are organized into separate platelet alpha granules and differentially released." Blood **111**(3): 1227-1233.

Jahn, R., T. Lang, et al., (2003). "Membrane fusion." Cell **112**: 519-533.

Jain, S., J. Harris, et al. (2010). "Platelets: linking hemostasis and cancer." Arterioscler Thromb Vasc Biol **30**(12): 2362-2367.

Jain, S., M. Zuka, et al. (2007). "Platelet glycoprotein Ib alpha supports experimental lung metastasis." Proc Natl Acad Sci U S A **104**(21): 9024-9028.

Joyce, J. A. and J. W. Pollard (2009). "Microenvironmental regulation of metastasis." Nat Rev Cancer **9**(4): 239-252.

Karpatkin, S., E. Pearlstein, et al. (1988). "Role of adhesive proteins in platelet tumor interaction in vitro and metastasis formation in vivo." J Clin Invest **81**(4): 1012-1019.

Kasper, B. and F. Petersen (2011). "Molecular pathways of platelet factor 4/CXCL4 signaling." Eur J Cell Biol **90**(6-7): 521-526.

Kerk, N., E. A. Strozyk, et al. (2010). "The mechanism of melanoma-associated thrombin activity and von Willebrand factor release from endothelial cells." J Invest Dermatol **130**(9): 2259-2268.

Kim, H. S., R. G. Ravi, et al. (2002). "Methanocarba modification of uracil and adenine nucleotides: high potency of Northern ring conformation at P2Y1, P2Y2, P2Y4, and P2Y11 but not P2Y6 receptors." J Med Chem **45**(1): 208-218.

Kim, Y. J., L. Borsig, et al. (1998). "P-selectin deficiency attenuates tumor growth and metastasis." Proc Natl Acad Sci U S A **95**(16): 9325-9330.

King, S. M., R. A. McNamee, et al. (2009). "Platelet dense-granule secretion plays a critical role in thrombosis and subsequent vascular remodeling in atherosclerotic mice." Circulation **120**(9): 785-791.

Knezevic, N., M. Tauseef, et al. (2009). "The G protein betagamma subunit mediates reannealing of adherens junctions to reverse endothelial permeability increase by thrombin." J Exp Med **206**(12): 2761-2777.

Korhonen, H., B. Fisslthaler, et al. (2009). "Anaphylactic shock depends on endothelial Gq/G11." J Exp Med **206**(2): 411-420.

Kottke-Marchant, K. and G. Corcoran (2002). "The laboratory diagnosis of platelet disorders." Arch Pathol Lab Med **126**(2): 133-146.

Kukulski, F., F. Ben Yebdri, et al. (2010). "Endothelial P2Y2 receptor regulates LPS-induced neutrophil transendothelial migration in vitro." Mol Immunol **47**(5): 991-999.

Kukulski, F., F. Ben Yebdri, et al. (2010). "The P2 receptor antagonist PPADS abrogates LPS-induced neutrophil migration in the murine air pouch via inhibition of MIP-2 and KC production." Mol Immunol **47**(4): 833-839.

Kwan, E. P., L. Xie, et al. (2007). "Interaction between Munc13-1 and RIM is critical for glucagon-like peptide-1 mediated rescue of exocytotic defects in Munc13-1 deficient pancreatic beta-cells." Diabetes **56**(10): 2579-2588.

Labelle, M., S. Begum, et al. (2011). "Direct signaling between platelets and cancer cells induces an epithelial-mesenchymal-like transition and promotes metastasis." Cancer Cell **20**(5): 576-590.

Lacy-Hulbert, A., R. Thomas, et al. (2001). "Interruption of coding sequences by heterologous introns can enhance the functional expression of recombinant genes." Gene Ther **8**(8): 649-653.

Lam, F. W., A. R. Burns, et al. (2011). "Platelets enhance neutrophil transendothelial migration via P-selectin glycoprotein ligand-1." Am J Physiol Heart Circ Physiol **300**(2): H468-475.

Langley, R. R., R. Carlisle, et al. (2001). "Endothelial expression of vascular cell adhesion molecule-1 correlates with metastatic pattern in spontaneous melanoma." Microcirculation **8**(5): 335-345.

Laurance, S., C. A. Lemarie, et al. (2012). "Growth arrest-specific gene 6 (gas6) and vascular hemostasis." Adv Nutr **3**(2): 196-203.

Lazarowski, E. R., W. C. Watt, et al. (1995). "Pharmacological selectivity of the cloned human P2U-purinoceptor: potent activation by diadenosine tetraphosphate." Br J Pharmacol **116**(1): 1619-1627.

Lemons, P. P., D. Chen, et al. (2000). "Molecular mechanisms of platelet exocytosis: requirements for alpha-granule release." Biochem Biophys Res Commun **267**(3): 875-880.

Li, Y., J. Y. Luo, et al. (2010). "Study on anti-metastasis of heparin derivatives as ligand antagonist of p-selectin." Biomed Pharmacother **64**(10): 654-658.

Lievens, D., A. Zernecke, et al. (2010). "Platelet CD40L mediates thrombotic and inflammatory processes in atherosclerosis." Blood **116**(20): 4317-4327.

Logan, M. R., S. O. Odemuyiwa, et al. (2003). "Understanding exocytosis in immune and inflammatory cells: The molecular basis of mediator secretion." J Allergy Clin Immunol **111**(5): 923-932.

Lonsdorf, A. S., B. F. Kramer, et al. (2012). "Engagement of alphaIIbbeta3 (GPIIb/IIIa) with alphanubeta3 integrin mediates interaction of melanoma cells with platelets: a connection to hematogenous metastasis." J Biol Chem **287**(3): 2168-2178.

Lowe, K.L., L. Navarro-Nunez et al. (2012). "Platelet CLEC-2 and podoplanin in cancer metastasis." Thromb Res **129**(Suppl 1):30-37.

Ma, L., R. Perini, et al. (2005). "Proteinase-activated receptors 1 and 4 counter-regulate endostatin and VEGF release from human platelets." Proc Natl Acad Sci USA **102**(1): 216-220.

Maree, A. O., H. Jneid, et al. (2007). "Growth arrest specific gene (GAS) 6 modulates platelet thrombus formation and vascular wall homeostasis and represents an attractive drug target." Curr Pharm Des **13**(26): 2656-2661.

Matsui, Y., H. Amano, et al. (2012). "Thromboxane A(2) receptor signaling facilitates tumor colonization through P-selectin-mediated interaction of tumor cells with platelets and endothelial cells." Cancer Sci **103**(4): 700-707.

May, F., I. Hagedorn, et al. (2009) "CLEC-2 is an essential platelet-activating receptor in hemostasis and thrombosis." Blood **114**(16): 3464-3472.

Maynard, D. M., H. F. Heijnen, et al. (2007). "Proteomic analysis of platelet alpha-granules using mass spectrometry." J Thromb Haemost **5**(9): 1945-1955.

McNicol, A. and S. J. Israels (2003). "Platelets and anti-platelet therapy." J Pharmacol Sci **93**(4): 381-396.

Meunier, F. A., G. Lisk, et al. (2003). "Dynamics of motor nerve terminal remodeling unveiled using SNARE-cleaving botulinum toxins: the extent and duration are dictated by the sites of SNAP-25 truncation." Mol Cell Neurosci **22**(4): 454-466.

Mishima K., Y. Kato Y, et al. (2006). "Increased expression of podoplanin in malignant astrocytic tumors as a novel molecular marker of malignant progression." Acta Neuropathol **111**:483-488.

Moncada, S., R. Gryglewski, et al. (1976). "An enzyme isolated from arteries transforms prostaglandin endoperoxides to an unstable substance that inhibits platelet aggregation." Nature **263**(5579): 663-665.

Muller, F., N. J. Mutch, et al. (2009). "Platelet polyphosphates are proinflammatory and procoagulant mediators in vivo." Cell **139**(6): 1143-1156.

Munnix, I. C. A., J. M. E. M. Cosemans, et al. (2009) "Platelet response heterogeneity in thrombus formation." Thromb Haemost **102**: 1149–1156.

Nguyen, D. X., P. D. Bos, et al. (2009). "Metastasis: from dissemination to organ-specific colonization." Nat Rev Cancer **9**(4): 274-284.

Nierodzik, M. L., A. Klepfish, et al. (1995). "Role of platelets, thrombin, integrin IIb-IIIa, fibronectin and von Willebrand factor on tumor adhesion in vitro and metastasis in vivo." Thromb Haemost **74**(1): 282-290.

Niers, T. M., L. W. Bruggemann, et al. (2009). "Differential effects of anticoagulants on tumor development of mouse cancer cell lines B16, K1735 and CT26 in lung." Clin Exp Metastasis **26**(3): 171-178.

Nieswandt, B., M. Hafner, et al. (1999). "Lysis of tumor cells by natural killer cells in mice is impeded by platelets." Cancer Res **59**(6): 1295-1300.

Nieswandt, B., I. Pleines, et al. (2011). "Platelet adhesion and activation mechanisms in arterial thrombosis and ischaemic stroke." J Thromb Haemost **9 Suppl 1**: 92-104.

Nieswandt, B., D. Varga-Szabo, et al. (2009). "Integrins in platelet activation." J Thromb Haemost **7 Suppl 1**: 206-209.

Nishihira, K., A. Yamashita, et al. (2006). "Inhibition of 5-hydroxytryptamine receptor prevents occlusive thrombus formation on neointima of the rabbit femoral artery." J Thromb Haemost **4**: 247-255.

Novak, E. K., H. O. Sweet, et al. (1988). "Cocoa: a new mouse model for platelet storage pool deficiency." Br J Haematol **69**(3): 371-378.

Nylander, M., A. Osman, et al. (2012). "The role of thrombin receptors PAR1 and PAR4 for PAI-1 storage, synthesis and secretion by human platelets." Thromb Res **129**(4): e51-58.

Oury, C., E. Toth-Zsamboki, et al. (2006). "The platelet ATP and ADP receptors". Curr Pharm Des **12**: 859-875.

Pakala, R., J. T. Willerson, et al. (1994). "Mitogenic effect of serotonin on vascular endothelial cells." Circulation **90**(4): 1919-1926.

Palumbo, J. S., K. E. Talmage, et al. (2005). "Platelets and fibrin(ogen) increase metastatic potential by impeding natural killer cell-mediated elimination of tumor cells." Blood **105**(1): 178-185.

Pearlstein, E., C. Ambrogio, et al. (1984). "Effect of antiplatelet antibody on the development of pulmonary metastases following injection of CT26 colon adenocarcinoma, Lewis lung carcinoma, and B16 amelanotic melanoma tumor cells into mice." Cancer Res **44**(9): 3884-3887.

Pearlstein, E., P. L. Salk, et al. (1980). "Correlation between spontaneous metastatic potential, platelet-aggregating activity of cell surface extracts, and cell surface sialylation in 10 metastatic-variant derivatives of a rat renal sarcoma cell line." Proc Natl Acad Sci U S A **77**(7): 4336-4339.

Peterson, J. E., D. Zurakowski, et al. (2010). "Normal ranges of angiogenesis regulatory proteins in human platelets." Am J Hematol **85**(7): 487-493.

Pivot-Pajot, C., F. Varoqueaux, et al. (2008). "Munc13-4 regulates granule secretion in human neutrophils." J Immunol **180**(10): 6786-6797.

Placke, T., H. G. Kopp, et al. (2010). "Glucocorticoid-induced TNFR-related (GITR) protein and its ligand in antitumor immunity: functional role and therapeutic modulation." Clin Dev Immunol **2010**: 239083.

Placke, T., H. G. Kopp, et al. (2011). "Modulation of natural killer cell anti-tumor reactivity by platelets." J Innate Immun **3**(4): 374-382.

Placke, T., M. Orgel, et al. (2012). "Platelet-derived MHC class I confers a pseudonormal phenotype to cancer cells that subverts the antitumor reactivity of natural killer immune cells." Cancer Res **72**(2): 440-448.

Polasek, J. (1989). "Lysosomal concept of platelet secretion--revisited." Eur J Haematol Suppl **50**: 3-24.

Polgar, J., S. H. Chung, et al. (2002). "Vesicle-associated membrane protein 3 (VAMP-3) and VAMP-8 are present in human platelets and are required for granule secretion." Blood **100**(3): 1081-1083.

Raqeeb, A., J. Sheng, et al. (2011). "Purinergic P2Y2 receptors mediate rapid Ca(2+) mobilization, membrane hyperpolarization and nitric oxide production in human vascular endothelial cells." Cell Calcium **49**(4): 240-248.

Ren, Q., H. K. Barber, et al. (2007). "Endobrevin/VAMP-8 is the primary v-SNARE for the platelet release reaction." Mol Biol Cell **18**(1): 24-33.

Ren, Q., C. Wimmer, et al. (2010). "Munc13-4 is a limiting factor in the pathway required for platelet granule release and hemostasis." Blood **116**(6): 869-877.

Ren, Q., S. Ye, et al. (2008). "The platelet release reaction: just when you thought platelet secretion was simple." Curr Opin Hematol **15**(5): 537-541.

Rendu, F. and B. Brohard-Bohn (2001). "The platelet release reaction: granules' constituents, secretion and functions." Platelets **12**(5): 261-273.

Rizo, J. and C. Rosenmund (2008). "Synaptic vesicle fusion." Nat Struct Mol Biol **15**(7): 665-674.

Rosenmund, C., A. Sigler, et al. (2002). "Differential control of vesicle priming and short-term plasticity by Munc13 isoforms." Neuron **33**(3): 411-424.

Rothwell, P. M., M. Wilson, et al. (2012). "Effect of daily aspirin on risk of cancer metastasis: a study of incident cancers during randomised controlled trials." Lancet **379**(9826): 1591-1601.

Ruiz, F. A., C. R. Lea, et al. (2004). "Human platelet dense granules contain polyphosphate and are similar to acidocalcisomes of bacteria and unicellular eukaryotes." J Biol Chem **279**:44250-44257.

Sachs, U. J. and B. Nieswandt (2007). "In vivo thrombus formation in murine models." Circ Res **100**(7): 979-991.

Sahai, E. (2007). "Illuminating the metastatic process." Nat Rev Cancer **7**(10): 737-749.

Schiavo, G., M. Matteoli, et al. (2000). "Neurotoxins affecting neuroexocytosis." Physiol Rev **80**(2): 717-766.

Schraw, T. D., T. W. Rutledge, et al. (2003). "Granule stores from cellubrevin/VAMP-3 null mouse platelets exhibit normal stimulus-induced release." Blood **102**(5): 1716-1722.

Secco, G. G., R. Parisi, et al. (2012). "P2Y12 inhibitors: pharmacologic mechanism and clinical relevance." Cardiovasc Hematol Agents Med Chem Epub ahead of print.

Sehgal, S. and B. Storrie (2007). "Evidence that differential packaging of the major platelet granule proteins von Willebrand factor and fibrinogen can support their differential release." J Thromb Haemost **5**(10): 2009-2016.

Seye, C. I., N. Yu, et al. (2004). "The P2Y2 nucleotide receptor mediates vascular cell adhesion molecule-1 expression through interaction with VEGF receptor-2 (KDR/Flk-1)." J Biol Chem **279**(34): 35679-35686.

Seye, C. I., N. Yu, et al. (2003). "The P2Y2 nucleotide receptor mediates UTP-induced vascular cell adhesion molecule-1 expression in coronary artery endothelial cells." J Biol Chem **278**(27): 24960-24965.

Shirakawa, R., T. Higashi, et al. (2004). "Munc13-4 is a GTP-Rab27-binding protein regulating dense core granule secretion in platelets." J Biol Chem **279**(11): 10730-10737.

Silverstein, R. L. and M. Febbraio (1992). "Identification of lysosome-associated membrane protein-2 as an activation-dependent platelet surface glycoprotein." Blood **80**(6): 1470-1475.

Sims, P. J. and T. Wiedmer (2001). "Unraveling the mysteries of phospholipid scrambling." Thromb Haemost **86**(1): 266-275.

Sixma, J. J., J. W. Slot, et al. (1989). "Immunocytochemical localization of platelet granule proteins." Methods Enzymol **169**: 301-311.

Smith, S. A., N. J. Mutch, et al. (2006). "Polyphosphate modulates blood coagulation and fibrinolysis." Proc Natl Acad Sci USA **103**: 903-908.

Smyth, S. S., R. P. McEver, et al. (2009). "Platelet functions beyond hemostasis." J Thromb Haemost **7**(11): 1759-1766.

Sollner, T. (2003). "Regulated exocytosis and SNARE function." Mol Membr Biol **20**(3): 209-220.

Sorensen, J. B., U. Matti, et al. (2002). "The SNARE protein SNAP-25 is linked to fast calcium triggering of exocytosis." Proc Natl Acad Sci USA **99**(3): 1627-1632.

Spano, D. and M. Zollo (2012). "Tumor microenvironment: a main actor in the metastasis process." Clin Exp Metastasis **29**(4): 381-395.

Stegner, D., B. Nieswandt (2011) "Platelet receptor signaling in thrombus formation." J Mol Med **89**: 109–121.

Stenberg, P. E., R. P. McEver, et al. (1985). "A platelet alpha-granule membrane protein (GMP-140) is expressed on the plasma membrane after activation." J Cell Biol **101**(3): 880-886.

Stokes, K. Y. and D. N. Granger (2012). "Platelets: a critical link between inflammation and microvascular dysfunction." J Physiol **590**(Pt 5): 1023-1034.

Suzuki, T., W. Li, et al. (2001). "The gene mutated in cocoa mice, carrying a defect of organelle biogenesis, is a homologue of the human Hermansky-Pudlak syndrome-3 gene." Genomics **78**(1-2): 30-37.

Suzuki-Inoue, K. (2011) "Essential in vivo roles of the platelet activation receptor CLEC-2 in tumour metastasis, lymphangiogenesis and thrombus formation." J Biochem **150**(2): 127-132.

Suzuki-Inoue, K., G. L. Fuller et al. (2006). "A novel Syk-dependent mechanism of platelet activation by the C-type lectin receptor CLEC-2." Blood **107**(2): 542-549.

Tapper, H. and R. Sundler (1990). "Role of lysosomal and cytosolic pH in the regulation of macrophage lysosomal enzyme secretion." Biochem J **272**(2): 407-414.

Terraube, V., I. Marx, et al. (2007). "Role of von Willebrand factor in tumor metastasis." Thromb Res **120 Suppl 2**: S64-70.

Tiruppathi, C., G. U. Ahmmed, et al. (2006). "Ca2+ signaling, TRP channels, and endothelial permeability." Microcirculation **13**(8): 693-708.

Vaidyanathan, V. V., N. Puri, et al. (2001). "The last exon of SNAP-23 regulates granule exocytosis from mast cells." J Biol Chem **276**(27): 25101-25106.

Vaidyanathan, V. V., K. Yoshino, et al. (1999). "Proteolysis of SNAP-25 isoforms by botulinum neurotoxin types A, C, and E: domains and amino acid residues controlling the formation of enzyme-substrate complexes and cleavage." J Neurochem **72**(1): 327-337.

van Gils, J. M., J. J. Zwaginga, et al. (2009). "Molecular and functional interactions among monocytes, platelets, and endothelial cells and their relevance for cardiovascular diseases." J Leukoc Biol **85**(2): 195-204.

Vandenbroucke St Amant, E., M. Tauseef, et al. (2012). "PKCalpha Activation of p120-Catenin Serine 879 Phospho-Switch Disassembles VE-Cadherin Junctions and Disrupts Vascular Integrity." Circ Res.

Varki, N. M. and A. Varki (2002). "Heparin inhibition of selectin-mediated interactions during the hematogenous phase of carcinoma metastasis: rationale for clinical studies in humans." Semin Thromb Hemost 28(1): 53-66.

Vidal-Vanaclocha, F., G. Fantuzzi, et al. (2000). "IL-18 regulates IL-1beta-dependent hepatic melanoma metastasis via vascular cell adhesion molecule-1." Proc Natl Acad Sci U S A 97(2): 734-739.

Voigtlander, C., A. Rand, et al. (2002). "Suppression of tissue factor expression, cofactor activity, and metastatic potential of murine melanoma cells by the Nterminal domain of adenovirus E1A12S protein." J Cell Biochem 85(1): 54-71.

Weiss, H. J. and B. Lages (1988). "The response of platelets to epinephrine in storage pool deficiency--evidence pertaining to the role of adenosine diphosphate in mediating primary and secondary aggregation." Blood 72(5): 1717-1725.

Weksler, B. B., A. J. Marcus, et al. (1977). "Synthesis of prostaglandin I2 (prostacyclin) by cultured human and bovine endothelial cells." Proc Natl Acad Sci U S A 74(9): 3922-3926.

White, J. G. (1999). "Platelet membrane interactions." Platelets 10(6): 368-381.

White, J. G. (1999). "Platelet secretory process." Blood 93(7): 2422-2425.

White, J. G. (2008). "Electron opaque structures in human platelets: which are or are not dense bodies?" Platelets 19(6): 455-466.

White, J. G. and M. Krumwiede (2007). "Some contributions of electron microscopy to knowledge of human platelets." Thromb Haemost 98(1): 69-72.

Yamamoto, M., N. Wada, et al. (2003). "Reversible suppression of glutamatergic neurotransmission of cerebellar granule cells in vivo by genetically manipulated expression of tetanus neurotoxin light chain." J Neurosci 23(17): 6759-6767.

Youssefian, T., J. M. Masse, et al. (1997). "Platelet and megakaryocyte dense granules contain glycoproteins Ib and IIb-IIIa." Blood 89(11): 4047-4057.

Yuan, P., S. Temam, et al. (2006) "Overexpression of podoplanin in oral cancer and its association with poor clinical outcome." Cancer 107: 563-569.

Yuasa, K., S. Takeda, et al. (2012). "A conserved regulatory element located far downstream of the gls locus modulates gls expression through chromatin loop formation during myogenesis." FEBS Lett 586(19): 3464-3470.

Zarbock, A., R. K. Polanowska-Grabowska, et al. (2007). "Platelet-neutrophil-interactions: linking hemostasis and inflammation." Blood Rev 21(2): 99-111.

Zigler, M., T. Kamiya, et al. (2011) "PAR-1 and thrombin: the ties that bind the microenvironment to melanoma metastasis." Cancer Res 71(21): 6561-6566.

9   <u>Appendices</u>

9.1   Zusammenfassung

9.1.1   Einleitung

In den letzten Jahrzehnten wurde in zahlreichen Publikationen gezeigt, dass Thrombozyten über ihre Funktion in der Hämostase hinaus an vielen weiteren Prozessen, vor allem pathologischen Veränderungen mit immunologischer Komponente, beteiligt sind. Ermöglicht wird dies durch die Sekretion einer breiten Palette proinflammatorischer Proteine sowie durch die Bildung reaktiver Mikropartikel nach Aktivierung der Thrombozyten. Thrombozyten besitzen zwei funktionell wichtige Arten von Vesikeln, *alpha* und *dense granules*. *Alpha granules* enthalten größere Moleküle wie die Adhesion-Proteine P-Selektin und vWF, Chemokine wie PF4, RANTES oder IL-1β sowie Wachstumsfaktoren wie VEGF und PDGF. In *dense granules* sind hingegen kleine Moleküle, vor allem ATP und ADP, aber auch Calcium, Serotonin und Histamin gespeichert.

Wie in allen sekretorischen Zellen wird die regulierte Exozytose in Thrombozyten von drei verschiedenen Klassen von SNARE-Proteinen, SNAP, Syntaxin und VAMP, vermittelt. SNARE-Proteine sind zu einem Teil an die Plasmamembran, zum anderen an die Vesikel-Membran gebunden, richten im Verlauf des Exozytose-Vorgangs cytosolische Alpha-Helices aneinander aus und lagern sich schließlich zusammen. Die so frei werdende Bindungsenergie reicht aus, um die Abstoßungskräfte der beiden Membranen zu überwinden und zur Fusion zu führen. Mehrere Isoformen o.g. Proteine sind in Thrombozyten nachweislich an sekretorischen Vorgängen beteiligt: SNAP-23, Syntaxin-2 und -4 und VAMP-3 und -8 (Chen, Lemons et al. 2000; Flaumenhaft, Rozenvayn et al. 2007). Andere, ebenfalls sehr konservierte Protein-Familien sind fast ausschließlich in der Nähe der Plasmamembran zu finden, der sogenannten *"active zone"* und beeinflussen die Sekretion, indem sie mit SNARE-Proteinen interagieren. Eines der wichtigsten Proteine dieser Art ist Munc13. Der Wirkungsmechanismus ist noch nicht vollständig geklärt, aber Verlust der zellspezifischen Isoform(en) führt oft zu starken Einschränkungen oder komplettem Verlust der Sekretion einzelner oder aller Vesikel-Arten dieser Zelle (Rosenmund, Sigler et al., 2002; Feldmann, Callebaut et al. 2003).

Thrombozyten verstärken das Fortschreiten atherosklerotischer Veränderungen, indem sie inflammatorische Stimuli wie PF4, RANTES und CD40L an Gefäßpartien, die ein dysfunktionales Endothel aufweisen, deponieren. Dies führt zu einer vermehrten Rekrutierung von Leukozyten, *"foam-cell"*-Bildung und atherosklerotischer Plaque-Formation (Gleissner, Shaked et al. 2010; Lievens, Zernecke et al. 2010).

Eine Beziehung zwischen Thrombozyten und Tumorerkrankungen wurde erstmals 1865 von dem französischen Arzt Armand Trousseau (Armand Trousseau, Phlegmasia alba dolens, in: Clinique Medicale de l'Hotel-Dieu de Paris, Vol 3, 2nd Edition, Ballière, Paris, 1865, pp 654-712) beschrieben. Er beobachtete, dass Krebs-Patienten eine erhöhte

Neigung zu thrombotischen Komplikationen haben und umgekehrt, dass bei Patienten mit akuter Thrombose das Risiko der Manifestation einer Krebserkrankung erhöht ist. Etwa seit den 1960er Jahren wird aber auch eine stetig steigende Anzahl an Studien veröffentlicht, die zeigen, dass Thrombozyten darüber hinaus direkt auf primäre Tumoren und besonders Tumor-Metastasierung einwirken können. Thrombozyten könnten in der direkten Umgebung von Primär-Tumoren dazu veranlasst werden, gezielt pro-angiogenetische Faktoren wie VEGF und PDGF freizusetzen. Dies erscheint durchaus plausibel, da in den letzten fünf Jahren immer mehr Belege veröffentlicht wurden, die zeigen, dass *alpha granules* heterogene Subpopulationen bilden, die kontextspezifisch und stimulusabhängig sezerniert werden können (Ma, Perini et al. 2005; Italiano, Richardson et al. 2008). Allerdings war es bisher nicht möglich, den Beitrag von Thrombozyten zu Tumor-Angiogenese von dem anderer Immunzellen zu differenzieren, die die gleichen Moleküle freisetzen können. Pharmakologische und genetische Depletion von Thrombozyten führt zu einem starken Rückgang der Metastasen-Bildung in verschiedenen Mausmodellen. Die diesem Phänomen zugrundeliegenden Mechanismen sind aber bisher unklar geblieben. Es ist bekannt, dass Thrombozyten an zirkulierende Tumorzellen binden und diese vor Lyse durch NK-Zellen, der effektivsten anti-metastatischen Immunabwehr des Körpers, sowie gegen Scherkräfte schützen. Thrombozyten lassen sich auch nach Andocken der Tumorzellen an der Gefäßwand in der Mikrozirkulation an deren Oberfläche nachweisen. Sie könnten durch verschiedene Oberflächen-Rezeptoren die indirekte Interaktion von Tumorzellen mit Leukozyten oder Endothelzellen erleichtern. Von Tumorzellen aktivierte Thrombozyten könnten aber auch Mediatoren freisetzen, die die Eigenschaften der Tumorzelle, insbesondere deren Aggressivität, beeinflussen (Labelle, Begum et al. 2011).

9.1.2 Ziele dieser Arbeit

Die Ziele dieser Arbeit waren

(I)   die Generierung und

(II)   Analyse genetisch modifizierter Mauslinien mit Sekretionsdefekten in Thrombozyten und

(III)   deren Nutzung zur Untersuchung der Rolle von Thrombozyten-Sekretion in Atherosklerose- und Tumor-Mausmodellen.

9.1.3 Ergebnisse

Der Wirkungsmechanismus der Toxine von *Clostridium* beruht auf der enzymatischen Spaltung verschiedener SNARE-Proteine durch die leichte Kette des Toxins. Um eine selektive Störung thrombozytärer Sekretion zu erzielen, ersetzten wir in einem bakteriellen artifizielle Chromosom die für das Thrombozyten-spezifische PF4-Protein kodierende Sequenz durch die cDNA der leichten Ketten von Tetanus-Toxin bzw. Botulinum-Toxin E und C. Diese Konstrukte wurden in den Pronukleus fertilisierter Maus-Oozyten injiziert, und die resultierenden *founder*-Tiere wurden in Bezug auf Toxin-Expression und Thrombozyten-

Sekretion untersucht. Auch nach zum Teil mehrmaliger Injektion war die beste Spaltungsrate in einem *founder*-Tier der Botulinum-E-exprimierenden Linie 40% des thrombozytären SNAP-23 und 60% der thrombozytären Menge von Syntaxin-2 in der Botulinum-C-exprimierenden Linie. Die Spaltung von VAMP-3 durch Tetanus-Toxin in Thrombozyten konnte nicht eindeutig nachgewiesen werden. Keine dieser Mauslinien zeigte eine gestörte Sekretion in isolierten Thrombozyten.

SNAP-23 ist die einzige SNAP-Isoform in Thrombozyten, während für die Syntaxin- und VAMP-Familie jeweils mindestens zwei Isoformen nachweislich an der Sekretion beteiligt sind. Durch die bekannte Promiskuität der SNARE-Proteine könnte also der Verlust einer Isoform eventuell kompensiert werden. Deshalb konstruierten wir zwei von anderen Publikationen hergeleitete dominant-negative Mutanten von SNAP-23 und exprimierten diese ebenfalls unter der Kontrolle des PF4-Promotors. Die eine Mutante wurde nicht in nachweisbarer Menge exprimiert, das andere Konstrukt wurde zwar exprimiert, führte aber auch in dem *founder*-Tier mit der höchsten Expression zu keiner funktionellen Einschränkung der Thrombozyten-Sekretion.

Munc13-4 ist die einzige Isoform des SNARE-assoziierten Proteins Munc13, die in Thrombozyten exprimiert wird. Deshalb erschien es vielversprechend, eine im Labor von Bruce Beutler hergestellte funktionelle Null-Mutante (Munc13-4*Jinx*) auf Defekte in Thrombozyten-Sekretion zu untersuchen. In der Tat war bei dieser Mauslinie die Sekretion von *dense granules*, bestimmt durch ATP-Ausschüttung, vollständig unterdrückt nach Stimulation mit Thrombin, dem Thromboxan A_2-Analog U46619 oder Kollagen. Demgegenüber war Sekretion von *alpha granules*, gemessen durch Freisetzung von PF4 oder vWF, unverändert in isolierten Munc13-4-defizienten Thrombozyten im Vergleich zu Wildtyp-Thrombozyten. Ebenfalls normal waren Morphologie, Thrombozytenanzahl, Gesamtmenge des *alpha-granule*-Proteins PF4 sowie die Anzahl repräsentativer Thrombozyten-Oberflächenrezeptoren. Die Aggregation der Munc13-4-defizienten Thrombozyten war nach Stimulation mit Kollagen oder U46619 deutlich gehemmt. Die Bildung großflächiger Aggregate in der Flusskammer, die Scherkräfte und Exposition von Kollagen in kleinen Gefäßen simuliert und mit heparinisiertem Blut durchströmt wird, war in Munc13-4-defizienten Thrombozyten im Vergleich zu Wildtyp-Thrombozyten vermindert. Munc13-4-defiziente Tiere zeigten eine stark verlängerte Blutungszeit nach Entfernung von 2 mm der Schwanzspitze. Auch im $FeCl_3$-Thrombosemodell war innerhalb der Versuchszeit von 60 min keine Bildung von stabilen Aggregaten in mesenterialen Arterien Munc13-4- defizienter Tiere zu beobachten, während die Arterien gleichaltriger Wildtyp-Mäuse nach etwa 10 min vollständig verschlossen waren. Diese Befunde zeigen, dass Verlust von Munc13-4 in Thrombozyten zu einer selektiven Unterdrückung der *dense-granule*-Sekretion führt, wodurch es zur Störung der Thrombozytenaggregation in vitro und in vivo kommt.

Um die Rolle von *dense-granule*-Sekretion im Rahmen chronischer Gefäßerkrankungen wie Atherosklerose zu untersuchen, bedienten wir uns eines Maus-Modells, bei dem der LDL-Rezeptor genetisch inaktiviert wurde. LDLR-KO Mäuse

entwickeln nach mehreren Wochen fett- und cholesterinreicher Diät atherosklerotische Veränderungen, die denen in humanen Gefäßen sehr nahe kommen. Wir transplantierten Knochenmark von Wildtyp- und Munc13-4-defizienten Donoren in LDLR-KO-Mäuse. Nach 16 Wochen fett- und cholesterinreicher Diät war kein Unterschied in atherosklerotischer Plaque-Bildung zwischen den Aorten beider Versuchsgruppen zu erkennen.

Da Depletion von Thrombozyten zu starker Verminderung der Metastasen-Bildung in Maus-Tumormodellen führt und Thrombozyten direkt an Tumorzellen binden, wollten wir überprüfen, ob Thrombozyten die Extravasation von Tumorzellen beeinflussen. Dazu wählten wir zunächst ein in-vitro-Testsystem, in dem die Transmigration zweier Maus-Tumorzelllinien (B16 Melanom und LLC1-Lungenkarzinom) durch eine murine Endothelzellschicht (MS1-Zellen) bestimmt wird. Zugabe von Wildtyp-Thrombozyten zu den Tumorzellen in den oberen Teil der *transwell*-Kammer führte bei beiden Tumorzelllinien zu einer zwei- bis dreifachen Erhöhung der Transmigrationsrate, während die Zugabe von Munc13-4-defizienten Thrombozyten die basale Transmigrationsrate nicht beeinflusste. Um zu überprüfen, ob die Unterdrückung eines Sekretionsproduktes in Munc13-4-defizienten Thrombozyten diesen Effekt verursachte, gaben wir nur den Überstand zuvor mit den entsprechenden Tumorzellen inkubierter Wildtyp-Thrombozyten in den Transmigrations-Versuch und erhielten die gleiche Erhöhung der Tumorzell-Transmigration. Das ATP/ADP-degradierende Enzym Apyrase verhinderte die Thrombozyten-abhängige Transmigration, während alleine die Zugabe von exogenem ATP eine vergleichbar erhöhte Transmigrationsrate zur Folge hatte. Inkubation von Thrombozyten mit Tumorzellen führte zu einer starken Ausschüttung von ATP in Wildtyp-, aber nicht in Munc13-4-defizienten Thrombozyten. Die Sekretion der *alpha granules* war jedoch auch nach Stimulation durch Tumorzellen in beiden Genotypen vergleichbar. Da die Erhöhung der Tumorzell-Transmigration durch Thrombozyten Endothel-abhängig war, untersuchten wir, welche Wirkung Überstände Tumorzell-stimulierter Thrombozyten auf die Morphologie und Permeabilität einer Endothelzellschicht haben. Die Adhäsionsverbindungen der Endothelzellen waren unter diesen Bedingungen gestört und lösten sich zum Teil ganz. Auch die Permeabilität der Endothelzellschicht für FITC-Dextran (70 kDa) war deutlich erhöht. Bei zusätzlicher Anwesenheit von Apyrase während der Inkubation von Thrombozyten und Tumorzellen waren Morphologie und Permeabilität hingegen normal. Um die Relevanz dieser Befunde in vivo zu untersuchen, injizierten wir B16- oder LLC1-Zellen in die Flanken von Wildtyp- und Munc13-4-defizienten Mäusen. Hierbei zeigten Munc13-4-defiziente Mäuse und Wildtyp-Mäuse vergleichbares Wachstum, Gewicht und Tumor-Angiogenese in B16- und LLC1-Tumoren. Die Metastasierung in der Lunge war jedoch unabhängig von der Größe der Metastasen um etwa 70% reduziert in Munc13-4-defizienten Tieren im Vergleich zu Wildtyp-Mäusen. Diese starke Verminderung in der Metastasierung stellte sich auch nach i.v.-Injektion von B16- oder LLC1-Zellen ähnlich dar. Um den Mechanismus unter Zellkultur-Bedingungen detaillierter zu charakterisieren, untersuchten wir die Expression von ionotropen und metabotropen ATP-Rezeptoren in

murinen Endothelzellen und fanden P2X$_4$ und P2Y$_2$ jeweils am höchsten exprimiert. Inhibierung oder *knockdown* von P2X$_4$ beeinflusste die Thrombozyten-vermittelte Tumorzell-Transmigration nicht, aber *knockdown* des P2Y$_2$-Rezeptors, für den es keinen spezifischen Antagonisten gibt, reduzierte diesen Effekt erheblich. Ob ein ähnlicher Mechanismus für die reduzierte Metastasen-Bildung in Munc13-4-defizienten Tieren in vivo verantwortlich ist, testeten wir, indem wir FITC-Dextran und kurz darauf B16-Tumorzellen i.v. injizierten. Nach drei Stunden war in den Lungen von Wildtyp-Mäusen eine deutliche extraluminale Akkumulation von FITC-Dextran zu beobachten, während Munc13-4-defiziente und P2Y$_2$-KO-Mäuse sowie Wildtyp-Mäuse ohne Injektion von Tumorzellen (Kontrollgruppe) eine ähnlich niedrige extraluminale FITC-Dextran-Präsenz zeigten. Die erhöhte Durchlässigkeit der Gefäße für FITC-Dextran korrelierte mit einer viel stärkeren Extravasation von CFSE-gefärbten B16-Zellen sechs Stunden nach Injektion in Wildtyp-Mäusen gegenüber Munc13-4-defizienten und P2Y$_2$-KO-Mäusen. Übereinstimmend mit einer Rolle endotheler P2Y$_2$-Rezeptoren in Thrombozyten-vermittelter Extravasation von Tumorzellen in vivo war die Metastasierung in den Lungen von P2Y$_2$-KO-Mäusen nach i.v.-Injektion von B16- oder LLC1-Zellen ähnlich stark reduziert wie in Munc13-4-defizienten Mäusen.

9.1.4 Diskussion

Von den im ersten Projektteil generierten fünf BAC-transgenen Mauslinien zeigte keine eine signifikante Störung der thrombozytären Sekretion. Fehlende Promotor-Elemente oder mangelhafter Transport zur *"active zone"* könnte die nicht ausreichende Expression und Wirkung der Toxin-Konstrukte und SNAP-23-Mutanten unter der Kontrolle des PF4-Promotors erklären. Mit der Munc13-4*Jinx*-Mutante konnten wir jedoch eine Mauslinie identifizieren, die einen isolierten, vollständigen Defekt in der Sekretion von *dense granules* in Thrombozyten aufweisen bei gleichzeitiger Erhaltung der *alpha-granule*-Sekretion und aller anderen wichtigen Thrombozyten-Merkmale. Damit stellt diese Mauslinie ein bisher einzigartiges Werkzeug dar, um die Rolle der *dense-granule*-Sekretion in verschiedensten Kontexten zu untersuchen.

Dass der Verlust von *dense-granule*-Sekretion die atherosklerotische Progression nicht beeinflusst, ist nicht unerwartet, da außer Polyphosphaten (Muller, Mutch et al. 2009) bisher keine potentiell inflammtorischen Mediatoren in *dense granules* beschrieben wurden.

Die vorliegende Arbeit liefert viele Belege für einen Mechanismus, der es Tumorzellen ermöglicht, Thrombozyten lokal in der Mikrozirkulation des Ziel-Organs zu nutzen, um durch eine hohe Ausschüttung von ATP und P2Y$_2$-vermittelte Destabilisierung der Endothel-Barriere diese leichter zu überwinden und Metastasen zu bilden. Auch eine andere Studie fand, dass P2Y$_2$-Rezeptoren die transendotheliale Migration von zirkulierenden Zellen vermitteln, in diesem Fall von Neutrophilen (Kukulski, Ben Yebdri et al. 2010). Desweiteren deckt sich mit unseren Ergebnissen, dass Aktivierung von endothelen P2Y$_2$-Rezeptoren über Koppelung an die G-Proteine G$_q$/G$_{11}$ zum Anstieg von

intrazellulärem Calcium (Abbracchio, Burnstock et al. 2006) und Aktivierung von Protein Kinase C führt, was die Destabilisierung der Endothel-Barrieren zur Folge hat (Gavard and Gutkind 2008; Knezevic, Tauseef et al. 2009; Korhonen, Fisslthaler et al. 2009). Eine in diesem Jahr erschienene Meta-Analyse kardiovaskulärer Verlaufsstudien (Rothwell, Wilson et al. 2012) kommt zu dem Schluss, dass tägliche Einnahme niedrig-dosierten Aspirins nach fünf Jahren zu einer Reduktion der krebsbedingten Todesfälle um ca. 15% führt, was ausschließlich auf die anti-metastatische Wirkung dieser Thrombozyten-hemmenden Dosis zurückzuführen sei. Unsere Ergebnisse legen einen Mechanismus nahe, der eine mögliche Erklärung für die vielfach beobachtete Beteiligung von Thrombozyten bei der Metastasen-Bildung liefert und gleichzeitig einen neuen Therapieansatz eröffnet, der die Gefahr von Einblutungen bei Gabe klassischer Thrombozyten-Inhibitoren umgeht. Wir konnten zeigen, dass die Metastasierung im murinen Modell durch Sekretion aus *dense granules* Tumorzell-aktivierter Thrombozyten stark beeinflusst wird. Wir fanden, dass ATP aus dense granules über endothele $P2Y_2$-Rezeptoren die Endothel-Barriere destabilisiert und den Tumorzellen so den Zugang zum Parenchym des Zielorgans erleichtert. $P2Y_2$-Rezeptoren könnten somit ein vielversprechendes Ziel pharmakologischer Intervention in der Tumortherapie darstellen.

9.2   Acknowledgements

I want to thank Nina Wettschureck and Stefan Offermanns for their guidance and support during the years of research underlying this thesis and for providing the productive, well-appointed environment that allowed me to learn and grow both scientifically and spiritually.

Additionally, I would like to thank all my colleagues at the Institute of Pharmacology in Heidelberg and the Max-Planck-Institute in Bad Nauheim, who have helped and supported me during my PhD.

I am grateful to Prof. Amparo Acker-Palmer for supervising my thesis for the University of Frankfurt and to Prof. Anna Starzinski-Powitz and the faculty of biology at the University of Frankfurt for enabling me to graduate in their faculty in cooperation with the MPI.

9.3 Curriculum vitae

Personal data

Name	Dagmar Schumacher (née Jaeneke)
Date of Birth	December 17th 1978 in Basel (Switzerland)
Address	Quinckestr. 9
	D-69120 Heidelberg
Email	d.jaeneke@gmail.com

Education

10/1998 – 10/2001 University of Bremen, **Psychology** (diploma)

Successfully completed lower-division requirements, GPA 1.0 (very good)

10/2001 – 03/2002 Gießen-Friedberg University of Applied Sciences, **Biotechnology** (diploma)

03/2002 – 09/2006 Mannheim University of Applied Sciences, **Biotechnology** (diploma)

Graduation Dipl.-Ing. (FH) September 2006, GPA 2.1 (good), thesis and oral examination 1.0 (very good)

Professional experience

10/2006 – 08/2012 **PhD:** 10/2006 – 08/2009: Institute of Pharmacology, University of Heidelberg; 09/2009 – 08/2012: Max-Planck-Institute for Heart and Lung Research, Bad Nauheim, Germany (supervisors: Stefan Offermanns, Nina Wettschureck)

Manuscript title: „Platelet-derived nucleotides promote tumor cell transendothelial migration and metastasis via $P2Y_2$ receptor." (under revision)

03/2006 – 09/2006 **Diploma thesis:** Neuroscience Research, Abbott GmbH and Company KG, Ludwigshafen, Germany (supervisor: Axel H. Meyer)

Title: „Investigation of the GPR7-NPB/NPW system and invasion of Schwann cells in experimental autoimmune encephalomyelitis (EAE)."

09/2004 – 02/2005 **Internship:** Pacific Biomedical Research Center, Department of Cell and Molecular Biology, Honolulu, USA (supervisors: Gillian D. Bryant-Greenwood, Claire Kendal-Wright)

Project title: „Role of NF-κB and AP-1 in gene expression of pre-B-cell-enhancing factor (PBEF) and other cytokines after IL-1β stimulation of amniotic epithelial WISH cells."

03/2003 – 08/2003 **Internship:** SLFA Neustadt a.d.W., Germany, Alplanta (previously Centrum Grüne Gentechnik, supervisor: Götz M. Reustle)

Project title: „Agrobacterium tumefaciens-mediated transformation of grape vine somatic embryos to introduce resistances to different viruses."

Project title: „Agrobacterium tumefaciens-mediated transformation of grape vine somatic embryos to introduce resistances to different viruses."

9.4   Publications

Peer-reviewed publications

- **Schumacher D**, Strilić B, Sivaraj KK, Wettschureck N, Offermanns S

  „Platelet-derived nucleotides promote tumor-cell transendothelial migration and metastasis via $P2Y_2$ receptor." (under revision)

- Herroeder S, Reichardt P, Sassmann A, Zimmermann B, **Jaeneke D**, Hoeckner J, Hollmann MW, Fischer KD, Vogt S, Grosse R, Hogg N, Gunzer M, Offermanns S, Wettschureck N

  „Guanine nucleotide-binding proteins of the G12 family shape immune functions by controlling CD4+ T cell adhesiveness and motility."

  Immunity, 708-720 (2009)

Abstracts & posters presented at meetings

- International Vascular Biology Meeting (IVBM) June 2nd - 5th (2012)

  Schumacher D, Strilić B, Wettschureck N, Offermanns S

  „Platelet-derived nucleotides promote tumor-cell transendothelial migration and metastasis via $P2Y_2$."

- Annual retreat Deutschen Gesellschaft für Experimentelle und Klinische Pharmakologie und Toxikologie (DGPT) March 19th - 22nd (2012)

  Schumacher D, Strilić B, Wettschureck N, Offermanns S

  „Platelet-derived nucleotides promote tumor-cell transendothelial migration and metastasis via $P2Y_2$."